EVALUATION OF INJURY MECHANISMS ASSOCIATED WITH ABUSIVE HEAD TRAUMA

by

Shaun Michael Evans

A thesis submitted to the faculty of
The University of Utah
in partial fulfillment of the requirements for the degree of

Master of Science

Department of Mechanical Engineering

The University of Utah

December 2014

The University of Utah Graduate School

STATEMENT OF THESIS APPROVAL

The thesis of **Shaun Michael Evans**

has been approved by the following supervisory committee members:

Brittany Coats	, Chair	**06/27/2014** Date Approved
Kenneth Monson	, Member	**06/27/2014** Date Approved
Antoinette Laskey	, Member	**06/27/2014** Date Approved

and by **Tim Ameel**, Chair of

the Department of **Mechanical Engineering**

and by David B. Kieda, Dean of The Graduate School.

ABSTRACT

Traumatic brain injury (TBI) is a leading cause of death and disability in children. One of the leading causes of severe TBI in infants is abusive head trauma (AHT). Shaken baby syndrome (SBS) is a subset of AHT in which brain injury is present without obvious signs of head impact, thus the head injury is thought to be caused by shaking. SBS is one of the most difficult forms of TBI to study as the injuries are complex and the histories surrounding the child's injuries are questionable, or unknown. In this thesis, we investigate potential mechanisms of brain and eye injury from AHT and SBS. In Chapter 2, we investigate the potential coupling effect of the physiological response to crying (i.e. increased intracranial pressure (ICP) and increased cerebral blood volume (CBV)) with repetitive head trauma. Increased ICP and CBV prior to and during head trauma did increase the amount of injury and there was some macroscopic findings unique to that group; however, levels of injury were not as severe as reported clinically in SBS.

In Chapters 3 and 4, we investigated two potential mechanisms of retinal hemorrhage (RH), a common ocular injury reported in AHT. The first study investigated whether repetitive occlusion of the optic nerve (ON) could lead to RH. Occluding the ON for 1-10 minutes and then releasing resulted in large RH that spanned the posterior pole and periphery of the retina. Cyclic, repetitive occlusion of the ON, however, resulted in no hemorrhage. In the second study, rapid increases in intraocular pressure (IOP) were evaluated as a possible mechanism of RH from AHT. A device mechanically

indented the eyes of 3-5-day-old piglets at different rates and depths to produce large changes in IOP. No hemorrhages were caused from the rapid changes in IOP, and it was concluded that rapid changes in IOP by itself does not cause RH. This work identified two mechanisms which can influence or cause injury from abuse, and another mechanism was shown to likely not be a factor in abuse.

TABLE OF CONTENTS

ACKNOWLEDGEMENTS

I would like to acknowledge and thank my advisor, Dr. Brittany Coats, for all of her help, support, and guidance. I would also like to thank the other members of my committee, Dr. Ken Monson and Dr. Toni Laskey, for their professional input and insight. I would also like to thank Dr. Gil Binenbaum for the opportunity to work with him on the eye studies.

I want to thank all of my lab mates: Jourdan Coulter, Kiffer Creveling, McKenna Drysdale, Justin Jones, Patrick Moran, John Muhs, Jami Saffioti, Greg Scott, Dan Shedd, and Alex Williams. You all helped me accomplish this work.

I would like to thank all of the staff at the U of U Comparative Medicine Center and all the staff at the animal care facility at the University of Pennsylvania for their assistance helping us with our animals.

I would like to thank Primary Children's Medical Center Foundation Early Career Grant for their financial support of the work in Chapter 2. I would also like to thank the University of Pennsylvania Vision Research Seed Grant Program (PI: Binenbaum) for their support of the work in Chapters 3 and 4.

I would like to thank my parents, Scott and Tracy, for always supporting me, and my siblings, Paul, Michelle, Spencer, and Tyler, for always being interested in my work. And finally, I cannot give enough thanks to my wife Ashley for her help, tireless support, and encouragement, and thank you Declan and Hazel for making bad days good.

CHAPTER 1

INTRODUCTION TO INJURY MECHANISMS OF ABUSIVE HEAD TRAUMA

1.1 Motivation

Abusive head trauma (AHT) is a serious problem in the US and Worldwide [1, 2, 3]. Shaken baby syndrome (SBS) is a term used to denote a subset of AHT that presents with traumatic brain and eye injury without any history of trauma or signs of head impact. Symptoms associated with SBS can include: subdural hematoma (SDH), subarachnoid hemorrhage, retinal hemorrhage (RH), encephalopathy, and other neurological abnormalities [4, 5]. Skeletal injuries, such as vertebral fractures and rib fractures, may also be associated with SBS [4].

The primary concern surrounding AHT is being able to correctly and consistently identify cases of abuse to protect the infant from further injury, and prosecute the perpetrator. The challenge in doing this, however, is that no testimony can be obtained from the victim and there are often no objective witnesses to the abusive act. Evidence is limited to the comparison of the injuries sustained by the victim to the description of the event by the person in charge of the infant's care. There is an obvious conflict of interest from the provided testimony of the caretaker as they may also be the perpetrator. A very strong understanding of the etiology of the injuries associated with AHT is necessary to

correctly identify cases of abuse.

The largest controversy related to AHT is whether or not shaking alone, as described in SBS, can cause severe head trauma in children. Some of the earliest observations of SBS were in the 1960s with Kempe's *The Battered-Child Syndrome* paper where they began to discuss how cases of abuse could be identified [6]. In the 1970s, Caffey and others began attributing shaking as the cause of injuries seen in abused infants based on the testimonies surrounding the abuse [7]. In 1987, Duhaime ran a series of biomechanical experiments with an instrumented infant surrogate doll. The surrogate was shaken and then struck against multiple surfaces [4]. The angular accelerations and angular velocities obtained from the surrogate were compared to scaled angular accelerations and velocities which caused concussion, subdural hematoma (SDH), and diffuse axonal injury (DAI) in adult primates [8]. Brain mass was the only factor used to scale the primate angular accelerations, velocities, and thresholds to the human infant. The angular accelerations and velocities measured by Duhaime were about 8 times lower than any of the scaled injury thresholds established in the adult primate studies. This comparison spurred the controversy surrounding the biomechanics involved with SBS.

Proving or disproving that shaking can cause severe injury is challenging. Clinicians can perform prospective or retrospective studies involving cases of suspected abuse, but conclusions regarding correlations of shaking and injury are only as valid as the testimonies given surrounding the incident. Instrumented anthropometric surrogate dolls can evaluate the kinematics surrounding a shaking event, but offer no insight into the prediction of injury [4, 9]. Furthermore, the validity of the kinematics is contingent

on matching material properties of the surrogate to that of a human infant. Animal models are potentially the most promising method to directly relate shaking to injury, but translating findings across species may be challenging and require large animal models. To date, all animal models investigating shaking have failed to reproduce exactly the types and severities of injuries associated with AHT, especially with respect to intracranial hemorrhage [10, 11, 12, 13, 14, 15].

Ocular hemorrhage, specifically RH, is an especially interesting aspect of AHT because it has been reported to occur in 53- 80% of suspected AHT cases [4, 16]. RH also has been reported in accidental head trauma, but only in approximately 10% of accidental cases [16, 17, 18, 19]. Bilateral RH, in particular, is much more likely to occur in AHT with a 40-100% occurrence versus only 1.5% reported in accidental injuries [16]. RH associated with AHT is typically widespread, covering 19.2-73.2% of the retina vs. 1.13-3.33% in accidental head trauma. RH is sometimes criticized as an identifier of AHT because RH can occur in as many as 37% of natural childbirths. These RH typically resolve within 6-9 days after birth [16].

Even though RH is thought to be one of the key identifiers of AHT, the mechanisms of RH are not entirely understood. Several theories exist to explain RH as it pertains to AHT. One theory postulates that collagen fibers from the vitreous extend into the retina and create traction on the retina during shaking, causing disruption of the retinal vasculature [20]. Another theory suggests that during shaking, there could be rapid changes in IOP, resulting in hemorrhages that are similar in appearance to those seen in ocular decompression retinopathy (ODR). One final theory, that has not been proposed in the literature, but will be addressed in this thesis, is that shaking results in

compression of the optic nerve, causing temporary but repetitive vein occlusions. Central retinal vein occlusion (CRVO) produces RH with descriptions similar to what has been reported in AHT (i.e. vitreal hemorrhaging, diffuse and flame shaped RH, retinal detachment) [4, 16, 21, 22].

For the past 40 years, little progress has been made to help differentiate abusive and accidental trauma in infants. This has resulted in not only costs to the physical and emotional well-being of children, but also to society as a whole. AHT is thought to occur in 30 out of 100,000 infants [23]. Several studies have found the average hospital bill from AHT to be anywhere from $18,000-$70,000. When you add in all the nonmedical costs (court fees, protective services, etc.), the average cost per child is between $790,000-$1,000,000 [2, 24]. The overall objective of this thesis is to increase our knowledge of mechanisms of injury associated with AHT, and to provide clinicians and law enforcement with data that may improve identification of AHT.

1.2 Thesis Overview

1.2.1 Chapter 2

Several animal models have attempted to simulate SBS without success. One of the reasons may be that the anesthetized animals do not accurately portray the physiological state of an infant just before shaking. In Chapter 2 *in vivo* experiments, on 3-5-day-old female piglets, are performed to test the hypothesis that the physiological effects of crying play a role in AHT. Crying is represented with increased intracranial pressure (ICP) and cerebral blood volume (CBV). A newly developed shaking device is used to mimic the theorized angular velocities, accelerations, and frequencies associated

with shaking. Axonal injury and intracranial hemorrhage will be compared between shaking only and shaking with increased ICP and CBV.

1.2.2 Chapter 3

In Chapter 3, we explore the potential of the piglet as a model for widespread RH. To do this, CRVOs were created in a newborn (3-5-day-old) piglet model. The chapter describes multiple methods and tools used to create the occlusion, and evaluates how those methods and results relate to RH in AHT.

1.2.3 Chapter 4

In Chapter 4, we evaluate sudden changes in IOP as a mechanism for RH. Changes in IOP were caused by an instrumented custom indentation device which allowed for controlled and repeatable test metrics. The results are discussed in relation to the mechanics of the ocular response and injury during AHT.

CHAPTER 2

THE PHYSIOLOGICAL EFFECTS OF CRYING AS AN ADDITIONAL INJURY MECHANISM OF THE BRAIN AND EYE IN A PIGLET SHAKING MODEL

2.1 Introduction

Traumatic brain injury (TBI) is one of the leading causes of hospitalization among children [1]. Pediatric TBI can lead to long-term neurological, behavioral, and cognitive problems, cortical blindness, as well as death. Abusive head trauma (AHT), or non-accidental head injury (NAHI), and infant shaking are some of the least understood forms of pediatric TBI. Common signs of AHT include retinal hemorrhage, diffuse axonal injury, subdural and subarachnoid hematoma, and skull fracture in the absence of a history of trauma. Shaken baby syndrome (SBS) is a subset of AHT that presents with the above intracranial injuries but with the absences of any clinical signs of head impact (e.g. skull fracture, bruising, soft tissue swelling). Some of the controversy surrounding infant shaking is due in large part to the inability of biomechanical researchers to be able to recreate the injuries commonly reported in SBS. This research is heavily reliant on biomechanical descriptions of the AHT events. Unfortunately, the history and biomechanical details in a suspected shaking incident are largely obtained from

confessions of perpetrators, which is subject to accuracy concerns.

Instead, studies have been performed using anthropomorphic dolls to recreate potential abusive events and determine approximate values for shaking frequency, and the angular velocity and acceleration of the head. The frequency of shaking in these studies has been reported to be 1.4-3 Hz [4, 9]. Peak to peak angular velocity has been reported to be between 50-60 rad/s [4, 9, 25]. The maximum angular acceleration was found to be 1138 [4], 2640 [9], and as high as 8693 rad/s^2 [25] although this high acceleration was generated by purposefully constructing the surrogate from the materials that would result in the highest accelerations by allowing impact between the head and torso.

The accuracy of these kinematic predictions in representing a true infant response is influenced by the mass distribution of the surrogate, the materials used to create the surrogate, and the methods used to represent joints in the surrogate. For example, a neck constructed out of a vertically coiled spring would allow movement in the anterior-posterior plane as well as the medial-lateral plane. Such a neck would also resist the applied forces in proportion to its spring constant. A neck made of one hinge would only allow movement in the anterior-posterior plane and would resist motion in proportion to its coefficients of friction. The effect of this type of change on kinematic predictions can be seen by the large range of values reported above for angular acceleration. In addition to surrogate construction, the method of shaking can also influence the kinematic results [25].

Surrogates are limited to kinematic predictions and cannot identify the types and amounts of injury that would be associated with shaking events. Therefore, the only

methods for studying injury from AHT are clinical studies, or animal studies. In clinical studies, the admissions concerning the shaking events are subject to uncertainty. Therefore, several groups have selected animal models to investigate the effect of repetitive head rotation similar to shaking. Two papers by Bonnier describe a mouse model used to investigate shaking [13, 14]. Animals in these studies were subjected to a 15 Hz shaking episode for 15 s. The shaking was induced mechanically using a "horizontally rotating shaker". No measurements of the kinematics were reported beyond the frequency. It should be noted that the frequency is five times higher than values reported in surrogate studies in the literature. The mice were shaken at 8 days after birth and then euthanized at different time points for histology. Microscopic retinal hemorrhage was found in about a third of the shaken animals. Animals which were shaken had an increase in white matter cell death. 27% of the animals in the longest survival group, of 31 days, died spontaneously between days 27 and 31 [14].

In three papers by, Finnie et al. 7-10-day-old lambs were manually shaken by the researchers 10 times for 30 seconds each time over the course of 30 minutes [10, 11, 12]. It was shown that axonal injury was only present in shaken animals vs. control animals. Neuronal injury was much higher in the shaken vs. control. Very little macroscopic hemorrhage was discovered. Several of the smaller animals died [11], but the deaths could be attributed to other causes, such as complications with anesthesia, and were not necessarily directly related to the shaking. In their most recent paper [10], the group described how only shaken animals had evidence of c-Fos, which has been associated with the identification of mild TBI [26]. Lacking from these studies was a repeatable method to apply shaking to the animals, as well as recording the kinematics involved in

the shaking. It is unclear if the number of shaking sequences and the duration over which the animals were shaken relates to real-world situations. It is known, however, that it is not uncommon for infants to be shaken more than once during a single event or during the course of several months [27]. It is acknowledged that recreating a real-world event of this nature can be very difficult due to the lack of information surrounding the events.

Coats et al. [15] performed experiments to determine if the repetitive nature of shaking affects injury. A mechanical device was developed to match the 3 Hz frequency found in the literature [9]. Shaking was performed on 3-5-day-old piglets with peak to peak angular velocities close to 30 rad/s. Single (noncyclic) head rotations were performed at similar angular velocities to the shaking. The duration of shaking (10 seconds vs. 30 seconds), and number of shaking episodes (continuous for 30 seconds vs. six 5-second shakes) were varied and compared to the single head rotation. Extra-axial hemorrhage, axonal injury, and ocular hemorrhage were used as injury metrics. They determined that the slight change in the duration of shaking did not significantly affect injury, but that the cyclic head rotations produced slightly more injury than the single head rotation. Despite some interesting findings, none of these studies were able to produce injuries at the severities typically thought to occur clinically. One potential reason for this may be the anesthetized relaxed state of the animal prior to shaking compared to the potential intense crying state of the infant prior to AHT. Crying is one of the primary triggers of AHT [28, 29]. During intense crying, intracranial pressure (ICP) increases 15 to 20 mmHg and cerebral blood volume (CBV) increases to 18% CBV from when not crying [30]. Crying alone is not known to cause severe brain injury or death. But, the increase in CBV and ICP could cause a compressive preload to the brain

which, when coupled with a repetitive head rotation, could lead to more injury than shaking alone.

The objective of this study was to test the hypothesis that increased levels of ICP and CBV resulted in more severe brain injury following a repetitive head rotation compared to shaking alone. A 3-5-day-old piglet model was chosen to evaluate the hypothesis because of the similarities in brain structure development and the use of the species in other head trauma research [31, 32, 33, 34]. A test method was devised to increase the ICP and CBV prior to and during a repetitive head motion. Axonal injury (AI) was used as the primary measure of head injury and was evaluated by staining for β-APP [35]. Completion of these studies may elucidate why animal models to date have not been able to reproduce injuries associated with shaking in infants.

2.2 Methods

To identify the effect of increased ICP and CBV on pediatric head trauma, 3-5-day-old piglets were place into one of four groups. Group 1 (n=5) experienced only an increase in ICP and CBV. This group was heavily instrumented as it was used to develop the procedures for increasing ICP and CBV throughout the study. Group 2 (n=5) experienced cyclic head rotations only. Group 3 (n=6) experienced a combination of increased ICP/CBV and cyclic head rotations. Group 4 (n=2) was a sham group that experienced everything in Group 3, except no head rotation was administered. This group was added because ICP in the animals in Group 3 was not able to be measured due to the invasive method used to measure ICP in Group 1, and may provide a more direct comparison to Group 3. All animals were cared for according to USDA standards and in

accordance with IACUC regulations. A special feeding system (Appendix A.1) was developed to ensure that all animals had a continuous supply of food and water throughout their care.

2.2.1 Group 1: ICP and CBV Protocol Development

Group 1 animals were anesthetized via nose cone with 5% isoflurane. After intubation, animals were maintained on 1-3% isoflurane. The head of the animal was shaved and a 1.5" incision was made above the mid-frontal bone. The scalp was reflected back to expose the skull. Using a hand drill, a 4.2 mm hole was carefully drilled through the skull, but stopped before the dura was punctured. The hole was located approximately 5 mm anterior to the coronal suture and 3 mm to the right of the sagittal suture. An injection port was inserted into the hole and adhered to the skull using dental cement (Ultradent UltraCem, South Jordan, UT). A small hole through the dura and arachnoid was made using a 20 gage needle. A blunted 20 gage needle was then inserted through the injection port to act as a guide and support structure for the fiber optic pressure transducer (Samba Preclin 420 LP, Gothenburg, Sweden). The pressure transducer was inserted through the blunted needle and into the sub-arachnoid space. Near infrared spectroscopy (NIRS) probes (Hamamatsu Niro-200NX, Middlesex, NJ) were placed onto the scalp approximately 1 inch posterior to the incision site and held in place with surgical tape. The NIRS probes report a normalized tissue hemoglobin index (nTHI) which is a normalized measure of the change in total hemoglobin in the animal. This was used to determine of the change in CBV from baseline. The intracranial pressure and NIRS data were monitored in real time and collected on a Dell laptop

(Latitude E6410, Round Rock, TX) at 1000 Hz (National Instruments NI 9201, Austin, TX).

A blood pressure cuff was wrapped around the abdominothorax of the animals and pressurized at different intervals and sequences to increase the ICP and CBV. This method has been previously used by Ratjen [36] to cause an increase in ICP in lambs. The exact pressurization protocol was determined by varying the amount of cuff pressure, the duration of the cuff pressure, and the order in which abdominothoracic pressurizations were applied. The final pressurization sequence resulted in an overall increase of ICP by 15-20 mmHg and increase in CBV by 12-18% from baseline (Figure 1). The exact sequence is as follows:

1. Wrap the cuff around the animal
2. Increase cuff pressure to 20 mmHg
3. Hold cuff pressure for 10 sec
4. Increase the pressure by 10 mmHg
5. Repeat steps 3 and 4 until 50 mmHg is reached
6. Hold cuff pressure for 10 sec
7. Release cuff pressure for 30 sec
8. Repeat the above steps 9 times.

2.2.2 Group 2: Repetitive Head Rotation

2.2.2.1 Head Rotation Device

A custom head rotation device was constructed to apply nonimpact repetitive back and forth head rotations to the piglet model (Figure 2A). An electric motor (Marathon Electric Motors, Wausau, WI) with a controller (Fuji Electric Systems, Edison, NJ) was fitted with a slotted eccentric cam attached to the drive shaft. As the drive shaft rotates the cam, the linkage arms raise up and down following the path of the slotted cam. The linkage arms travel in a slot on the rotation arms which rotate the head

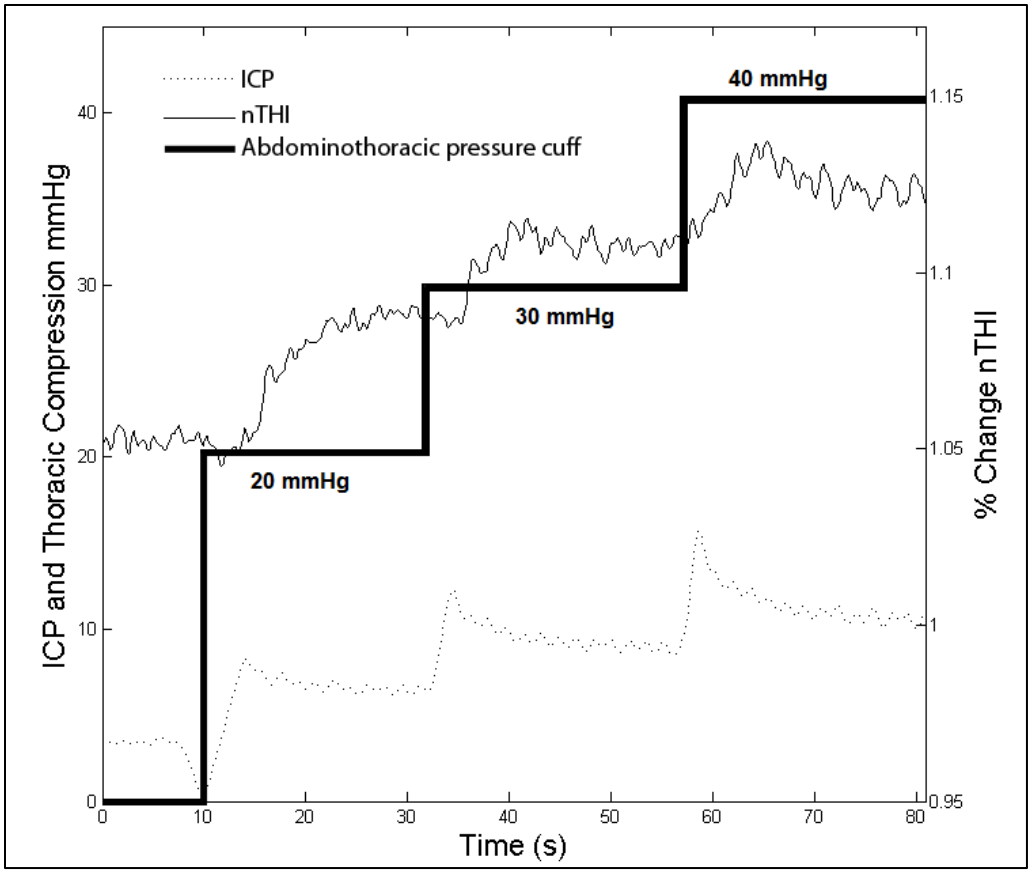

Figure 1: Example of a representative plot of ICP and nTHI with the compression cuff stepping sequence superimposed on top. Not shown is the 50 mmHg step.

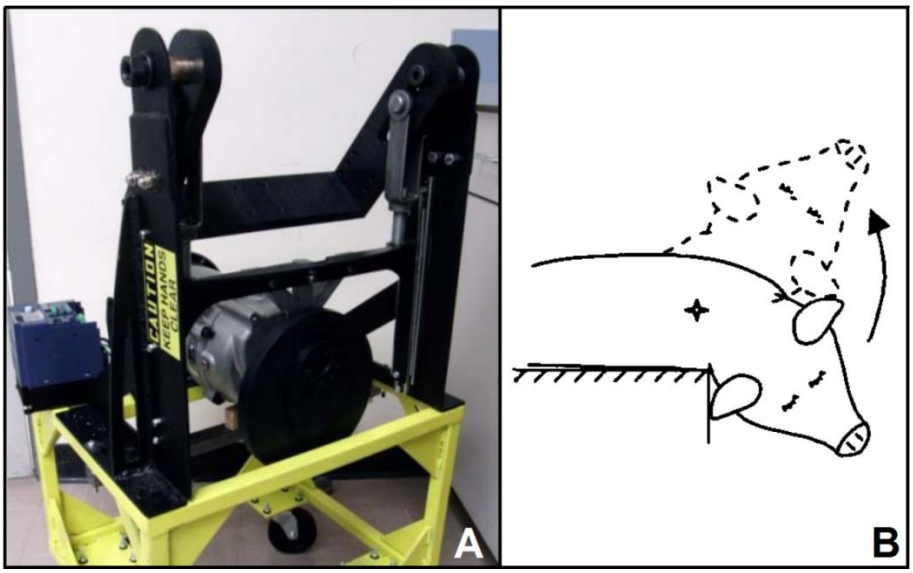

Figure 2: Image of the head rotation device. (A) schematic of piglet head motion (B) adapted from Eucker [37].

mounting assembly. The frequency of the cyclic rotations was adjusted with the motor controller. An angular velocity (DTS ARS 8K, Seal Beach, CA) sensor was attached to the rotation arms and the data collected at 1000 Hz.

2.2.2.2 Head Rotation Protocol

The animals in Group 2 were anesthetized as described in Group 1. Lying in the prone position, a bite plate was inserted in the mouth of the animal. Padded straps were used to firmly hold the animal to the bite plate. The animal was then rotated onto its side and the bite plate was bolted to the rotation arms (Figure 2B). This positioning resulted in a horizontal rotation of the head. The animal's head was slowly rotated through the entire range of motion (-50° to 50°) to ensure the center of rotation was approximately located in line with the C2 vertebrae. Once the center of rotation was verified, the cyclic device was initiated. The animal's head rotated back and forth at approximately 2.5-3 Hz for 20 seconds. Upon completion, the animal was removed from the device and returned to the animal care facility for recovery and monitoring.

2.2.3 Group 3: Combined Head Rotation and Increased ICP/CBV

Animals were anesthetized as described in Group 1. The hair on the head of the animal was shaved and the NIRS probes attached using surgical tape. ICP measurements were not made in Group 3 due to the invasive measurement method. Animals were attached to the head rotation device in the exact same manner as Group 2. Upon verification that the center of rotation was approximately located on the C2 vertebrae, the protocol to increase the ICP and CBV developed in Group 1 was implemented. During

the final step of the ICP/CBV protocol, the cuff pressure was held at 30 mmHg and the cyclic head rotation device was activated for 20 seconds. After the head rotation, cuff pressure was released and the animal was removed from the device. The animal was returned to the animal care facility as in Group 2.

2.2.4 Group 4-Increased ICP/CBV Shams

There was some concern that the animals in Group 1 might have had slightly lower ICP than those in Group 3 because of the hole drilled through the skull for the pressure transducer placement in Group 1. Therefore, Group 4 acted as a sham group for Group 3. Animals (n=2) were anesthetized in the same manner as previously described and attached to the bite plate of the head rotation device. NIRS probes were attached to the skull. The abdominothoracic protocol was administered as in Groups 1 and 3. After the final step of the compression protocol, the cuff pressure was increased to 30 mmHg and held for 20 seconds, but no cyclic head rotation was applied. The animals were then allowed to wake and recover as in the previous groups.

2.2.5 Post Procedure

Group 1 animals were euthanized immediately following the procedure. Animals in Groups 2-4 were euthanized 24 hours after completion of the procedure. All animals were perfusion fixed with 10% formalin. The brain and eyes were removed and stored in 10% formalin, and a 1%/1.25% formaldehyde glutaraldehyde mixture, respectively. After at least a week, the brains were switched to a PBS solution.

2.3 Data Analysis

2.3.1 Axonal Injury (AI)

AI was used as the primary measure of brain injury. Each fixed brain was cut into 3 mm slices using a custom brain mold (Figure 3). Slices were photographed with a high resolution digital color camera (Nikon D-3000, Melville, NY), and the digital images were turned into a pdf for the neuropathologist to use as an injury identification sheet. The pathologist circled regions on the digital image of each slice of brain which correlated to regions of the brain that stained positive for ß-APP on the microscopic slides. The total pixel area of each brain slice was determined using Photoshop and the total pixel volume of the brain was calculated by summing the areas of each slice in a brain. A total pixel volume of AI was defined as the sum of all the regions circled by the pathologist across all slices of the brain. The final percentage of AI in the brain was calculated as the total volume of AI divided by the total volume of the brain.

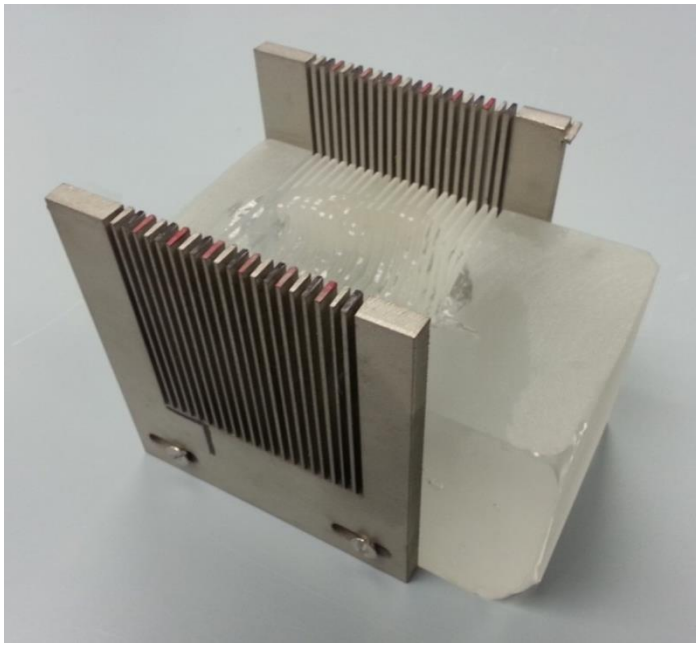

Figure 3: Brain matrix used to slice 3-5-day-old piglet brains into 3 mm slices.

2.3.2 Ocular Hemorrhage

The eyes were examined both macroscopically at removal and microscopically after H & E staining for hemorrhage. The macroscopic hemorrhage was determined as a binary value; either the animal had macroscopic hemorrhage or it did not. The animals with microscopic hemorrhage were identified using a CX41 brightfield microscope (Olympus Center Valley, PA). The presence and type of hemorrhage (i.e. extraocular, ciliary body, retinal, scleral, etc.) for each eye was noted.

2.3.3 Cyclic Head Rotation Kinematics

The collected angular velocity data were filtered using an algorithm to determine the optimum cutoff frequency for a 4^{th} order digital Butterworth filter [38]. Infinite impulse response (IIR) Butterworth filters are known to cause linear phase shifts in data. To overcome this, the data were first filtered using a 2^{nd} order Butterworth filter. The data were then inverted and filtered again with the same filter. This resulted in a 4^{th} order filter and removed the phase shift. After filtering, the angular velocity data were numerically integrated to obtain the angular displacement, and then numerically differentiated to obtain the angular acceleration. See Appendix A.2 for the MATLAB code.

2.2.3.1 Angular Displacement

A semi-automated peak finding algorithm was created in MATLAB (see Appendix A.2). The user designated the size of a boundary region within which the algorithm searched for either the maximum or minimum value. Using the plotted data, the user picked the approximate peak or valley they wished to find and that location

would become the center of the boundary region the algorithm used to find the peak or valley. The valleys were subtracted from the peaks to obtain the overall angular excursion. All peaks and valleys were selected over the steady state portion of the data and the mean and standard deviation were reported for each animal.

2.2.3.2 Frequency

The shaking frequency was calculated by using the peaks from the angular displacements. The frequency was calculated by dividing the total number of peaks by the elapsed time from the first peak chosen until the final peak chosen.

2.2.3.3 Angular Velocity

The peak finding algorithm was used to find the peaks and valleys of the angular velocity data. The valley was subtracted from the peaks to define peak to peak velocities throughout the steady-state region. The mean and standard deviation of the peak to peak velocity for each animal was reported.

2.2.3.4 Angular Acceleration

The peak finding algorithm was used to find the peaks and valleys of the angular acceleration data. The mean of the peaks was compared to the inverse of the mean of the valleys, and the larger of the two was reported.

2.4 Results

2.4.1 Test Metrics

The mean increase and standard deviation of ICP in Group 1 and nTHI in Groups 1, 3, and 4 is shown in Table 1. The nTHI data in Group 4 was determined to be unstable due to poor attachment of the NIRS probes. Only a partial nTHI data set was available for this group. Thus, the reported 0.2% increase is representative for only the final 4 compressions of the sequence.

The mean and standard deviation of the applied peak to peak angular velocities, maximum angular accelerations, peak to peak angular displacements, and angular frequencies from Groups 2 and 3 are also reported in Table 1. There were no significant differences between groups, suggesting that all kinematic loading was equivalent between the groups. Characteristic plots of the angular displacement, angular velocity, and angular acceleration are shown in Figure 4.

2.4.2 Macroscopic Brain Injury

No subdural or subarachnoid hemorrhages were seen in any of the groups. Of interest was a large thrombosis in the transverse sinus at the top of the cerebellum for two

Table 1: Test metrics from all 4 groups.

Group	Peak to Peak Angular Displacement (std) deg.	Peak to Peak Angular Velocity (std) rad s^{-1}	Average Angular Acceleration (std) rad^{-2}	Rotation Frequency (std) Hz	nTHI (std) %	ICP (std) mmHg
Group 1	-	-	-	-	14.9 (5.98)	23.5 (16.4)
Group 2	119.6 (5.2)	45.8 (0.7)	1731 (324)	2.84 (0.23)	-	-
Group 3	122.6 (2.2)	45.3 (2.2)	1908 (246)	2.74 (0.02)	8.32 (4.14)	-
Group 4	-	-	-	-	0.2 (**)	-

– Metric was not available for the corresponding test group.
** Lack of data to complete a standard deviation.

of the Group 3 animals (Figure 5).

2.4.3 Microscopic Brain Injury

Axonal injury was found in all four groups (Figure 6) and was located primarily in areas surrounding the thalamus. The combined cyclic and increased ICP/CBV group (Group 3) demonstrated the most AI followed by the ICP/CBV sham group (Group 4). The cyclic rotation only group and the ICP/CBV only group (Groups 2 and 1, respectively) had the least amount of AI. Large variability among the animals precluded any significant differences among the means. A chi square analysis was performed to identify significant effects in the incidence of AI (as several animals had no injury), but no significance was seen. In Group 3 (combined cyclic with ICP/CBV), there appeared to be a correlation between AI with the % increase of CBV (as determined by the nTHI measurement, Figure 7) though the correlation coefficient was 0.60, R^2 value was 0.36, and p=0.21. Group 1 (ICP/CBV only) did not exhibit a similar effect.

2.4.4 Macroscopic and Microscopic Ocular Hemorrhage

Large macroscopic extra ocular hemorrhage was found only in Group 3, upon removal of the eyes from the head (Figure 8A). Similar to axonal injury, microscopic hemorrhage occurred in all groups (Figure 9) but the amount and type of hemorrhage varied. In Group 1 (increased ICP/CBV), 2 of the 3 animals had hemorrhage, one with an extraocular, the other an intradural. In Group 2 (cyclic only), 2 of the 5 animals had extraocular hemorrhage, and 1 of those animals also had an intradural hemorrhage. Group 3 (combined cyclic and increased ICP/CBV) showed the highest number of

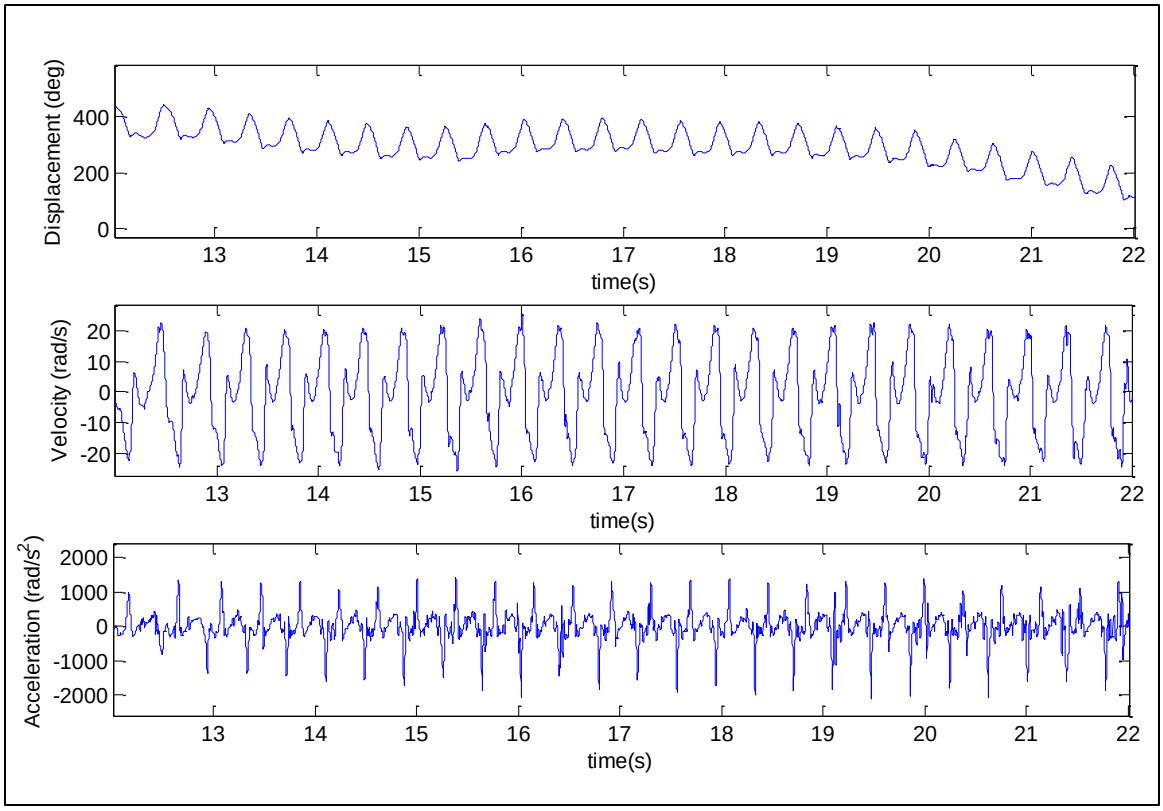

Figure 4: Representative angular displacement, velocity, and acceleration traces from the cyclic head rotation applied to Groups 2 & 3.

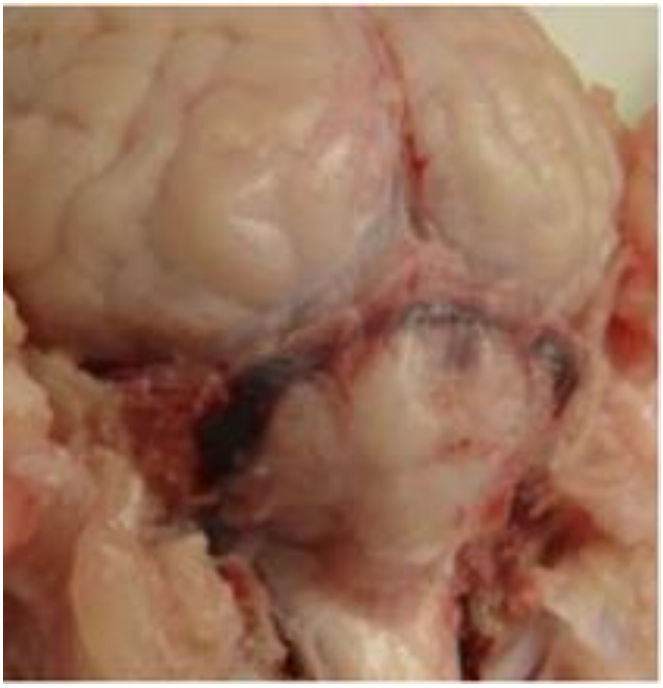

Figure 5: Image of the thrombus above the cerebellum prior to removal of the dura.

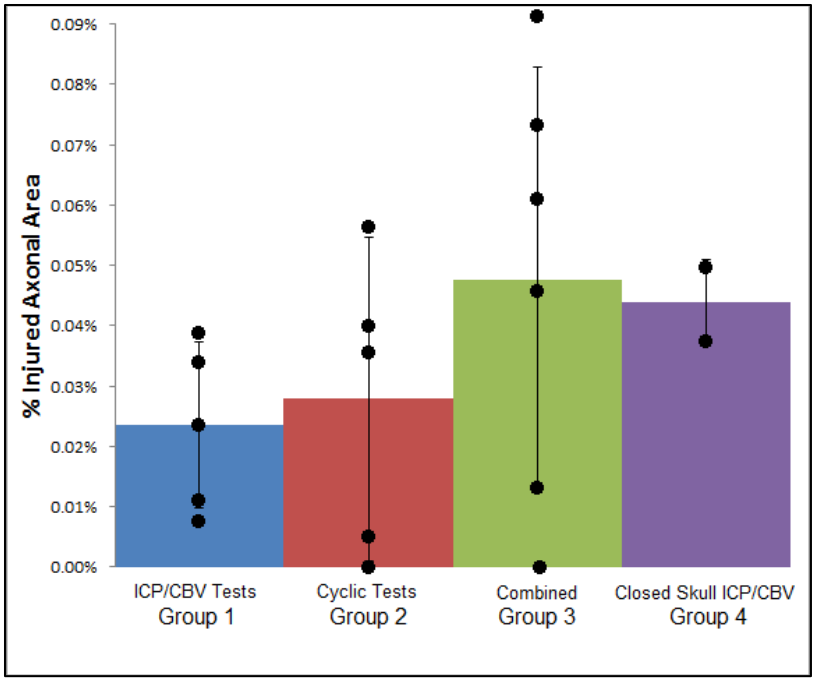

Figure 6: Axonal injury by group. Error bars show one standard deviation. Dots indicate injury from individual animals.

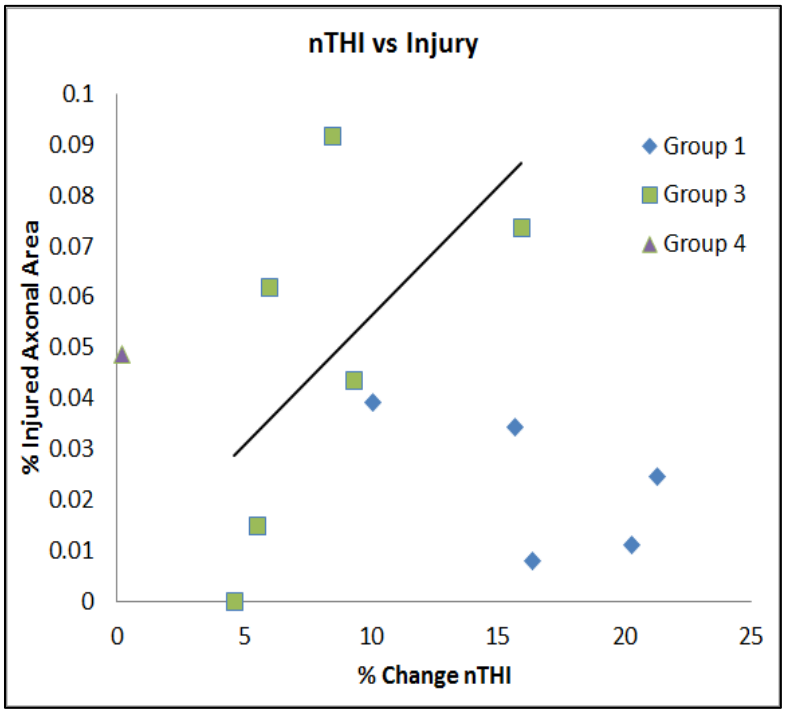

Figure 7: Percent change in nTHI by group vs. AI. nTHI appears to have a random effect within Group 1, but AI appears to increase with the increase of nTHI in the presence of a cyclic load.

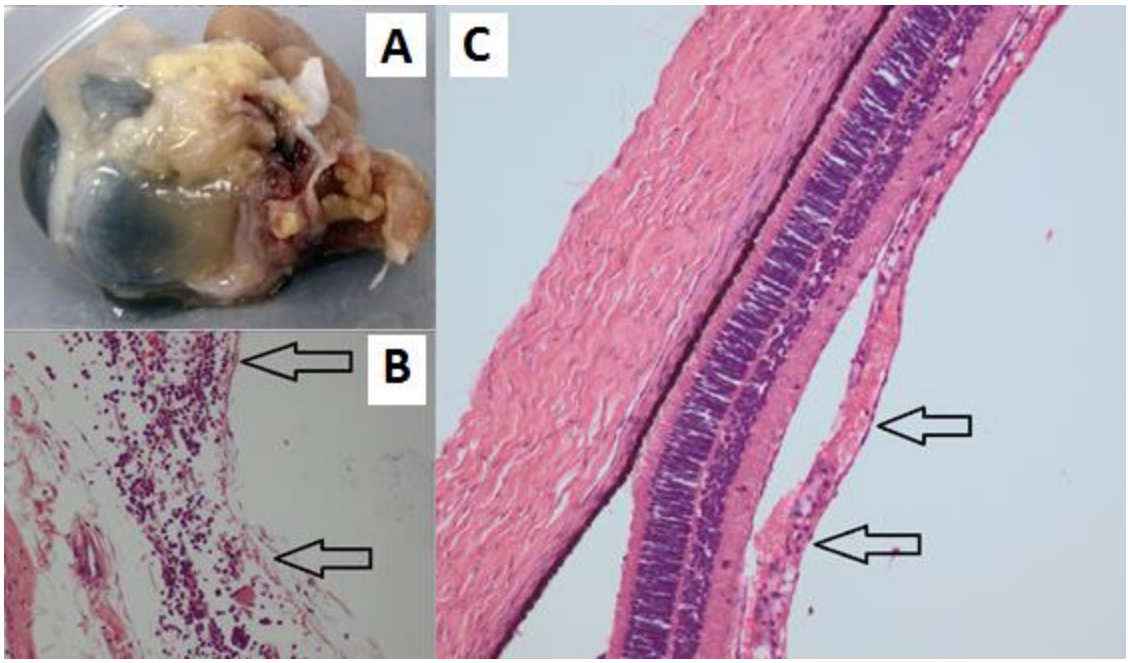

Figure 8: Extraocular hemorrhage on the optic nerve sheath (A), macroscopic extraocular hemorrhage (B), and retinal hemorrhage from Group 3 animals (C).

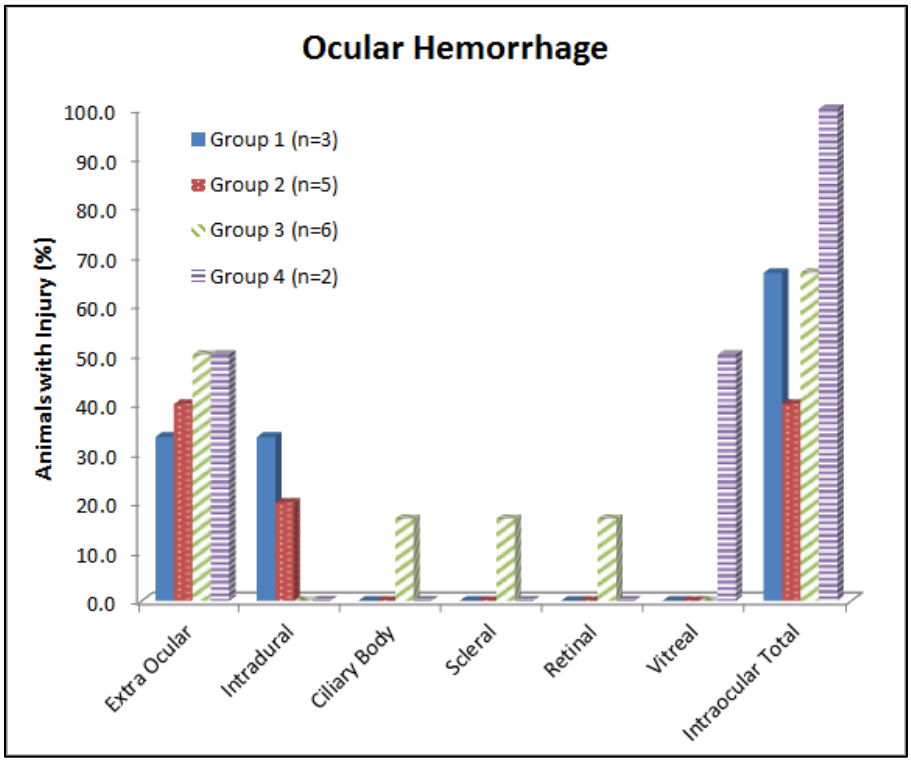

Figure 9: Ocular hemorrhage by group. The group total represents the total percentage of animals in each group with ocular hemorrhage.

incidences of microscopic hemorrhage and was the only group to present with a retinal hemorrhage. Three of the 6 animals contained extraocular hemorrhage. One of those also had a scleral hemorrhage (Figure 8C) and another had the retinal hemorrhage. Lastly, one of the 6 Group 3 animals had a ciliary body hemorrhage. In Group 4, 1 of the 2 animals had a vitreal hemorrhage. The other animal had an extraocular hemorrhage.

2.5 Discussion

AHT is a very challenging topic to study. Many of the mechanisms of AHT are unknown and/or controversial, and the emotional, legal, and medical implications are immense. Doctors are often asked if injuries seen clinically correlate with the history offered by the caregivers. Shaking related injuries are probably the most difficult to understand and diagnose due to the small amount of empirical data on the subject. Biomechanical studies have not been able to replicate injuries from shaking, but the complexity of the kinematics and the lack of biomechanical data as to how infants are abused makes reenactment challenging. In this study, we investigated how injury from shaking was influenced by increased ICP/CBV. We found that the combined effects of increased ICP/CBV and shaking led to the most diverse and highest amounts of injury in our study. However, none of the injuries seen compare, in terms of amount and severity, to what is seen clinically.

2.5.1 Macroscopic Brain Injury

There was no evidence of SDH or SAH in any of the animals. The cause of the thrombus seen in the transverse sinus above the cerebellum (Figure 5) is unclear. After

discussing the test sequence with a pediatric radiologist that specializes in AHT, it was postulated that there may have been excessive compression, due to a small hemorrhage or unknown force. This would have slowed the blood flow enough to cause the thrombus. However, there was no macroscopic evidence of hemorrhage near the thrombus and microscopy of the dural tissue has not been performed.

2.5.2 Axonal Injury

Interestingly AI was present in all groups, even within the sham group, but was limited in its scope to regions surrounding the thalamus vs. the diffuse AI seen clinically. This could be partly in response to using ß-APP as the identifier for injury. ß-APP is a commonly recognized marker for many types of neurotrauma and disease [39].

The function of the amyloid precursor protein (APP) is unknown [40]. What is known is that APP is transported along axons and when the transport method is interrupted, an accumulation of ß-APP forms around the location of the disruption. This can be caused by an axon breaking, or being compressed enough to hinder functionality. ß-APP will accumulate even if the axon transport is only temporarily disrupted. It is thought that ß-APP can be present for some time after the disruption [41]. It is possible that the increased ICP in our study caused a compression on the axons and disrupted the axonal transport of APP, resulting in a positive staining for ß-APP in Groups 1 and 4 [41].

The fact that Group 3 had the most AI on average lends credibility to the hypothesis that the physiological effects of crying play a role in head injury. Interestingly, Group 4 (ICP/CBV sham) presented with the second highest AI. This

could be due to several reasons. The ICP in Group 4 was not measured and it is possible that ICP was actually greater than Group 1. It is also possible that the 2 animals are outliers which reacted more strongly in the production of ß-APP. With a higher sample size, the mean AI of that group could decrease. Regardless, the findings in this study suggest that increased ICP and CBV can cause axonal disruption. It is unknown, however, if this disruption is permanent or temporary.

Maximum ICP, maximum steady state ICP, maximum angular acceleration, average angular velocity, and frequency of shaking were all evaluated for a correlation to the presence of AI. None of these evaluated correlated except nTHI in the combined cyclic ICP/CBV group. It is not surprising that the kinematics did not correlate with AI because the variability in these parameters was designed to be too small.

2.5.3 Ocular Injury

Ocular injury was present in each of the groups. Group 1 and 4 had equal occurrence of injury as Group 3 but both had smaller sample sizes. Group 3 had a diverse array of hemorrhages and was the only group to have a retinal hemorrhage. No intraocular pressure (IOP) measurements were taken during these studies to determine if the method to increase ICP and CBV drastically increased the IOP of these animals. Currently there is a debate surrounding the correlation of IOP and ICP, with some groups reporting no correlation [42, 43], and some groups reporting a positive correlation [44, 45]. Regardless of the link between ICP and IOP, increased ICP has been reported to cause RH in the absence of trauma [46, 47, 48]. One study by Binenbaum et al. [48] measured the opening pressure (OP) from routine lumbar punctures in children (3-17

years) and evaluated their eyes for RH. RH was seen in 23.5% of the children with elevated OP (> 20.6 mmHg). RH was only found in the areas surrounding the optic nerve disc and not in the far periphery, as is typical of AHT. The hemorrhages seen in our study were microscopic and sparse, which is also atypical of hemorrhages associated with AHT [4, 16, 21, 22].

2.5.4 Kinematics

As seen in Table 1, the kinematics between groups are very similar. Shaking studies report peak to peak angular velocities of 50-60 rad/s, angular accelerations between 1100-2700, and shaking frequencies of around 3 Hz [4, 9, 25]. Because of the smaller mass of the piglet brain than that of an infant, a greater load needs to be applied to the piglet head to create similar brain deformations between species. Equations were developed by Holbourn [49] and Ommaya and Hirsch [50] which allow the scaling of angular velocity (Eq. 2.1) and acceleration (Eq. 2.2) by mass.

$$\dot{\Theta}_p = \dot{\Theta}_{in} \left(\frac{M_{in}}{M_p}\right)^{\frac{1}{3}} \quad \text{Eq. [2.1]}$$

$$\ddot{\Theta}_p = \ddot{\Theta}_{in} \left(\frac{M_{in}}{M_p}\right)^{\frac{2}{3}} \quad \text{Eq. [2.2]}$$

$\dot{\Theta}_p$ and $\ddot{\Theta}_p$ are the angular velocity and accelerations, respectively, of the piglet, $\dot{\Theta}_{in}$ and $\ddot{\Theta}_{in}$ are the angular velocity and acceleration, respectively, of the human infant. M_p and M_{in} are the masses of the piglet and human, respectively. These equations are intended

for use on objects of similar geometry with the same material properties. As a result, modifications to those equations were made to allow for differences in material properties [51].

$$\dot{\Theta}_p = \dot{\Theta}_{in} \left(\frac{M_{in}}{M_p}\right)^{\frac{1}{3}} * \left(\frac{G_p}{G_{in}}\right)^{\frac{1}{2}} \quad \text{Eq. [2.3]}$$

$$\ddot{\Theta}_p = \ddot{\Theta}_{in} \left(\frac{M_{in}}{M_p}\right)^{\frac{2}{3}} * \left(\frac{G_p}{G_{in}}\right) \quad \text{Eq. [2.4]}$$

G_p and G_{in} are the shear moduli of the piglet and human, respectively. Equations 2.3 and 2.4 then allow us to make comparisons between a human infant with a brain mass of approximately 400 g. [4] and a piglet with a brain mass of approximately 39 g. The shear modulus of the piglet is 529.9 Pa [52]. Shear modulus data are unavailable for the human infant and was scaled from adult human data. It was assumed that the ratio between human adult and infant shear moduli is similar to that of an adult pig and newborn, which was found to be 0.49 [52]. Therefore, the shear modulus of adult human (295.7 Pa) [52] was divided 0.49 and the infant a shear modulus was estimated to be 601.8 Pa.

Based on the inputs from the surrogate studies and the estimated material properties, the peak to peak angular velocity and peak acceleration that will produce similar brain deformation in a piglet as from shaking an infant is approximately 102-122 rad/s, and 4,572-11,223 rad/s^2, respectively. Due to the limited range of motion of the pig neck, the cyclic device was unable to generate the exact combination of frequencies, angular velocities, and angular accelerations that were desired. Therefore, the shaking

frequency was set to 3 Hz and the angular velocity and acceleration maximized by rotating the piglet head through its max angle of rotation without causing injury to the neck. It should be noted that 2 of the animals in Group 2 had shaking frequencies just above 3 Hz (3.09 and 3.07 Hz) and those 2 animals had the highest AI of all the animals in Group 2, 33% and 90% higher than the group average. The scaled peak to peak angular velocity was calculated to be 2.7 times higher than our obtained velocities. The scaled angular accelerations were calculated to be 2.6 times higher than our obtained accelerations. This could clearly have an impact on the amount of injury present for this study.

In addition to neck range of motion, another reason for not obtaining the desired velocity and acceleration could stem from the design of the device. Due to space and storage concerns, and the need to perform these studies in different surgical suites, the device needed to be mobile. During use, close to 110 lbs of weight was added to the device to stabilize the device and reduce bouncing. Even with the added weight, the entire device bounced as the animal was shaken. The device also used a single-sided eccentric cam to guide the rotation of the swing arms. During high frequency use, the guide pin slipped out of the guide path on the cam, scraping off portions of the cam. The peak values for velocity and acceleration were likely diminished due to the portion of time the swing arms were not being forced by the cam. One final downside of the cam system was that it was impossible to match both the frequency and angular velocity of the surrogate studies simultaneously. Increasing the angular velocity also increased the frequency.

One option is to replace the cam system with a rotation arm that is driven directly

by the motor. This would allow a nonsinusoidal input to drive the system. A path can be programmed to specify the frequency and peak to peak angular velocity independent of one another. Physical stops with adjustable springs can be used to obtain target peak kinematics.

Our study is similar to Coats et al. [15], but their AI percentage for a 30-second shaking duration is closer to double our Group 2 (cyclic only) AI injury and they report extra-axial hemorrhage in several animals. The 20-second cyclic duration in our study was shorter than the duration reported in Coats et al., but they report little to no difference in AI between a shaking duration of 10 seconds vs. 30 seconds. Their angular accelerations (~900 rad/s^2) and angular velocities (~28.1 rad/s) were lower than those reported in our study. The differences between injury levels could be differences between animals, or perhaps differences in breeding between animal suppliers.

The above discussion has been based on scaling between a human and porcine newborns via brain mass and brain material properties. If ocular injury was of greater interest than the brain, then it would be more appropriate to scale based on ocular mass and eye material properties. The eyes of an infant are similar in size and shape to the eyes of a piglet [53], so little scaling would be required. The material properties of the infant and piglet eye are largely unknown, so it is unknown how much scaling would be required to account for differences in deformation due differences in ocular material properties across species.

2.5.5 Intracranial Pressure

Any pressure differences due to volume change from the insertion of the transducer between Groups 1, 3, and 4 were assumed to be minimal. The total volume of CSF around the brain (not including any of the spinal CSF space) has been measured in a single animal in our lab to be around 1500-3000 mm^3. The volume of the 20 G needle with the fiber optic transducer cable inside was only around 5 mm^3. It is possible that the invasive method by which the ICP was measured (i.e. the puncturing of the dura to insert the pressure transducer) could lead to a lower intracranial pressure in Group 1 than in Groups 3 and 4. No CSF was seen around the injection port, or coming out of the needle. If CSF was leaking from the pressure port, we would expect a gradual decline in measured pressure. Instead, our data show an initial spike in pressure and then a reduction to a steady state pressure. This response is thought to be at least partially as a result of a stress relaxation of the tissues involved (i.e. brain, pia, arachnoid, and dura).

2.5.6 Normalized Tissue Hemoglobin Index

Normalized tissue hemoglobin index was used as the metric to monitor the change in CBV of the animals. nTHI was used by Ancora et al. to measure changes in CBV in infants, and by Brazy to quantify the change in CBV in infants during crying [30, 54]. This allows for a direct comparison to our study. Brazy found that nTHI increased 18% from baseline during intense infant crying. The nTHI values in our study were a little lower than this, but each animal responded slightly different. Excluding the Group 4 nTHI outlier, an ANOVA did show significance between Groups 1 and 3 ($p=0.0099$). This could simply be a result of poor adhesion of the NIRS probes to the skull of the

animal, as it is unlikely that simply puncturing the dura could affect CBV in such a manner.

The nTHI data were excluded for 1 of the Group 4 animals due to unrealistic interaction between the oxygenated (O_2Hb) and deoxygenated (HHb) hemoglobin. Physiologically, the total hemoglobin in the brain remains relatively constant [55, 56, 57, 58]. This means that O_2Hb and HHb typically respond opposite of each other (i.e. if one rises the other falls, Figure 10 A). In this study, the total hemoglobin will increase slightly in response to the abdominothoracic pressurization sequence applied in Groups 1, 3, and 4. Despite this increase, the O_2Hb and HHb should mostly mirror each other, with O_2Hb increasing slightly more than HHb decreased. In the excluded data set, O_2Hb and HHb mimicked each other. As one rose so did the other and these data traces were nearly identical. This led to very large changes in the total hemoglobin. The reason for this response is not entirely known. It is likely that there was a coupling of the signals during data acquisition.

The second animal in Group 4 also had inconsistencies in the nTHI data. A short period of drift occurred at the beginning of data collection because the tension and adhesion in the tape were not in equilibrium and the tape slipped slightly. Typically, once the sensor has settled, the NIRS is re-zeroed to reset the initial conditions. However, the second animal in Group 4 continued to drift for close to half of the test (~14 minutes). The probes did eventually reach equilibrium, but due to the skewed initial conditions, the NIRS calculated using the initial data as a baseline the nTHI continued to exhibit drift. To correct for the drift, a linear approximation of the drift was taken and the inverse of the approximation was added back onto the nTHI data. The nTHI data were

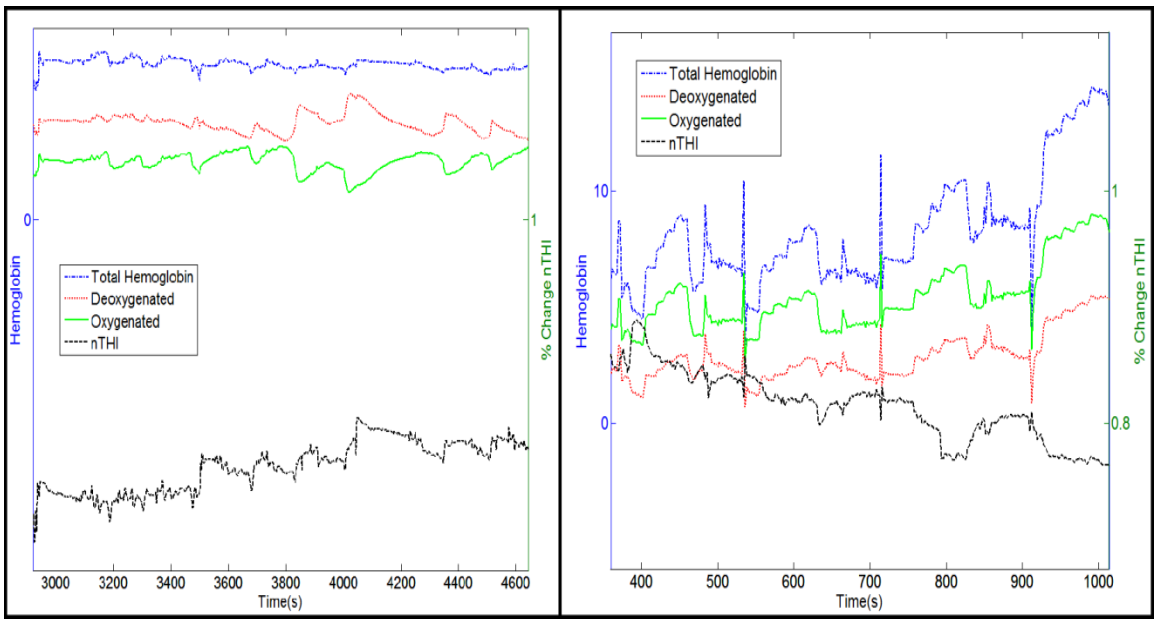

Figure 10: Comparison of normal and abnormal nTHI signals. (A) Representative plot of a typical O_2Hb and HHb relationship. (B) Plot of the atypical results of the excluded data set in Group 4.

only considered valid, however, for the region where the O_2Hb and HHb values were in equilibrium. This occurred after 5 compression sequences had been performed. There was a 0.2% increase in nTHI for the final four compressions, but it is unknown what the nTHI was for the entire sequence.

2.6 Conclusion

As a first study to investigate the effect of intense crying on head trauma, the results appear to be promising. Increased ICP/CBV with cyclic head rotation does result in greater amounts of AI. Macroscopic findings were present but the injuries seen still fall short of injuries seen clinically. Group 3 (increased ICP/CBV with cyclic head rotation) had more axonal injury than the other 3 groups, and had the most widely distributed ocular injury. An increase in the sample size of each group is needed to

determine if significance exists between groups. Higher angular velocities and accelerations are also needed to accurately represent kinematics of infant shaking.

2.7 Future Work

More work needs to be done to be able to definitively say that the physiological effects of crying (i.e. increased ICP/CBV) play an important role in AHT. A revision of the head rotation device should be made to increase the angular accelerations and velocities to scaled values from human infant surrogate studies. Upgrades to the cyclic device could include a closed loop control system, a more stable base to allow for higher prescribed accelerations and velocities, and a rotation arm directly controlled by a motor. The inclusion of physical stops would increase angular acceleration.

CHAPTER 3

CENTRAL RETINAL VEIN OCCLUSION IN THE PIGLET: A POTENTIAL MECHANISM OF RETINAL HEMORRHAGE IN CASES OF ABUSIVE HEAD TRAUMA

3.1 Introduction

As mentioned in the previous chapter, ocular hemorrhage is often associated with abusive head trauma (AHT). Retinal hemorrhage (RH) occurs in 53-80% in cases of suspected abuse and approximately 10% of accidental cases [16]. Even though there is a high occurrence of RH associated with abuse, the mechanisms which cause RH in cases of abuse is still unknown. A clearer understanding of these mechanisms may lead to better diagnostic tools for clinicians.

RH in AHT cases are typically described as diffuse or widespread, preretinal, flame shaped, and may be associated with vitreal hemorrhage and/or retinal detachment [4, 16, 21, 22]. Interestingly, vitreal hemorrhaging, diffuse and flame shaped RH, and retinal detachment have all been used to describe ocular injury associated with central retinal vein occlusion (CRVO) [59, 60]. Because of these similarities, it may be possible that the mechanisms that lead to RH due to CRVO are similar to those in AHT.

To evaluate mechanisms of RH, the newborn piglet was selected as a potential

animal model. The piglet model was selected because it is already a well-documented model for infant head injury, which is often associated with ocular hemorrhage in trauma [61]. Additionally, 3-5-day-old piglets have similar ocular mass and dimensions to a human infant, approximately 16.5 mm in diameter [62]. The piglet model has been shown previously to produce retinal hemorrhage when subjected to high velocity head rotation [63]. However, this hemorrhage was near the vitreous base and it is unknown if piglets can experience RH in the posterior pole that is widespread and may reach the periphery of the eye, as described clinically in AHT. Therefore, the two objectives of this study were to: 1) evaluate the piglet's ability to develop widespread RH, and 2) evaluate CRVO as a potential mechanism for RH in AHT.

3.2 Methods and Procedures

To evaluate the ability of the immature porcine model to develop diffuse RH, CRVO was experimentally induced in 3-5-day-old piglets (n=4). All testing was approved by the International Animal Care and Use Committee at the University of Pennsylvania. Animals were anaesthetized using 5% isoflurane, intubated, and maintained at 1-3% isoflurane throughout the duration of the study. Consciousness was determined by using a pinch tests, heart rate monitoring, and ocular response to touch. All animals were euthanized at the completion of the study without being allowed to awake from the anesthesia.

CRVO was created by carefully dissecting extraocular tissue to provide access to the optic nerve (ON). This included dissection of extraocular musculature and conjunctiva. Once a path to the ON was cleared, curved forceps were inserted behind the

eye until the clamping end was around the ON. The forceps were gently clamped on the ON to occlude the venous return from the eye while still allowing arterial blood to flow into the eye. This was verified via visual inspection of the retina by an ophthalmologist using an indirect ophthalmoscope. To create the CRVO in a systematic and repeatable manner, an instrumentation system was created that could mount to forceps and measure the clamping forces in real time. All surgical procedures were performed by an ophthalmologist; all data acquisition and analysis was performed by the author.

3.2.1 Instrumented Clamp Design

A custom mounting frame was designed into which the forceps could be mounted, without hindering their usage (Figure 11). Removable mounts were included in the design so that the entire assembly could be held in a magnetic base if long, stationary durations were required during the study. The mounting frame was instrumented with a 10 lb Futek (LSB200, Columbus, OH) load cell to measure clamping force at a sample rate of 300 Hz using a National Instruments (NI 9201, Austin, TX) data acquisition system, and recorded on a Dell laptop (Round Rock, TX). The forces measured by the load cell were measured at the handle end and not the tip. The clamping force at the tip was solved for based on static equilibrium equations and the geometry of the forceps. The tip clamping force was found to be approximately 4 times higher than the handle force, see Appendix B.1 for calculations. These calculations were validated by testing the entire clamping assembly with an Instron (5943, Norwood, MA) testing machine. From these tests, the measured tip clamping force was on average 3.89 times higher than the handle.

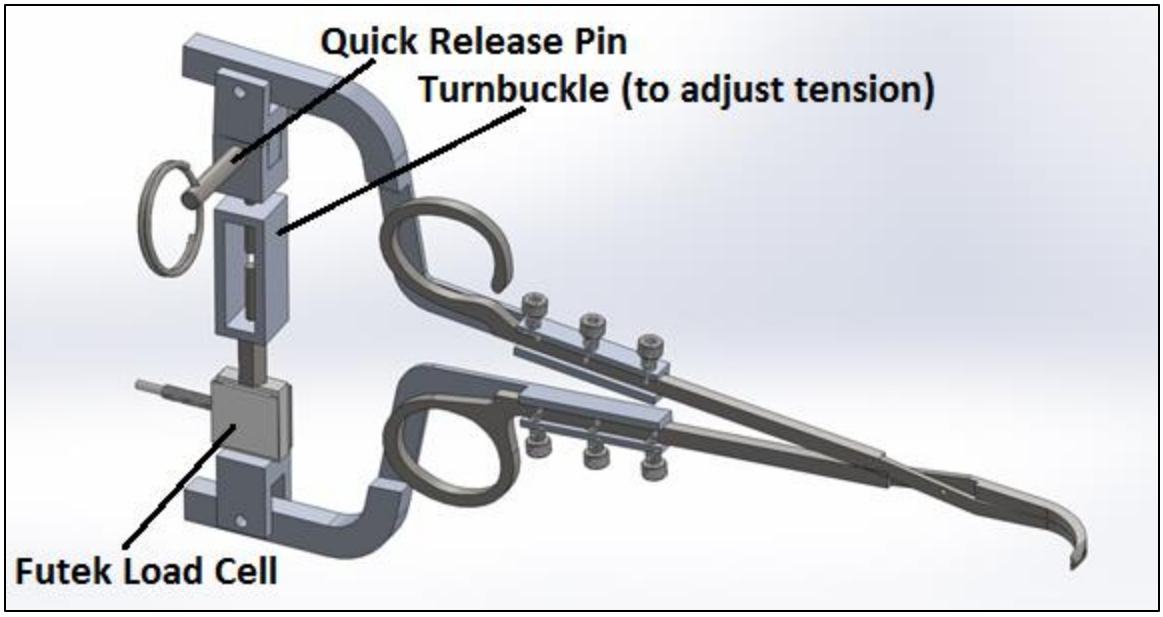

Figure 11: CAD drawing of the forceps within the mounting frame.

3.2.2 Test Protocol

In addition to evaluating the ability of our model to form RH, the second objective of our study was to evaluate whether RH could occur during shaking due to periodic kinking or occlusion of the ON. To investigate our objectives, three test groups were created: Group 1 (n=2 eyes) had only the ON clamped. Group 2 (n=5 eyes) received abdominothoracic compressions and the ON clamped. If no RH resulted in Group 2, the eyes were used to evaluate the effect of cyclic loading in Group 3 (n=2 eyes), which received abdominothoracic compressions and manual cyclic clamping.

A Tono-Pen Avia VET Veterinary Tonometer (Reichert Technologies, Depew, NY) was used to determine a baseline intraocular pressure (IOP) of each eye. Two drops of cyclopentolate 2% ophthalmic solution were then administered to the eye to dilate the pupil. Once dilated, the ophthalmologist inserted an eye speculum and examined the eye with an indirect video ophthalmoscope (Keeler, Vantage Plus LED Digital, Windsor,

UK) to verify the absence of any pre-existing hemorrhages or injuries. Digital video of the examinations was recorded on a Dell (Round Rock, TX) laptop.

3.2.2.1 Single Clamping

Using the instrumented surgical forceps, the ON was clamped and held in place between 1 and 10 minutes for Groups 1 and 2. The ophthalmologist used the indirect video ophthalmoscope to examine the eye during clamping and after the clamp was released. The first eye in Group 1 was used to determine appropriate clamping forces. In this eye, the ON was clamped at 0.4 lbs, 0.6 lbs and 0.9 lbs. Each subsequent eye was clamped to at least 0.9 lbs prior to examination. After the clamp was released, the eye was monitored every minute for up to 10 minutes for RH. The abdominothoracic compressions in Groups 2 and 3 were generated in the exact same manner as was described in Chapter 2 section 2.1.

3.2.2.2 Cyclic Clamping

If no hemorrhage was noted after the completion of the single clamp with increased ICP and CBV in Group 2, cyclic clamping was performed to simulate possible repetitive occlusion of the ON during shaking. To do this, the clamp was placed on the ON of the eye, clamped to 1 lb, and locked in place. The locking mechanism of the mounting fixture was designed to hold the forceps in a closed position with a specific clamping force. The locking mechanism contained a quick release pin that allowed the clamps to be quickly released and then reclamped with the same clamping distance. The clamp was removed from the ON of the eye using the quick release pin and the eye was

allowed to relax for 2 minutes. The forceps were then clamped and unclamped to the predetermined clamping distance in a cyclic pattern as quickly as possible for approximately 1 minute. Following cyclic clamping, the eye was monitored every minute up to 10 minutes for RH.

Following completion of the studies, all animals were perfusion fixed with 10% formalin. The brain and eyes were removed and stored in 10% formalin and 1%/1.25% formaldehyde glutaraldehyde mixture, respectively.

3.2.3 Data Analysis

To evaluate the potential of the piglet model to produce hemorrhage and better understand vascular changes associated with CRVO, the occurrence of RH and changes in retinal vessel diameter were tracked throughout the study. The maximum clamping force and number of clamping sequences were also recorded for each eye. Hemorrhage was determined as a binary value. If hemorrhage occurred at any point during the study, the eye was determined to have hemorrhage and the ophthalmologist provided a description of the hemorrhage (e.g. flame shaped, diffuse).

3.2.3.1 Vessel Diameter Quantification

The change in diameter of blood vessels in the major vascular arcade was quantified in all eyes before, during, and after clamping. Single image frames were extracted from the indirect video ophthalmoscope using video processing software (Avidemux 2.6). The first image in the set of images from each eye was defined as the reference state. Subsequent images were evaluated at multiple clamping states (e.g.

clamped, post-clamp). These images were labeled with a randomly assigned identifier to blind reviewers and avoid bias from measuring the images consecutively. Only one image was selected for each clamping state. The selected image was chosen based on the clarity of the vasculature in the image. The vessels were labeled alphabetically starting with the vessel closest to "noon" on the optic nerve disk (OND) and continuing clockwise until all measurable vessels were labeled (Figure 12).

Because indirect video ophthalmoscope is taken by using a handheld magnifying loupe, different magnifications occur during and between videos based on the position of the loupe. Therefore, the pixel lengths were not constant between images. To overcome this, the diameter of the OND was assumed to be constant throughout the study and image measurements were scaled by comparing the diameter of the OND in each image to that of the reference image. The scaling factor used to scale the images was defined as

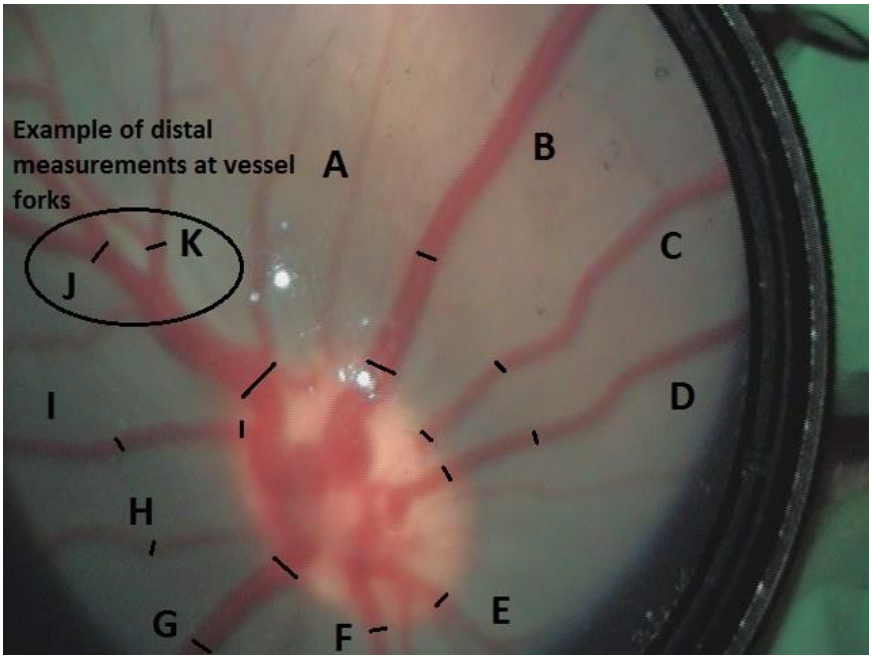

Figure 12: Example of a reference image from an eye. Each label indicates a vessel of the arcade evaluated for diameter changes during and after clamping. Example of the diameters measured (black lines) proximal and distal to the optic nerve.

the longest length of the OND in the reference image divided by the longest length of the OND in the current image. Each OND length was measured 4 times and the average was used for the scaling.

Vessel diameter measurements were taken proximal and distal to the OND. Proximal measurements were taken at the intersection of the vessel with the OND. Distal measurements were taken at very distinct landmarks, such as a fork in a vessel (Figure 12). These measurements were taken directly before the vessel began to widen as it approached the fork. In the absence of a distinct landmark, the distal vessel diameter measurement was taken 75 pixels away from the optic nerve. This distance was scaled appropriately by the same scale factors defined above. Each measurement was made four times and the average was used in further calculations. All lines drawn to measure the diameter were as close as possible to perpendicular to the vessel walls. Care was taken to ensure that all measurements were taken at the same locations between each image of the same eye.

From each series of vessel diameter measurements, a percent change in diameter from the reference image was defined as the difference between the current image vessel diameter and the reference image diameter (d_{ref}) divided by d_{ref}. Each image set was evaluated by 3 people. The outlying value of the three measurements was dropped and the average of the remaining two values was recorded. The outlier from the three measurements was defined as either: 1) a value that had an opposite sign from the other two values, or 2) the value farthest away from the median of the three values.

3.2.3.2 Clamping Forces

The force data were filtered post-hoc using a 4th order Butterworth filter. An appropriate cutoff frequency was determined by evaluating the spectral density of the data (Figure 13). To avoid the phase shifting associated with IIR digital filtering, force data were filtered first with a 2nd order Butterworth filter, then inverted, filtered again with the same 2nd order filter, and inverted back. A MATLAB program (Appendix B.2) was written to extract the peak clamping force, average plateau force, rate of force application, total clamping time, and total time clamped starting from the peak force for Groups 1 and 2 (Figure 14). A second MATLAB (Appendix B.2) program was written for Group 3 to extract the total cycling time and frequency of clamping.

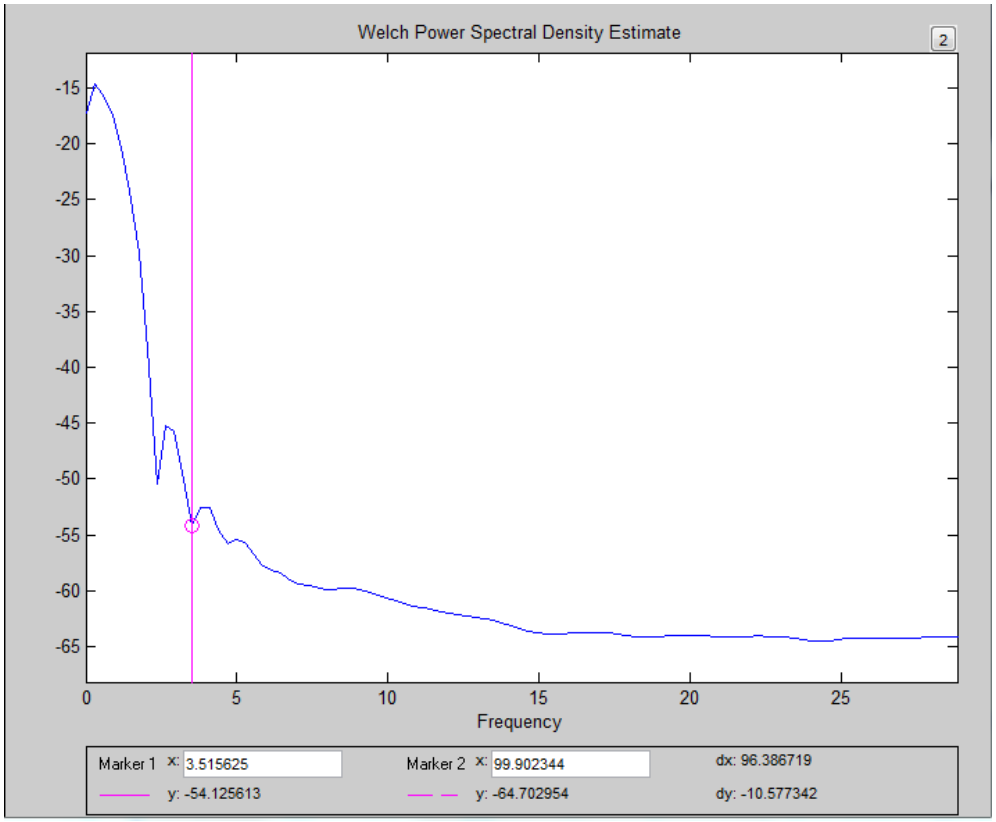

Figure 13: Spectral analysis used to determine 3.5 Hz cutoff frequency, shown by the vertical line. Image zoomed in to lower frequencies to better show cut-off frequency.

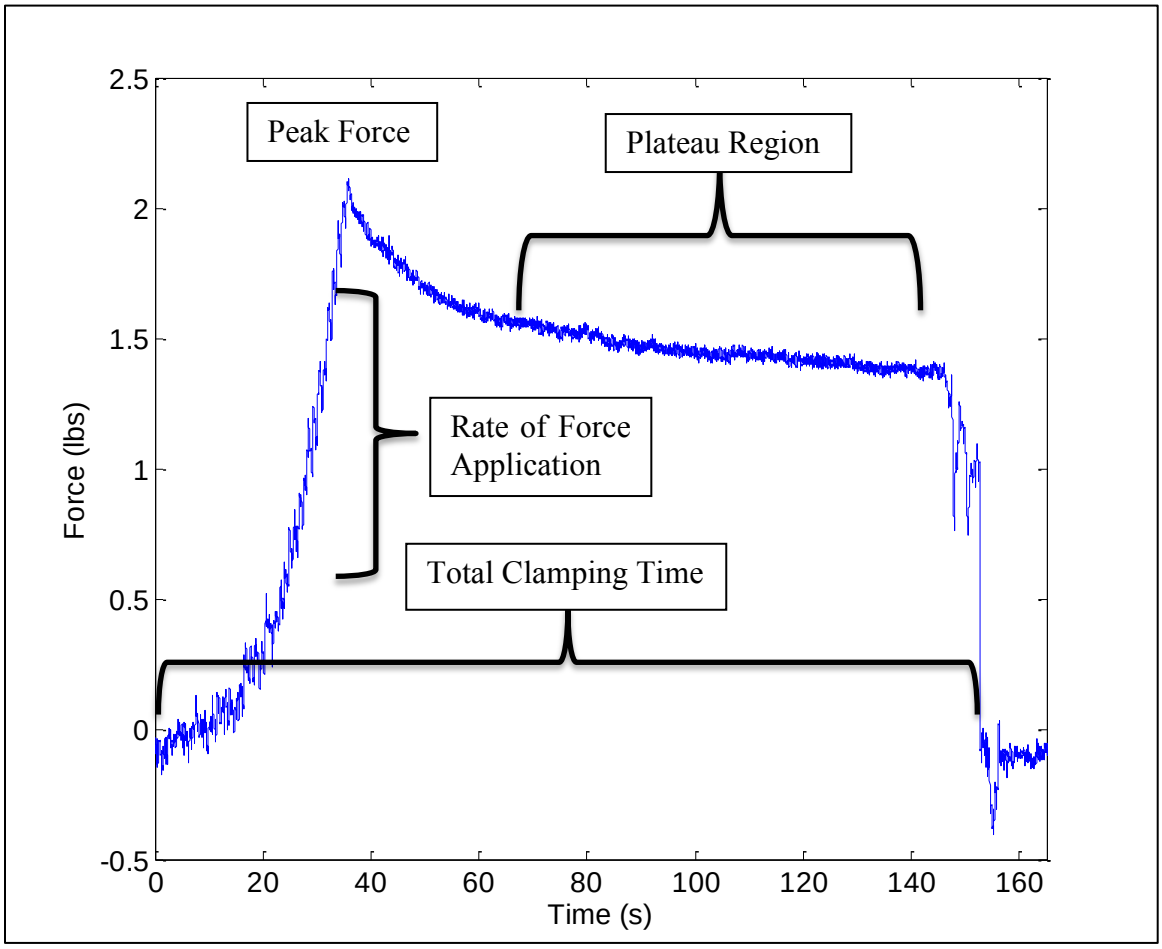

Figure 14: Representative force plot during clamping of a Group 2 eye. The rate of force application was the slope of the initial linear segment of the force-time trace. Peak force was defined as the peak force measured and the plateau force was the average force over the plateau region. The total clamping time was the time between the initial application of force to when the force returned back to zero.

3.2.3.3 Intraocular Pressure

Tonopen measurements were made before and after the abdominothoracic compressions in Group 2 to measure changes in IOP.

3.3 Results

3.3.1 Hemorrhage

Table 2 details the clamping metrics for each eye in the study. Retinal hemorrhage occurred in 1 of the 2 eyes in Group 1. The hemorrhages were small intraretinal peripapillary hemorrhages that extended into the superior periphery, indicating that the piglet retina is capable of producing hemorrhages across the span of the retina (Figure 15). The peak ON clamping force in the eye with hemorrhage was 2.9 lbs, where the peak clamping force in the eye without hemorrhage was 5.4 lbs. The eye which hemorrhaged was clamped 4 times with an average clamped duration of 4.42 minutes. The eye without hemorrhage was clamped 2 times with an average clamped duration of 4.06 minutes. The eye with hemorrhage had a higher average rate of force application at 0.15 lbs/s vs. 0.06 lbs/s in the eye without hemorrhage.

Two out of 5 eyes in Group 2 had RH (Figure 16 and Figure 17). The first eye had peripapillary hemorrhage (Figure 16A), large subretinal and intraretinal hemorrhage (Figure 16B). The subretinal hemorrhage extended through most of the retina. The second eye had a very large preretinal, possibly subhyaloid, hemorrhage (Figure 17). The eyes which produced hemorrhage were clamped with peak forces of 6.2 lbs and 2.0 lbs, while the other three eyes had peak clamping forces of 4.3, 4.5, and 5.7 lbs, respectively. The first eye hemorrhaged within 1 minute after the release of the clamp, the second eye

Table 2: Clamping metrics by eye and whether clamping resulted in hemorrhage.

Group	Eye	Hemorrhage	Average Clamping Force (lbs)	Average Rate of Force Application (lbs/s)	Number of Clamps	Avg Clamp Time (min)
1	1	Y	3.29	0.15	4	4.42
1	2	N	5.36	0.06	2	4.06
2	1	Y	2.09	0.08	2	1.86
2	2	Y	6.26	0.05	2	2.70
2	3	N	4.28	0.03	2	3.77
2‡	4	N	4.33	0.27	2	3.78
2*	5	N	5.71	0.06	2	6.29
3‡	1	N	-	-	1	1.15
3*	2	N	-	-	2	0.68

Matching symbols indicate which Group 2 eye a Group 3 eye came from.
– indicates data were not available.

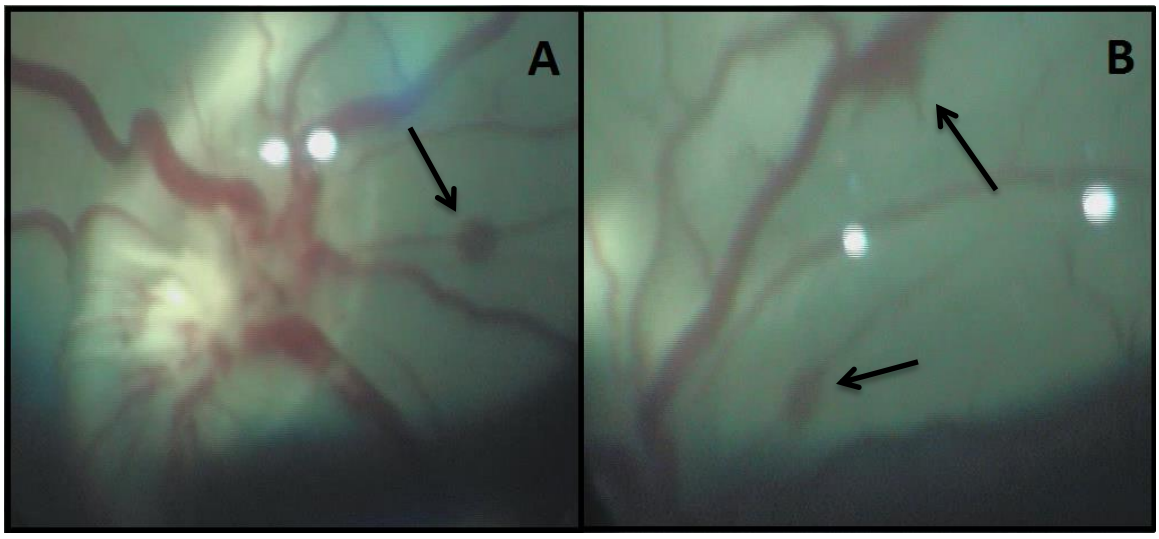

Figure 15: The arrows indicate retinal hemorrhage which occurred in a Group 1 eye. Near the ON (A), in the periphery (B).

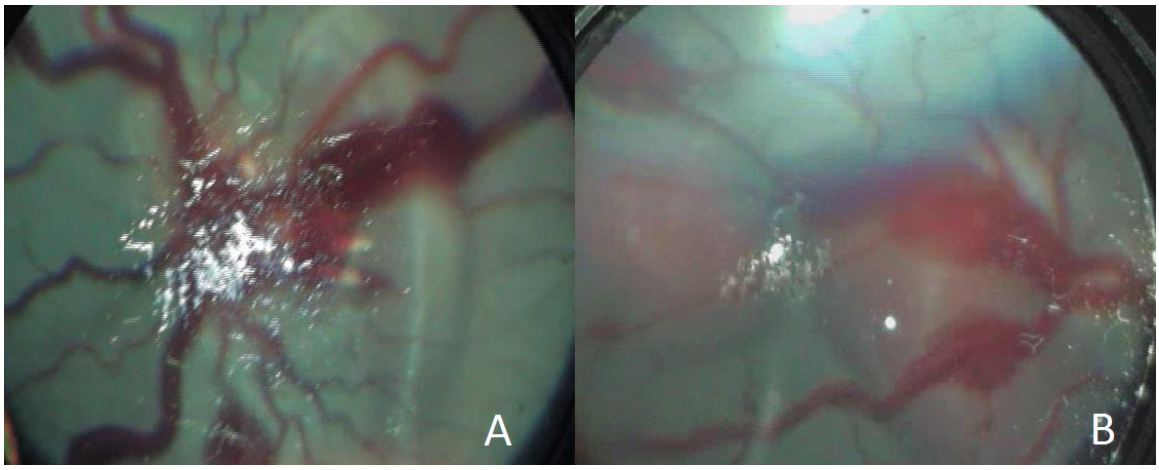

Figure 16: Retinal (A) and Subretinal (B) hemorrhages from a Group 2 eye clamped to 6.2 lbs. Image B was found on the periphery.

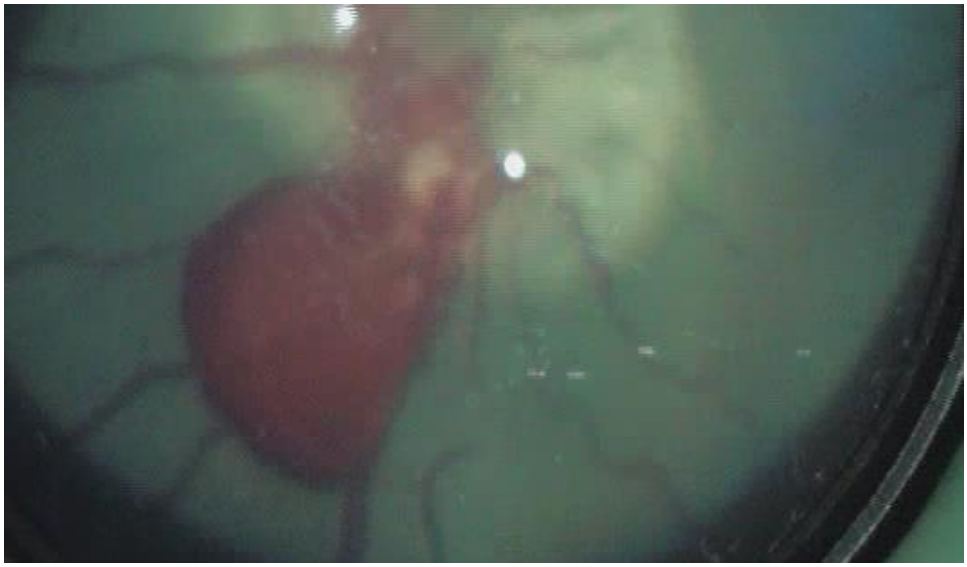

Figure 17: Preretinal hemorrhage which occurred in a Group 2 eye clamped to 2 lbs.

began hemorrhaging during clamping. The average clamp time for Group 2 eyes which hemorrhaged was 2.28 minutes. The eyes that did not produce hemorrhage were clamped for an average of 4.61 minutes. Each eye in Group 2 was clamped twice. No eyes in Group 3 had any RH. Each eye was cyclically clamped to approximately 4 lbs at an average frequency of 0.61±0.23 Hz for 55 seconds.

3.3.2 Vessel Diameter Change

Overall proximal vessels (Figure 18) show larger absolute diameter changes than distal vessels (Figure 19). Around half of all the individual measurements show an increase from baseline. The first measureable clamped state usually showed a decrease in vessel diameter. A comprehensive table with all of the vessel changes can be found in Appendix B.3. Some videos, or frames in videos, were unable to be analyzed due to being out of focus.

3.3.3 Intraocular Pressure

A t-test was performed comparing the IOP of the Group 2 animals before and during abdominothoracic compressions. Before compression, the mean IOP was 13.4 mmHg; the mean IOP after completing the compression sequence was 15.6 mmHg. These differences were statistically significant ($p=0.03$).

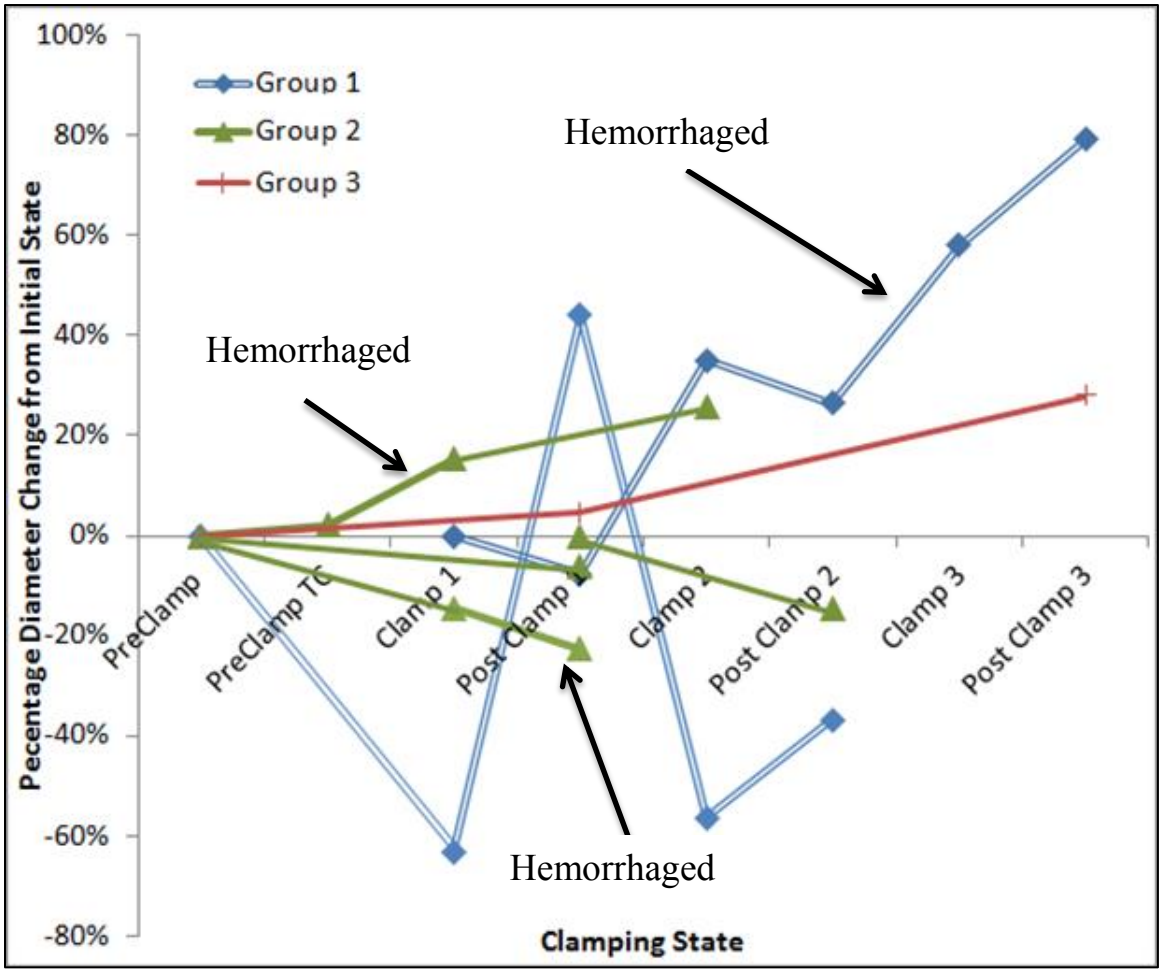

Figure 18: Percentage diameter change from the reference state for all of the proximal measurements. PreClamp TC was a state prior to clamping but after abdominothoracic compressions.

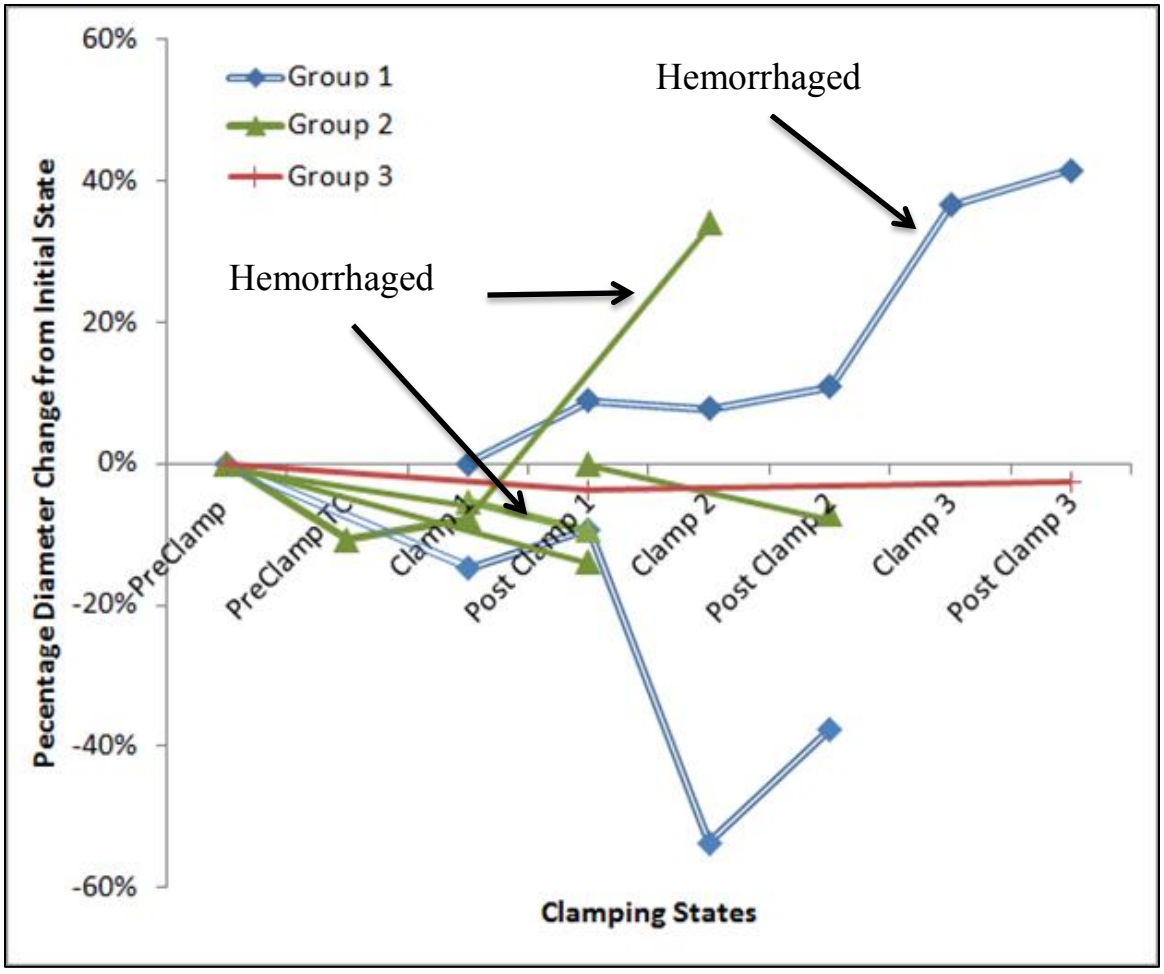

Figure 19: Percentage diameter change from the initial reference state of all the distal measurements.

3.4 Discussion

3.4.1 Hemorrhage

The hemorrhaging seen in this small sample of piglets is inconsistent. All of the hemorrhages occurred in 3 eyes from 2 animals. No hemorrhages occurred in the eyes of the other 2 animals, which were part of Groups 2 and 3. What this indicates is that piglets are capable of getting substantial RH (as seen in Figure 16 and Figure 17). However, there may be microstructural variations among the animals that preclude them all from getting hemorrhages. RH has been reported to occur within 53-86% of cases of

suspected abuse [16], which may also suggest that there could be microstructural differences among infants that make some less prone to RH. Of course the application of loading in all abusive head trauma scenarios can vary widely and this is also likely to have a major effect on ocular injury outcome. Care was taken to perform the same exact methods to every animal in this study, but because the ON was unable to be visualized during clamping, there may have been slight differences in the location of clamping that might have affected the results. The hemorrhages that resulted from the CRVO varied between small in limited regions, to large subretinal, intraretinal, and preretinal hemorrhage. The types of hemorrhage seen are similar to what might be seen clinically, though, apart from the subretinal hemorrhage, the hemorrhages were more localized in this model. This sparser occurrence of hemorrhage could be a result of the lack of the clamping being ceased as soon as RH formed rather than continuing to clamp and release.

Given the similarities in injury between CRVO and traumatic RH from AHT, it is feasible that there is overlap in the mechanisms of injury. The optic nerve is not a straight conduit. It naturally has multiple bends as it exits the eye and connects to the brain. During shaking, the ON may kink and get temporarily occluded. While a temporary occlusion may not be enough to create hemorrhage, a repetitive occlusion may lead to a buildup of blood in the eye without adequate venous return. To investigate this possibility, we performed cyclic clamping on the ON. No hemorrhages resulted. The frequency of the cyclic clamping was 0.61 Hz, which is much lower than published estimates of vigorous shaking on infant surrogates [4, 9]. A higher clamping frequency may inhibit more venous return and more closely simulate a central retinal vein occlusion.

The range of forces needed to cause hemorrhage ranged from 2.05 -6.22 lbs. With a larger statistical power, these numbers could help determine injury risks from occlusion, but in our study, the smallest force led to a hemorrhage and larger forces did not. Therefore, additional factors are likely involved and force may not directly correlate to injury. A finite element model may assist in identifying these additional factors.

As discussed in Chapter 2, physiological changes due to crying (i.e. increased intracranial pressure and cerebral blood volume) could be a potential factor on the injuries seen in conjunction with AHT. It is currently unclear whether increases in intracranial pressure (ICP) directly correlate to increases in intraocular pressure (IOP) [42, 43, 44, 45, 64]. Han [42] and Kirk [43] both showed no correlation between ICP and IOP, but IOP and ICP were not measured simultaneously, but rather 2-5 hours (Han) and 1 hour (Kirk) apart. Li [45] showed a weak correlation ($r=0.32$, $R^2=0.1$) and found that IOP could accurately predict ICP in 65% of the cases in their study. The time between measurements was not mentioned in the Li study. Sajjadi [64] and Lashutka [44] showed very high correlations, $r=0.95$ and 0.83, respectively. Sajjadi recorded IOP measurements within 1 minute of recording the ICP. Lashutka did not mention the exact time between measurements, but it was implied that they were both recorded in a short amount of time.

The IOP in our study significantly increased in animals that experienced abdominothoracic compressions. In Chapter 2, we showed these compressions increased ICP, so it appears IOP likely does increase with an increase in ICP. It is interesting to note that 1 of the eyes with increased ICP and CBV led to the lowest force which caused a hemorrhage at 2.09 lbs. It is possible that increasing the ICP led to a compression on the ophthalmic veins, making it easier to occlude the vein. Due to the bilaterality of RH

in many AHT cases, it is likely that the mechanism of RH can affect both eyes simultaneously. An increase in ICP and CBV (which would be systemic) combined with the potential symmetric nature due to shaking in the anterior-posterior plane would satisfy this characteristic. It is also a possibility that the increase in CBV extends to the ocular blood volume as well prestressing the retinal vasculature before the CRVO is superimposed.

It is possible that the metallic clamp itself caused hemorrhages because it is harder and sharper than the eye. However, no extraocular hemorrhage occurred as a result of any of the clamping, and eyes with higher clamping forces did not necessarily result in hemorrhage. This suggests that hemorrhages were due to the CRVO and not iatrogenic damage from the clamps.

3.4.2 Vessel Diameter Change

The diameter of the vessels decreased during the first clamp of every eye. This is expected as there would be a drop in pressure within the vessel. It would also be expected after a series of clamping and releasing, which lead to a hemorrhage, that rapid reperfusion of the vessels would cause the diameters to increase. A sustained increase in diameter after subsequent occlusion may be due to vessels stretching near or beyond the inelastic limit of the material. Additional increases in the diameter may lead to strains eventually resulting in rupture and hemorrhage. Three of the eyes (1 from each group) showed an overall trend of increasing vessel diameter; however, only 2 of these eyes hemorrhaged. The other 4 eyes showed no obvious correlation between change in vessel diameter and hemorrhage, as the 2 hemorrhaged eyes in Group 2 had a similar magnitude

of change, but opposite sign.

Vessel diameter change was greatest near the ON disk. The majority (72%) of the proximal diameter changes were larger than the corresponding distal diameter changes. However, when a hemorrhage occurred in an eye, it was not isolated to the areas around the ON disk. In fact, several hemorrhages were noted peripherally away from the ON disk. Most of the video capture was focused on the ON and as such, we were unable to take measurements of the vessels in the more distal regions due to a lack of available images to compare against and the absence of the ON in the periphery, needed for scaling. As a result, we were unable to correlate percent change in the diameters of the peripheral vessels to hemorrhage.

The vessel diameter measurements are highly variable and it is unclear exactly how much these results are being influenced by the manual vessel measurements of the volunteers. Error in one of the less focused images was quantified to determine an appropriate estimate of the precision of our manual measurements. Each vessel measurement was taken four times, and the maximum and minimum measurements were used to determine a maximum error. The maximum and minimum measurements in that blurred image differed by 28%. While this was a worst case approximation, it indicates that the vessel diameter measurements were likely influenced by error induced during the measurement process. Methods to automate or semi-automate the measurement procedure need to be developed to decrease this error. Using registration techniques to obtain scaling ratios along with image thresholding to convert to a black and white binary image could be used to improve the repeatability of the measurements.

3.5 Conclusion

This study was able to show that large retinal hemorrhages can occur in the piglet model. It also showed that a mechanical occlusion of the ON can result in RH. The range of forces needed to occlude the ON varied widely and may be dependent on predisposed increased systemic pressure or microstructural variability within each animal.

There was a distinct change in vessel diameter during the vein occlusion and immediately after. However, these changes did not correlate to the presence or absence of RH. Nor was hemorrhage found in locations of large diameter changes.

CHAPTER 4

RAPID CHANGES IN INTRAOCULAR PRESSURE IN THE IMMATURE PIGLET

4.1 Introduction

To date, there are no definitive conclusions about the mechanisms which cause traumatic RH from AHT. Some theories proposed are: hemorrhage from vitreoretinal traction, hemorrhage due to central retinal vein occlusion (CRVO), and hemorrhage due to rapid changes in intraocular pressure (IOP) similar to what occurs with ocular decompression retinopathy (ODR) [20, 65, 66]. In Chapter 3, we investigated CRVO as a potential mechanism. In this chapter, we investigate the potential for rapid changes in IOP to cause RH. Changes in IOP during AHT may occur from compression of the thorax during shaking [36] or from the globe repeatedly impacting the walls and soft tissues in the orbit. This latter mechanism may be similar to what occurs with ODR, which has been shown to share many of the same clinical signs as CRVO [66] and RH in AHT. ODR is most commonly associated with glaucoma drainage and several other procedures which lead to a decrease in IOP [66]. It is not uncommon to see IOP decreases from 16-50 mmHg in association with ODR [65, 66]. The purpose of the study was to observe the effects of rapid changes in IOP in a 3-5-day-old piglet model. A custom indentation device was constructed to allow for different indentation depths and

rates to achieve this purpose.

4.2 Methods and Procedures

In order to evaluate rapid changes in IOP as a cause of RH, the eyes of immature 3-5-day-old piglets (n=4) were subjected to a series of eye indentations. To test conditions similar to ODR, a single indentation to depths ranging from 1-7 mm was performed at two indentation rates (1 mm/s and 50 mm/s). A cyclic indentation was also performed at 3 Hz for 30 seconds to the same depths as the single indentation portion of the study. The 3 Hz frequency was chosen to match the frequency of shaking reported in surrogate studies recreating abusive scenarios [9]. IOP was monitored continuously throughout the indentations with a fiber optic pressure transducer (Samba Preclin 420 LP, Gothenburg, Sweden). All testing was approved by the International Animal Care and Use Committee at the University of Pennsylvania.

4.2.1 Indentation Device

4.2.1.1 Device Specifications

In order to achieve systematic and repeatable indentation depths and rates, a computer controlled indentation device was designed and constructed. The indentation device was capable of indenting between 0 and 7 mm. It could perform single “indent and hold” tests as well as repetitive indentations at 3 Hz. The device was small enough to easily move around a surgical table. Force and displacement instrumentation were included to correlate the indentation depth and eye contact force with the resulting IOP.

4.2.1.2 Device Design

The actuation of the indenter was created by attaching a rack and pinion (Stock Drive Products, New Hyde, NY) to a stepper motor controlled by an Arduino (Uno R3, IDE 1.0.5, Italy) microcontroller. Connected to the rack was a 10 lb force transducer (LSB200, Futek, Columbus OH) which attached to a 4 mm diameter stainless steel tip. The indentation tip was flat with rounded edges to contact the eye uniformly without damaging the sclera. A linear variable differential transformer (LVDT) (Transtek 240 series, Ellington, CT), was attached to the nonindentation side of the rack to accurately measure the indentation depth (Figure 20). Data from the fiber optic pressure sensor, LVDT, and force transducer were continuously collected at 300 Hz using a data acquisition system (National Instruments NI 9201, Austin, TX), and stored on a Dell (Round Rock, TX) laptop.

The indentation device was equipped with its own power supply and circuitry to regulate voltage for the Arduino, LVDT, and stepper motor. A stepper motor driver board (Big Easy Driver, Sparkfun, Boulder, CO) powered and controlled the stepper motor. Custom Arduino code with a simple user interface was created to control the rate, direction (forward and backward), and depth of the indentation tip. See Appendix C.1 for a more detailed explanation about the Arduino code. The device was equipped with a locking hinged bracket to adjust the angle at which the indentation occurs. A fine threaded screw was included to allow precision advancement of the indentation tip. The whole assembly was mounted to an adjustable base to facilitate use at different heights.

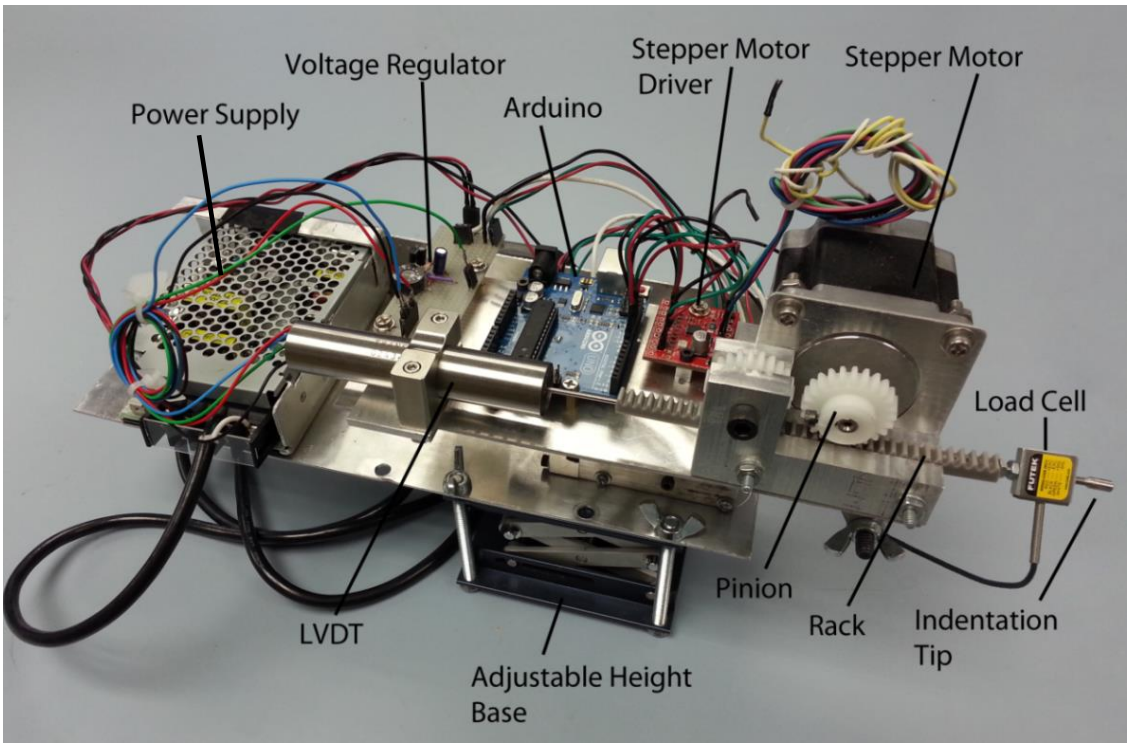

Figure 20: Indentation device designed to apply compressions to the eye at variable depths and speeds.

4.2.2 Animal Preparation

Animals were anesthetized with 5% isoflurane and maintained at 1-3% isoflurane via intubation tube. Two drops of cyclopentolate 2% ophthalmic solution was applied to the eye of each animal to dilate the pupil. An ocular speculum was inserted and an ophthalmic exam performed by an ophthalmologist to determine the presence of any preexisting ocular conditions. Hemostatic forceps were clamped on the canthus (outer corner of the eye) for a short period of time then removed. This prevented hemorrhage while a small incision was made in the canthus to allow better access to the sclera. The conjunctiva of the eye was incised and reflected to expose the sclera. A 25 gage trocar was inserted into the eye and the fiber optic pressure transducer was threaded through the trocar until its tip sat in the middle of the vitreal space. This was verified by the

ophthalmologist through an optical indirect ophthalmoscope. The sensor was held in place throughout the duration of the test either by hand or by a stand. Baseline IOP measurements were taken with the fiber optic pressure sensor and compared to non-invasive measurements made with a Tono-Pen Avia VET Veterinary Tonometer (Reichert Technologies, Depew, NY) prior to the trocar insertion.

4.2.3 Testing Protocol

4.2.3.1 Single Indentation

The tip of the indentation device was placed close to the sclera of the eye, but not touching. The tip was advanced using the precision screw until the force sensor registered a noticeable contact force. The indenter was activated to indent the eye to a depth of 1 mm at the "slow" rate of 1 mm/s. The indentation was held for 5 seconds and then returned to the starting position, withdrawing the indentation tip at a 1 mm/s rate. The eye was allowed to return to a baseline IOP. If after 1 minute the IOP did not return to baseline, a new baseline IOP was established using the fiber optic pressure sensor and Tono-pen. Then, the eye was indented to 1 mm at a "fast" rate of 50 mm/s. The depth was held for 5 seconds and then returned to the starting point, withdrawing the tip at the fast rate. The eye was again allowed to settle to a baseline IOP. This indentation procedure was repeated in 1 mm increments up to a maximum depth of 7 mm.

4.2.2.2 Cyclic Indentations

The indentation device was aligned in a manner similar to the single indentations. The indenter tip was indented to a depth of 1 mm at a rate of 6 mm/s and immediately

withdrawn at the same rate. This was repeated for 30 seconds, resulting in a cyclic compression frequency of 3 Hz. Following the 30-second cyclic compression to 1 mm, the eye was allowed to return to a baseline IOP. The cyclic compression was then repeated at 1 mm increments from 2-7 mm, maintaining a 3 Hz indentation frequency for each new depth by increasing the indentation rate.

4.2.4 Data Analysis

All data were filtered post-hoc using a 4^{th} order Butterworth filter. An appropriate cutoff frequency was determined by evaluating the spectral density of the data, and finding the frequency that contained approximately 95% of the power cumulative sum distribution. To avoid the phase shifting associated with IIR digital filtering, force data were filtered first with a 2^{nd} order Butterworth filter, then inverted, filtered again with the same 2^{nd} order filter, and inverted back. MATLAB programs (Appendix C.2) were written to extract the indentation velocity, final indentation depth, maximum pressure, average plateau pressure, rate of pressurization, and maximum force from the appropriate sensor data. Plateau pressure was not available for the cyclic indentations as there was no dwell period. An analysis of variance (ANOVA) was performed on the peak and plateau pressures (Figure 21) to determine differences between indentation velocity and depth. The linear region of the pressure vs. time response was extracted as the rate of pressurization. An ANOVA was performed to determine if differences existed between the pressurization rates between the slow and fast rates.

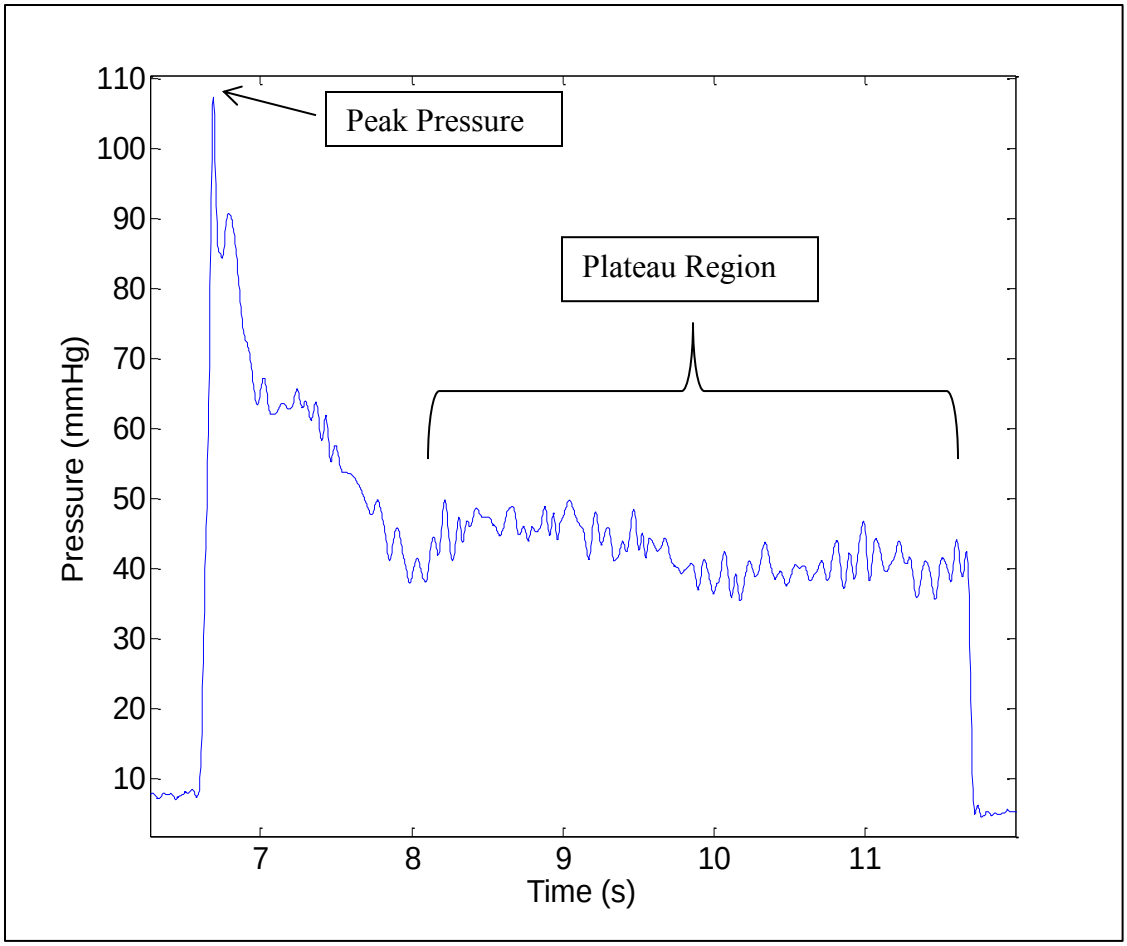

Figure 21: Typical pressure profile indicating peak pressure and plateau region.

4.3 Results

The average depths for each test type are shown in Table 3. No test depth was less than 89% of the desired depth. The average ± standard deviation of the fast indentation rate was 52 ± 9.19 mm/s, the average ± standard deviation of the slow indentation rate was 0.945 ± 0.03 mm/s.

4.3.1 Single Indentation

Both the average plateau ($r=0.98$, $p<0.0001$, $R^2=0.96$), and peak IOP ($p<0.0001$, $R^2 = 0.95$) pressures were strongly correlated to the average plateau and maximum

Table 3: Average and standard deviations of measured depths for the various study conditions.

	Desired Depth	1 mm (std)	2 mm (std)	3 mm (std)	4 mm (std)	5 mm (std)	6 mm (std)	7 mm (std)
Actual Depths	Slow Single indent.	1.013±0.080	1.90±0.044	2.86±0.068	3.84±0.059	4.78±0.073	5.76±0.065	6.73±0.056
	Fast Single indent.	0.989±0.028	1.89±0.031	2.88±0.078	3.82±0.052	4.75±0.051	5.58±0.345	6.55±0.079
	Cyclic Indent.	0.89±0.012	1.84±0.016	3.05±0.008	3.68±0.008	4.58±0.007	5.53 ±0.007	6.54±0.009

applied force of the eye, regardless of the rate of indentation (Figure 22). The plateau pressures were not significantly dependent on indentation rates ($p = 0.559$) (Figure 23A). Due to large variability, the peak pressures were also not statistically different between the two rates ($p = 0.057$), but there is a definitive increase in the mean of the peak pressure with increased rate (Figure 23C). Indentation rate was determined to be the only significant factor ($p < 0.0001$) in the rate of pressure response (Figure 24). The pressurization rate was not significantly different in any of the slow rate depths, but the 1 mm depth in the fast rate was significantly different than all the other depths ($p=0.0346$, Figure 25).

4.3.2 Cyclic Indentations

The cyclic indentations did not have a plateau region (Figure 26 inset). As such, only the peak pressure and average rate of pressurization were reported. Figure 26 shows a representative pressure trace from a cyclic indentation. Similar to the single indentation studies, there was a very strong correlation between peak force and peak pressure ($R^2 = 0.99$) (Figure 27). Figure 28 shows the mean peak pressure at each of the cyclic indentations, where the peak pressure across all animals was averaged at each indentation peak. The response of the pressure to the cyclic loading was nonlinear. This non-linearity was more distinct at the larger depths (depths>4 mm). Significant differences

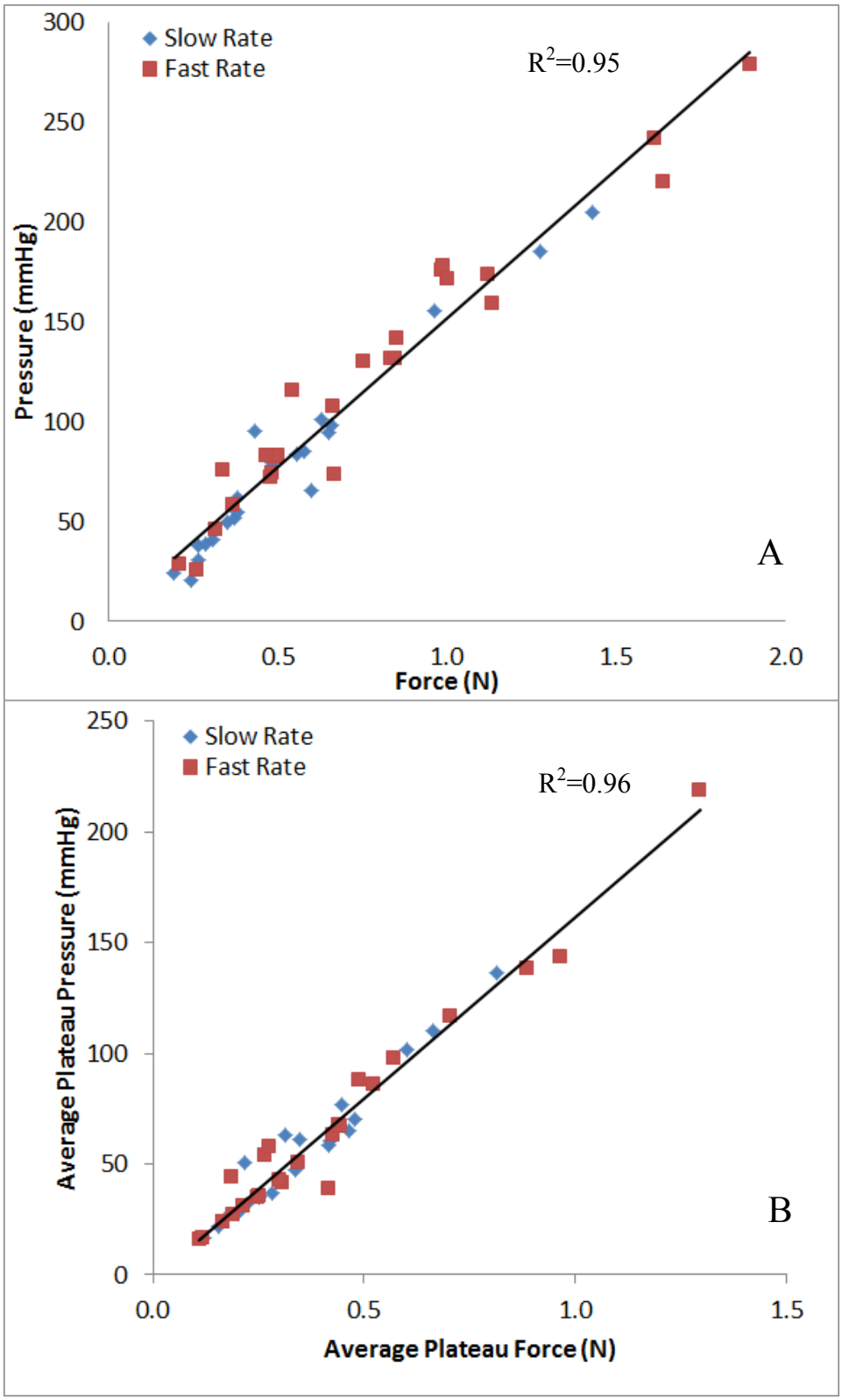

Figure 22: Pressure and force response from single indentation studies. (A) Maximum force and peak pressure response and (B), average plateau force and average plateau pressure response.

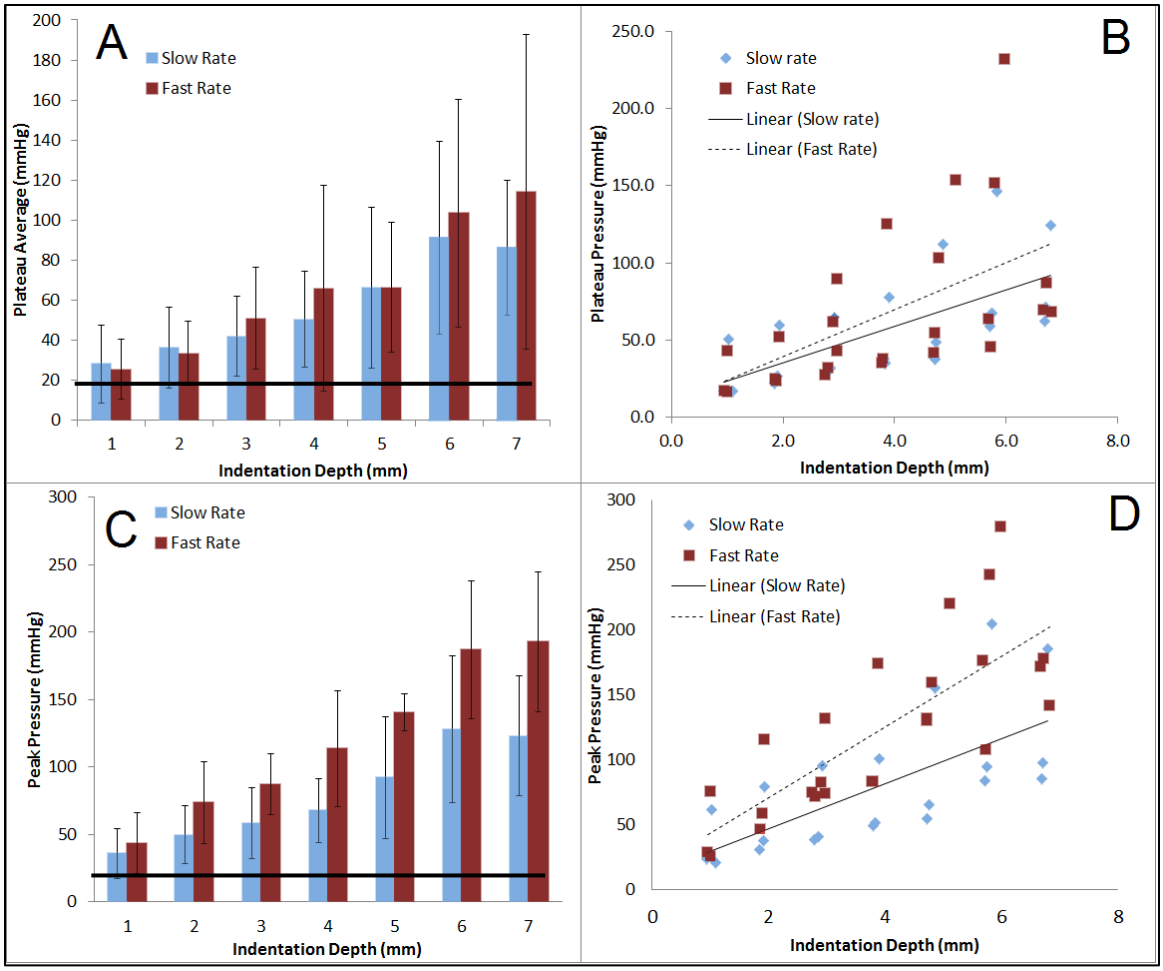

Figure 23: Pressure response due to indentation depth from single indentation studies. (A) Mean and standard deviation of the plateau pressure response. The bar indicates the average baseline IOP. (B) Plateau pressures by rate with linear regressions. (C) Mean and standard deviations of peak pressure response. The bar indicates the average baseline IOP. (D) Peak pressures by rate with linear regressions.

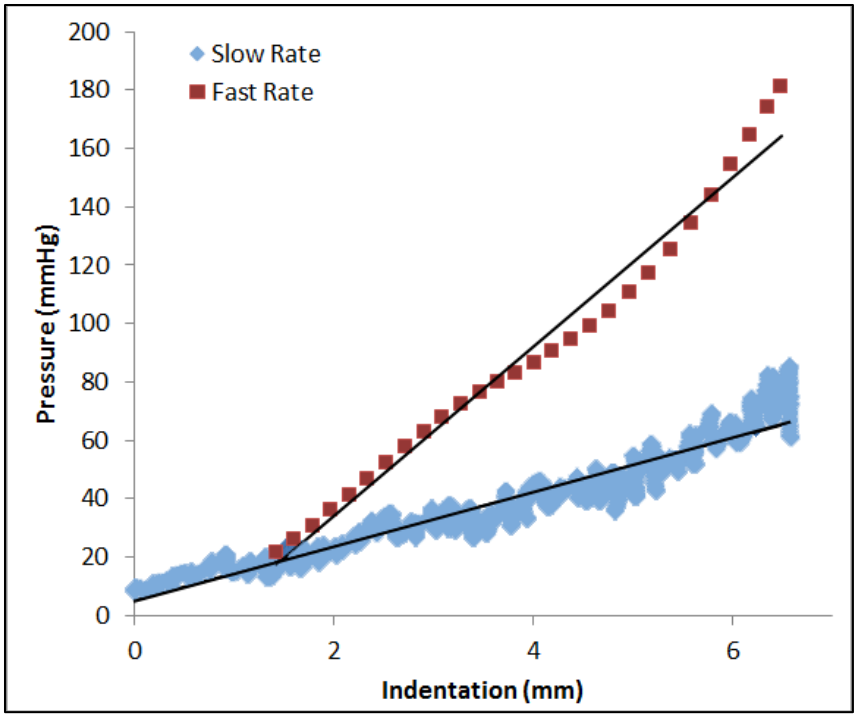

Figure 24: Representative plot of the pressure response by indentation depth with linear regression lines.

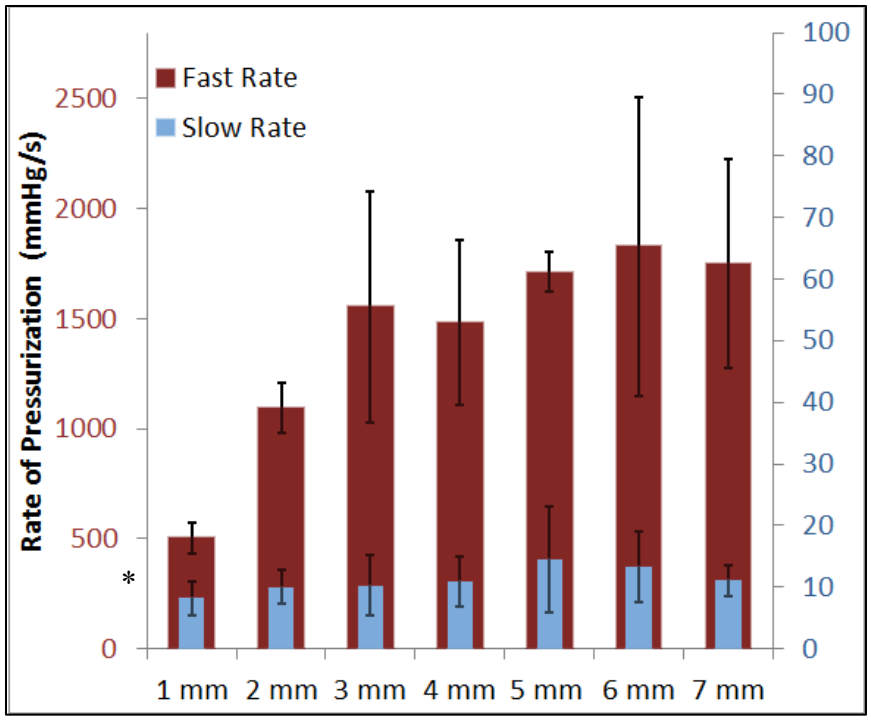

Figure 25: Average and standard deviation of the rate of pressurization by indentation rate and depth. The slow rate uses the scale on the right-hand side of the figure. *indicates significance.

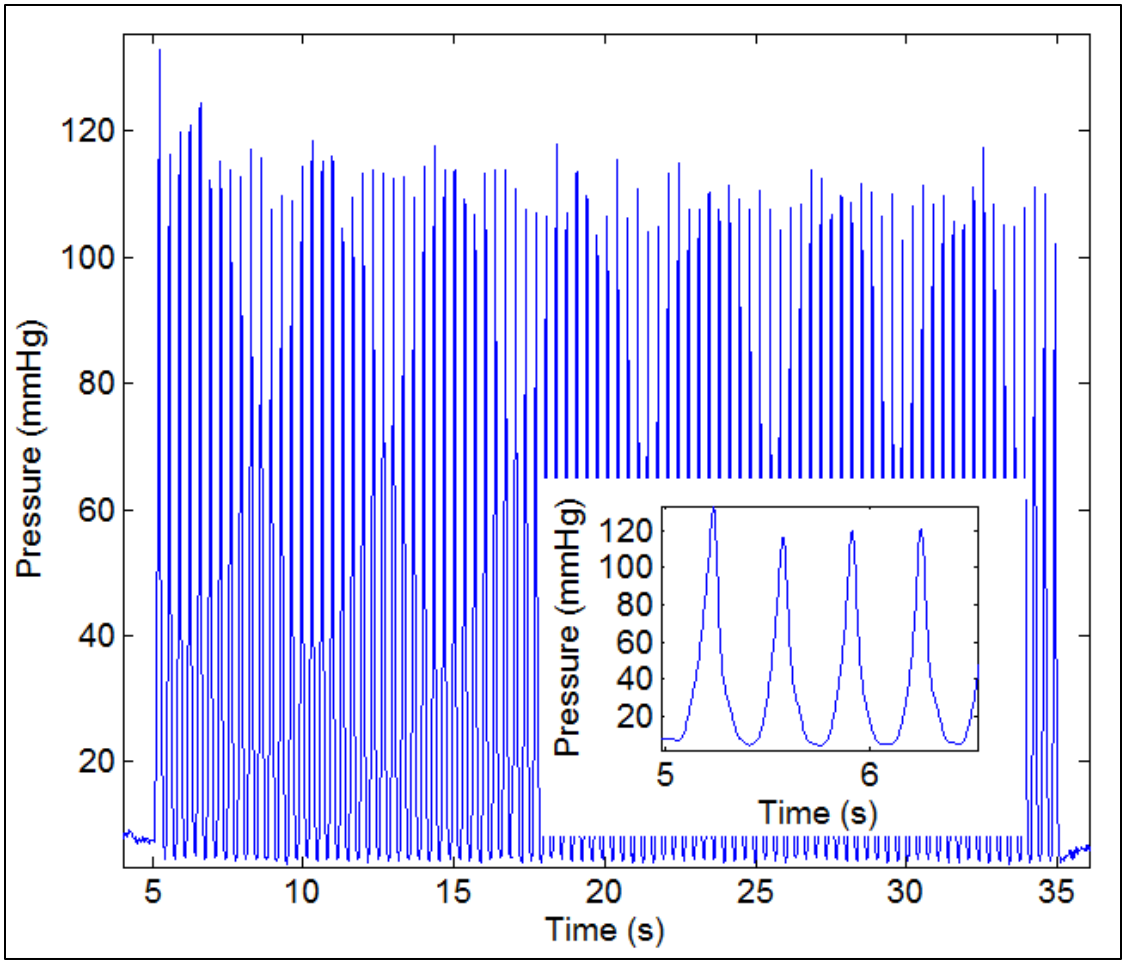

Figure 26: Representative cyclic indentation pressure trace at an indentation depth of approximately 6 mm. Inset: Pressure response from the first 4 indentation peaks.

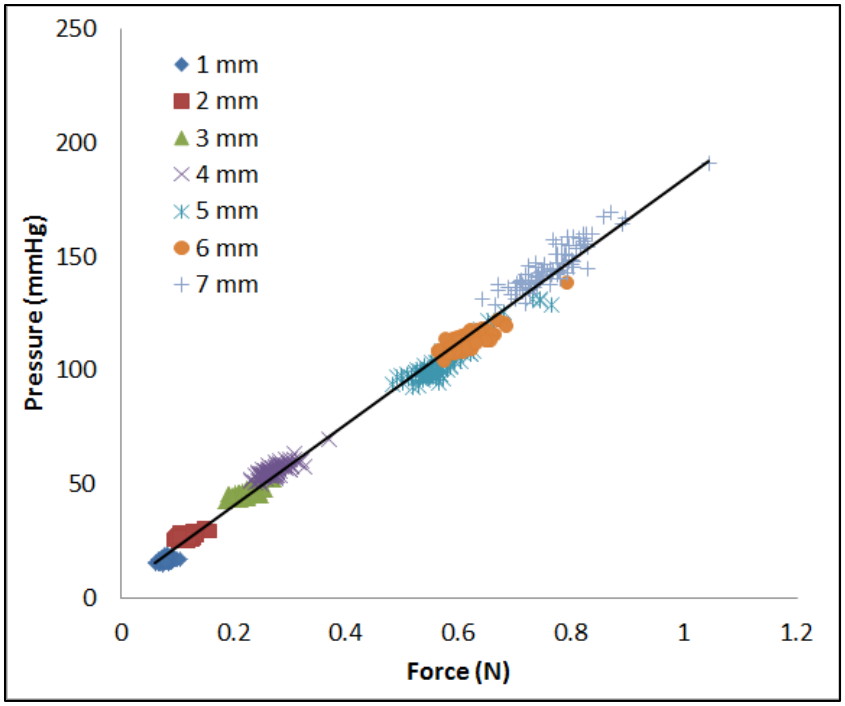

Figure 27: Correlation of force and pressure from cyclic indentation studies.

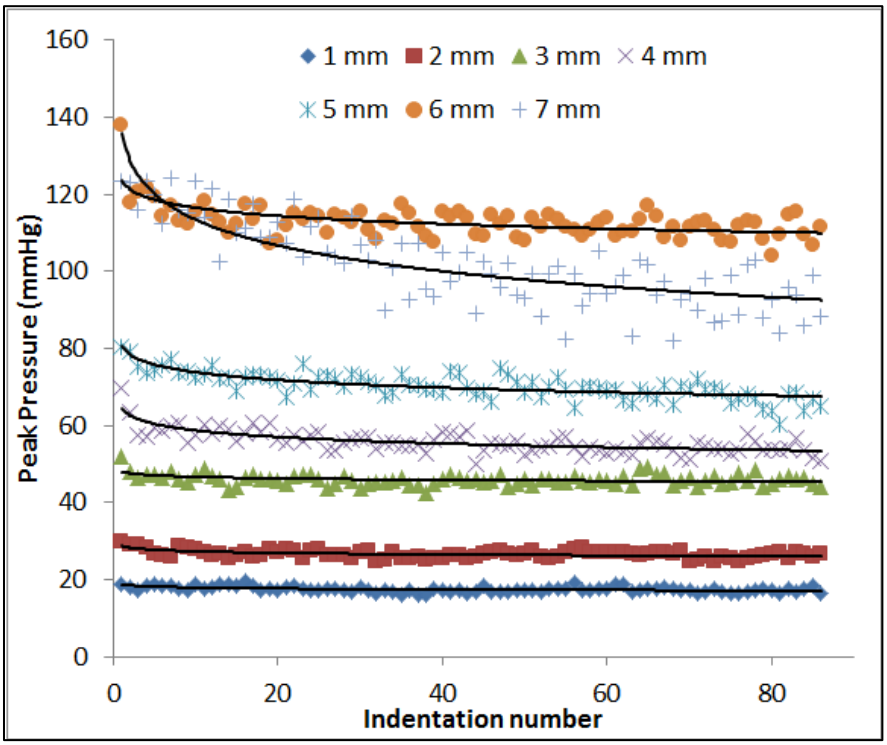

Figure 28: Peak pressure values averaged at each indentation peak with superimposed logarithmic regression lines showing the nonlinear decrease in peak pressure during subsequent cycles.

were shown between the pressurization rates ($p<0.0001$) at the various cyclic indentation depths (Figure 29).

4.3.3 Ocular Hemorrhage

No ocular hemorrhage was noted in this study. Regardless of the peak pressure, or pressurization rate, no hemorrhage was produced in either of the single indentation groups or cyclic indentation groups.

4.4 Discussion

The exact mechanisms which cause RH in abuse are still unknown. RH is often a key finding in AHT. A better understanding of the mechanisms that cause RH is needed to give clinicians more diagnostic power. We sought to determine if rapid changes in IOP could be a mechanism of RH from abuse. IOP was increased 18-178 mmHg above baseline at pressurization rates ranging from 10-1441 mmHg/s.

A pressure change of 16 mmHg has been associated with hemorrhage due to ODR. All but 3 of the 46 single indentation tests experienced a change in IOP greater than the minimum reported change in IOP of 16mmHg [65, 66]. All but 2 of the 22 cyclic indentations had each peak pressure above 16 mmHg. 57% of the indentation groups were significantly higher than reported values, with group averages ranging from 72.7-178.9 mmHg, with a single eye as high as 279 mmHg. This signifies that a change in pressure alone is not sufficient to cause RH in this model.

ODR usually occurs in conjunction with glaucoma drainage and a rapid decrease in IOP. Glaucoma causes the IOP of the eye to increase due to a lack of drainage through

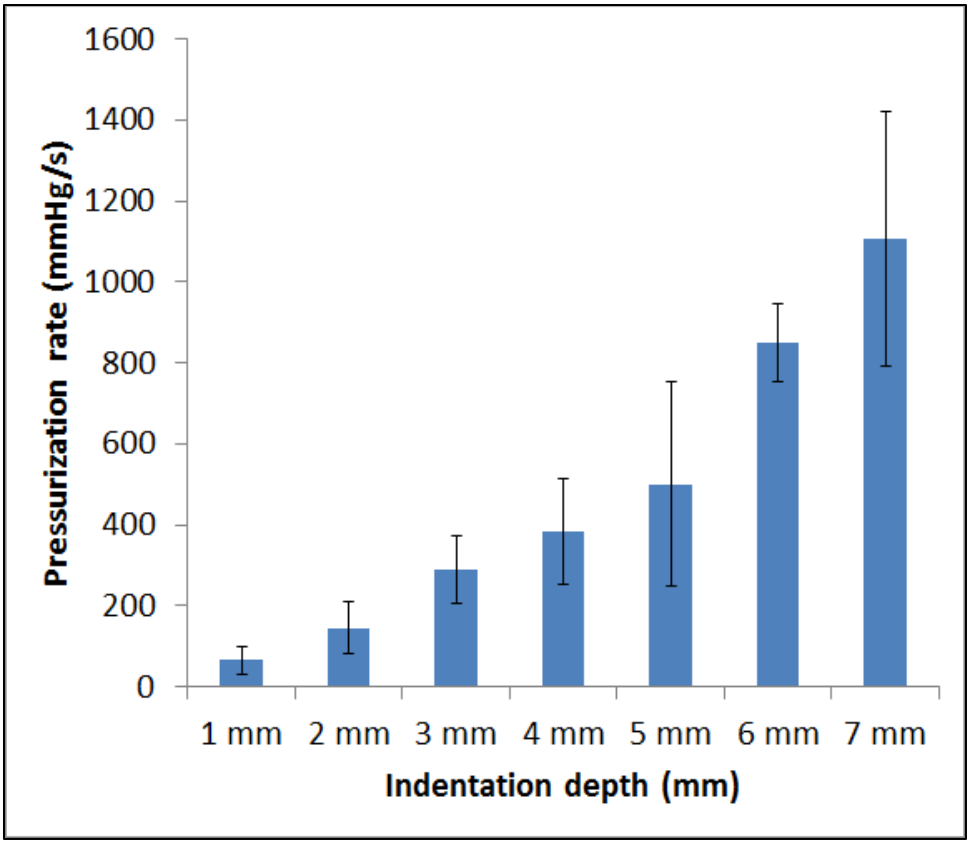

Figure 29: Rate of the pressure response as a function of the indentation rate, combined from all groups.

the open angle. The IOP builds slowly with time and it is possible that experiencing increased IOP for an extended period of time is important to ODR. This study most likely did not reproduce any of the long time periods inherent with glaucoma and ODR. It is possible that if a child had been crying for an extended period, as is typical prior to shaking [28, 29], that this could increase IOP for a duration closer to the time periods associated with glaucoma or ODR but there are no data in the literature providing durations of IOP increase for these diseases.

The eyes were successfully indented at various indentation rates which resulted in pressurization rates from 10.7-1441 mmHg/s. The mechanical response of the eye during indentation was nonlinear and displayed a viscoelastic response. The rate of pressure

change with respect to displacement at slow rates was notably lower than the rate of pressure change of the fast rate indentations. Peak pressure also exhibited this trend, but it was not statistically significant by a very small margin. At the faster indentation rates, a toe region can be seen prior to the linear elastic region of the indentation (Figure 30). This may be due to the alignments of microstructures or a viscoelastic response of the structure. Sclera and vitreous, which likely contribute the most to the IOP response, have both been shown to have viscoelastic material responses [67, 68]. If IOP is a factor in RH from AHT, the viscoelastic material responses will dictate the resulting pressures within the eye based on the reaction forces of the orbit onto the sclera.

After the initial peak pressure, the pressure relaxed toward a plateau. This plateau pressure was not significantly influenced by the indentation rate or peak pressure. This falls in line with spring and damper models of viscoelasticity such as a Maxwell, or Kelvin-Voigt model (Figure 31). The initial pressure response would be largely governed by the rate-dependent damper, but the final relaxation would be governed by the equilibrium position of the spring. If the eyes in our studies were allowed to relax longer than the prescribed 5 seconds, it is possible that the final plateau pressure compared between indentation rate groups would be even closer. It is unlikely, however, that the relaxed material response would play a role in RH due to the fast repetitive application of load associated with the 3 Hz shaking frequency of AHT.

The cyclic indentations resulted in a similar material response. The initial peak pressures decayed to an equilibrium pressure with continued indentations. Other biosolids, such as rabbit mesentery and porcine aortic valves, show similar decreases in peak stress with cyclic testing [65, 66], and may be due to the response of the collagen in

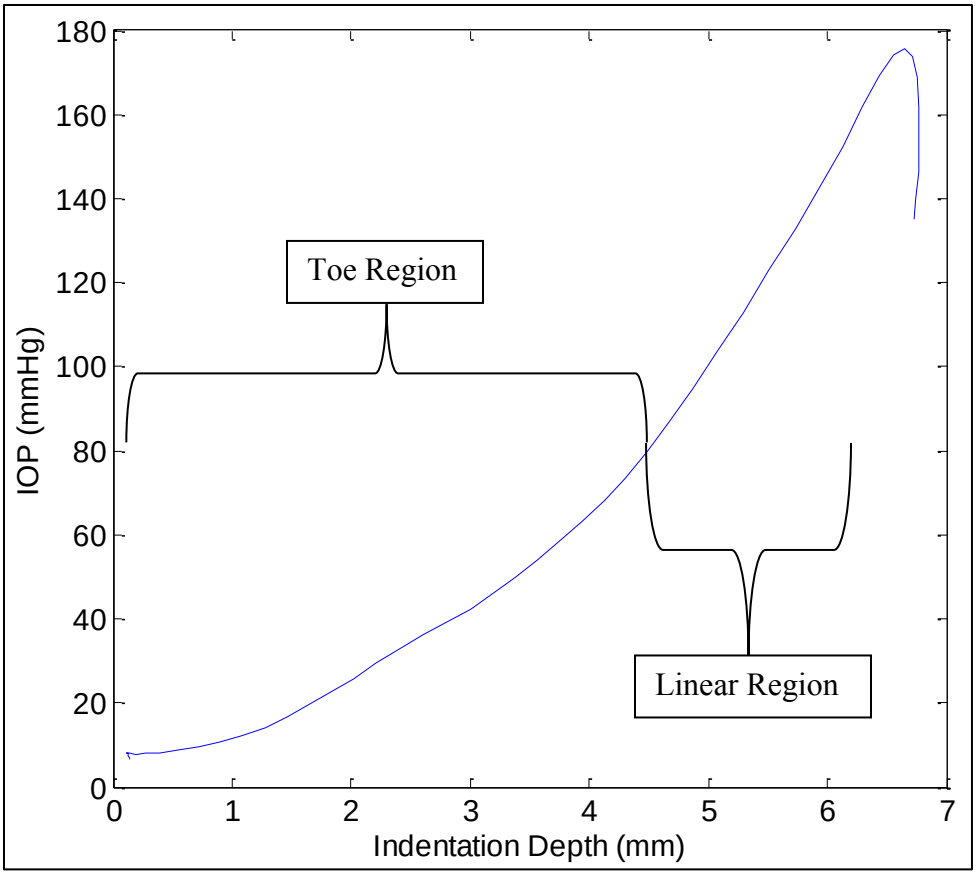

Figure 30: Example of a pressure response from a fast rate single indentation to approximately 7 mm.

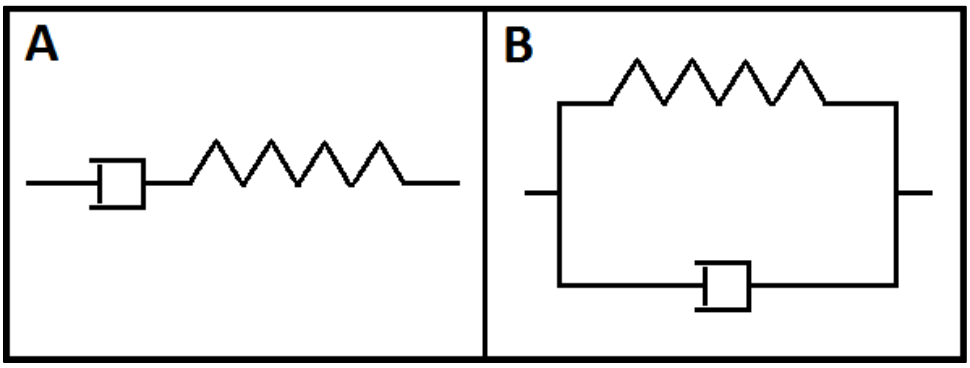

Figure 31: Models of viscoelasticity: (A) Maxwell model (B) Kelvin-Voigt model.

the eye. Collagen naturally undulates [67] and it is possible that as the collagen stretches the fibers lose their undulations. The shortest fibers could become stretched such that they either break, or break loose from the matrix in which they are embedded, causing less resistance to deformation in the next cycle and lowering the IOP. Because the repeated indentations are to the same depth, progressive damage would cease and equilibrium would be reached as demonstrated in Figure 28. It is also possible that instead of damage, there is merely a reorganization of the collagen fibers within the matrix. A decrease in pressure due to the loss of fluid through the trocar would also cause a decay similar to that seen in Figure 28, but this was never visualized and IOP quickly returned to baseline values after removal of the indenter tip. These observations lend more credibility to the decay being a material response rather than due to leakage.

The strong correlation between IOP and force signifies that these studies could possibly be performed without the invasive insertion of the trocar and IOP sensor. This could have implications on studying ODR outside of the context of AHT, as long increased IOP durations could be implemented that were not possible in this study. To identify inertial effects, the indentation device was tested without an eye. There were small inertial forces, but these inertial forces fell within the noise of the load cell and were eliminated during filtering.

4.5 Conclusion

The methods used in this study demonstrated that rapid changes in IOP do not result in RH. Levels of IOP in this study went as high as 279 mmHg, or 15 times higher than the average baseline levels, and no hemorrhages found. A fast indentation rate

increased peak IOP more than a slow rate of indentation, but this rate effect did not lead to hemorrhages. The mechanical responses of the ocular tissues demonstrated an overall viscoelastic response which was dependent on indentation rate. Long durations of increased IOP could be a factor in RH from ODR but are less likely in AHT.

The cyclic indentation studies showed a decrease in peak pressure over the duration of the indentations. This effect was greater at higher indentation depths, which corresponds to higher pressurization rates. This suggests that peak IOP from cyclic indentations would not be higher than IOP from a single rapid indentation or ocular impact.

CHAPTER 5

CONCLUSION

Abusive head trauma (AHT), especially shaken baby syndrome (SBS), remains difficult to diagnose and investigate. The exact circumstances surrounding abuse and specifically shaking are often unclear or unknown. As we understand more about injury mechanisms, clinicians will have better diagnostic tools to distinguish between cases of abuse vs. accident. In this thesis, several possible injury mechanisms were studied and evaluated in the context of abuse.

5.1 Chapter 2

Shaking as the sole injury mechanism in SBS is a controversial theory. It is not clear if shaking alone can cause the injuries seen clinically [4]. In Chapter 2, we examined how the physiological effects of crying, increased intracranial pressure (ICP), and cerebral blood volume (CBV) along with shaking can affect injury in a 3-5-day-old piglet model. It was shown that animals which were shaken along with increased ICP and CBV showed higher amounts of axonal injury, along with the formation of a thrombus in the transverse sinus in 2 of the animals. The animals which experienced the increased ICP and CBV with shaking had a wider variety of ocular hemorrhage, including macroscopic extraocular hemorrhage, and the only retinal hemorrhage (RH),

seen microscopically, in any of the animals.

Our results were somewhat weakened by the high variability between animals as no statistical significance was shown. Another weakness of the study was the low angular accelerations and velocities. Our cyclic device was able to match the shaking frequency of 1.5-3 Hz found in the literature [4, 9], but the angular acceleration and angular velocity were 86% and 60% lower, respectively, than infant surrogate angular velocities and accelerations scaled from the human infant to the newborn pig by brain mass and material properties. A larger sample size along with a redesigned cyclic device is needed to definitively quantify the injurious effects of increased ICP and CBV due to crying during shaking.

5.2 Chapter 3

Retinal hemorrhage is heavily associated with AHT but the mechanisms which cause RH in abuse is unknown [16]. In Chapter 3, a 3-5-day-old piglet model was evaluated as a model for RH by creating central retinal vein occlusions by mechanically clamping the optic nerve (ON). Widespread subretinal and intraretinal hemorrhage was seen due to the occlusions. It was concluded that 3-5-day-old piglets can produce widespread RH. It was also concluded that if the ON becomes occluded or otherwise kinked that hemorrhage could result. ON occlusion could therefore be one mechanism which causes RH during abuse.

All of the hemorrhages came from 2 of the 4 animals, so the small sample size makes it difficult to draw strong conclusions. Also the methods used to quantify vessel diameter change were subject to human error; as such, no correlations were made

between vessel diameter change and hemorrhage. A larger sample size and a more automated system to measure vessel diameter change are needed to draw stronger conclusions.

5.3 Chapter 4

In a continuation of the investigation into the mechanisms of RH, Chapter 4 evaluated the possibility of rapid changes in intraocular pressure (IOP) to cause RH during abuse. Large changes in pressure were created in the eyes of 3-5-day-old piglets at different rates of pressurization and depths of indentation. No hemorrhages were seen in any of the study groups. Pressure changes were as high as 174 mmHg in one of the groups, which is close to 3 times higher than reported pressure changes related to ocular decompression retinopathy. It was concluded that rapid changes in pressure alone do not cause RH.

5.4 Overall Conclusions

We were able to show that increased ICP/CBV from crying can lead to increased levels of injury from shaking, which has never before been explored in the literature. We also showed that 3-5-day-old piglets can be used as a model to simulate hemorrhage, and occlusions of the ON can lead to hemorrhage. This is a potential mechanism of RH which can be further explored. Finally, we showed that RH does not occur due to rapid changes in IOP. This thesis was able to clarify some of the uncertainties associated with SBS.

APPENDIX A

CHAPTER 2 APPENDIX

A.1 Description of Animal Feeding System

The food consumed by 3-5-day-old pigs is a powder-based milk replacement to be mixed into water. Typically, this milk replacement is used in conjunction with a very expensive feeding system which includes a large tank with a constant stirrer to keep the powder agitated and floating in the water. The milk replacement is then pumped to a bowl as needed by the animal. The Comparative Medicine Center is not equipped with any such feeding systems, where typically, a dry food is given to the animals and water through a ball-bearing-stopped water bottle, the kind of water bottles associated with pet mice, rats, and gerbils.

A recirculating feeding system was designed to continuously agitate the milk replacement in a form the piglets could feed with. The same system was used to give the piglets water as well. FDA approved pumps were used to pump the milk replacement and water into specially modified pet food bowls. Two holes were drilled into the bowls and bulkhead pass-throughs were inserted through the holes. The bulkhead pass-throughs allowed tubing to be attached to the bowls. One of the pass-throughs was the feed line the other the return. The liquid would fill up the bowl and then start draining out the

return pass-through, so the height of the return pass-through determined the height of the liquid in the bowl.

A.2 MATLAB Code

A.2.1 Filter Angular Velocity. Calculate Angular Acceleration and Displacement

```
clear all
close all

Program, based on Yu et al., 1999, determining optimum cutoff frequency from kinematic
data.

filename=['120628_1CR.txt'];
uppertime=20;
lowertime=10;
data=load(filename);
cal=(.187*180/pi/1000);
sampling=1000;
dt=1/sampling;
T=length(data)*dt;
time=dt:dt:T;
datatime = [data,time'];

Convert velocity data
baseline=mean(data(1:50));
vel=(baseline-data)./cal;

Integrate to determine excursion
disp=0;
for i=2:length(data)
  disp(i)=disp(i-1)+dt*vel(i);
end
disp=disp*180/pi;

correct for drift
slope=disp(length(disp))/time(length(time));
disp=disp-time*slope;

Differentiate to determine acceleration
for i=1:length(vel)-1
  accel(i)=(vel(i+1)-vel(i))/dt;
end
accel(length(vel))=0;

Determine optimum cutoff frequency based on sampling rate
MOCF=abs(0.071*sampling-0.00003*sampling^2);
```

```
Filter data using MOCF
cutoff=MOCF;
Wn=cutoff*2/sampling;
[z,p,k]=butter(2,Wn,'low');
[sos,g]=zp2sos(z,p,k);
h1=dfilt.df2sos(sos,g);
a=filter(h1,vel);
b=flipud(a);
c=filter(h1,b);
velf=flipud(c);

Integrate filtered signal to determine excursion
dispf=0;
for i=2:length(data)
  dispf(i)=dispf(i-1)+dt*velf(i);
end
dispf=dispf*180/pi;

Differentiate filtered signal to determine acceleration
for i=1:length(velf)-1
  accelf(i)=(velf(i+1)-velf(i))/dt;
end
accelf(length(velf))=0;

Estimate the relative mean residual between filtered and unfiltered data
SSN=sum((vel-velf).^2);
SSD=sum((vel-mean(vel)).^2);
vel_e=sqrt((SSN/SSD)*100);
SSN=sum((disp-dispf).^2);
SSD=sum((disp-mean(disp)).^2);
disp_e=sqrt((SSN/SSD)*100);
SSN=sum((accel-accelf).^2);
SSD=sum((accel-mean(accel)).^2);
accel_e=sqrt((SSN/SSD)*100);

Calculate final optimum cutoff frequency
cut_vel=abs(0.06*sampling-0.000022*sampling^2)+5.95/vel_e;
cut_disp=abs(0.06*sampling-0.000022*sampling^2)+5.95/disp_e;
cut_accel=abs(0.06*sampling-0.000022*sampling^2)+5.95/accel_e;

Refilter data using new cutoff frequency
cutoff=cut_vel;
Wn=cutoff*2/sampling;
[z,p,k]=butter(2,Wn,'low');
[sos,g]=zp2sos(z,p,k);
h1=dfilt.df2sos(sos,g);
```

```
a=filter(h1,vel);
b=flipud(a);
c=filter(h1,b);
vel_vel=flipud(c);
cutoff = 40;
Wn=cutoff*2/sampling;
if Wn>=1
  Wn=0.99;
end
[z,p,k]=butter(2,Wn,'low');
[sos,g]=zp2sos(z,p,k);
h1=dfilt.df2sos(sos,g);
a=filter(h1,vel);
b=flipud(a);
c=filter(h1,b);
vel_disp=flipud(c);
cutoff=cut_accel;
Wn=cutoff*2/sampling;
[z,p,k]=butter(2,Wn,'low');
[sos,g]=zp2sos(z,p,k);
h1=dfilt.df2sos(sos,g);
a=filter(h1,vel);
b=flipud(a);
c=filter(h1,b);
vel_accel=flipud(c);

Integrate filtered signal to determine excursion
disp2=0;
for i=2:length(data)
  disp2(i)=disp2(i-1)+dt*vel_disp(i);
end
disp2=disp2*180/pi;

correct for drift
slope=disp2(length(disp2))/time(length(time));
disp2=disp2-time*slope;

Differentiate filtered signal to determine acceleration
for i=1:length(vel_accel)-1
  accel2(i)=(vel_accel(i+1)-vel_accel(i))/dt;
end
accel2(length(vel_accel))=0;

Plots to check filtering

figure(1)
```

```
plot(time,disp,time,disp2)
title('Disp')
legend('unfiltered','filtered')

figure(2)
plot(time,vel,time,vel_vel)
title('Vel')
legend('unfiltered','filtered')

figure(3)
plot(time,accel,time,accel2)
title('Accel')
legend('unfiltered','filtered')
```

Plots for analysis

```
figure(4)

subplot(3,1,1)
plot(time,disp2)
xlabel('time(s)')
ylabel('displacement (deg)')
title(filename)

subplot(3,1,2)
plot(time,vel_vel)
xlabel('time(s)')
ylabel('velocity (rad/s)')

subplot(3,1,3)
plot(time,accel2)
xlabel('time(s)')
ylabel('acceleration (rad/s)')

figure(5)
subplot(3,1,1)
plot(time,disp2)
xlabel('time(s)')
ylabel('displacement (deg)')
title(filename)
axis([lowertime uppertime min(disp2) max(disp2)])

subplot(3,1,2)
plot(time,vel_vel)
xlabel('time(s)')
ylabel('velocity (rad/s)')
axis([lowertime uppertime min(vel_vel) max(vel_vel)])
```

```
subplot(3,1,3)
plot(time,accel2)
xlabel('time(s)')
ylabel('acceleration (rad/s)')
axis([lowertime uppertime min(accel2) max(accel2)])
```

A.2.2 Peak To Peak Angular Velocity, Displacement, and Acceleration

```
figure(1)
plot(vel_vel)

 The first data collection is for the velocity the second is for the displacement.
[vtupper, VelUpper] = ginput;
[vtlower, VelLower] = ginput;
 vtupper = round(vtupper);
buffer = 100; this buffer can be changed to look further ahead or behind the picked point
for the max value

VelPeaks = ones(length(vtupper),1);

This loop finds the max value near the picked value
for cntr=1:length(vtupper)
  lb = vtupper(cntr)-buffer;
  ub = vtupper(cntr)+buffer;
  maxmat = vel_vel(lb:ub);
  VelPeaks(cntr) = max(maxmat);
end
vtlower = round(vtlower);
buffer = 50;
VelVals = ones(length(vtupper),1);
for cntr=1:length(vtlower)
  lb = vtlower(cntr)-buffer;
  ub = vtlower(cntr)+buffer;
  minmat = vel_vel(lb:ub);
  VelVals(cntr) = min(minmat);
end
figure(1)
plot(disp2)

Data collection for displacement
[dtupper, DispUpper] = ginput;
[dtlower, DispLower] = ginput;
dtupper = round(dtupper); this rounds the values so you have an array of useable indices
from clicked points

buffer = 50;     This can be adjusted to give a larger or smaller window to select your
peak or valley

DispPeaks = ones(length(dtupper),1);
for cntr=1:length(dtupper)
  lb = dtupper(cntr)-buffer;
  ub = dtupper(cntr)+buffer;
```

```
  maxmat = disp2(lb:ub);
  DispPeaks(cntr) = max(maxmat);
end
dtlower = round(dtlower); this rounds the values so you have an array of useable indices from clicked points

buffer = 50;     This can be adjusted to give a larger or smaller window to select your peak or valley

DispVals = ones(length(dtlower),1);
for cntr=1:length(dtlower)
  lb = dtlower(cntr)-buffer;
  ub = dtlower(cntr)+buffer;
  minmat = disp2(lb:ub);
  DispVals(cntr) = min(minmat);
end
TotalDispVel = VelPeaks-VelVals;
AvgVelDisp = mean(TotalDispVel);
StdVel = std(TotalDispVel);
TotalDisp = DispPeaks-DispVals;
AvgDisp = mean(TotalDisp);
StdDisp = std(TotalDisp);
CombinedVelDisp = [TotalDispVel';TotalDisp'];
[Cycles columns] = size(DispUpper);
CycFreq = Cycles/(time(dtupper(Cycles))-time(dtupper(1)));
[maxacc t] = max(accel2);
[minacc t] = min(accel2);

change the file name each time the program is run or you will overwrite the data you had previously collected.
FileId = fopen('AngVelResults45.txt','w');
fprintf(FileId,'%50s\r\n','Peak to Peak values for velocity(rad/s) and displacement(deg)');
fprintf(FileId,'\r\n%15s %15s\r\n','P to P Velocity','P to P Disp.');
fprintf(FileId,'%4.4f     %4.4f\r\n', CombinedVelDisp);
fprintf(FileId,'\r\n%15s %15s\r\n','Avg Velocity','Avg Disp.');
fprintf(FileId,'%4.4f     %4.4f\r\n', AvgVelDisp, AvgDisp);
fprintf(FileId,'\r\n%15s %15s\r\n','Std Velocity','Std Disp.');
fprintf(FileId,'%4.4f     %4.4f\r\n', StdVel, StdDisp);
fprintf(FileId,'\r\n%20s\r\n','Max and Min Acceleration rad/s^2');
fprintf(FileId,'%4.4f    %4.4f\r\n',maxacc,minacc);
fprintf(FileId,'\r\n%20s\r\n','Frequency Hz');
fprintf(FileId,'%4.4f\r\n',CycFreq);

 closes the document so you can delete etc
fclose('all');
```

```
Acceleration extraction
figure(4)
plot(accel2)
[xxx yyy] = ginput;
xxx = round(xxx);
accel2 = accel2(xxx(1):xxx(2));
figure(4)
plot(accel2)

The first data collection is for the velocity the second is for the displacement.
[atupper, accUpper] = ginput;
[atlower, accLower] = ginput;
atupper = round(atupper);
buffer = 100; this buffer can be changed to look further ahead or behind the picked point
for the max value

AccPeaks = ones(length(atupper),1);

This loop finds the max value near the picked value
for cntr=1:length(atupper)
  lb = atupper(cntr)-buffer;
  ub = atupper(cntr)+buffer;
  maxmat = accel2(lb:ub);
  AccPeaks(cntr) = max(maxmat);
end
atlower = round(atlower);
buffer = 50;
AccVals = ones(length(atlower),1);
for cntr=1:length(atlower)
  lb = atlower(cntr)-buffer;
  ub = atlower(cntr)+buffer;
  minmat = accel2(lb:ub);
  AccVals(cntr) = min(minmat);
end
AvgAccVals = -1*mean(AccVals);
StdVals   = std(AccVals);
AvgAccPeaks = mean(AccPeaks);
StdPeaks = std(AccPeaks);
result = [AvgAccPeaks, StdPeaks, AvgAccVals, StdVals];
```

Table 4: Cyclic Study Test Data

ID	Test type	Avg PtoP Vel (rad/s)	Std Vel (rad/s)	Avg PtoP Disp (deg)	Std Disp (deg)	Avg Freq (Hz)
120531	2	45.666	1.7001	121.012	8.0158	2.6601
120629	2	45.3995	1.3446	118.581	4.4449	2.6954
121218	2	45.3609	2.8222	118.615	6.1813	2.6667
121220_1	2	47.008644	4.760667228	127.007	34.37227939	3.09768
121220_2	2	45.679225	2.975819693	112.626	10.25253952	3.07898
130116_1	1	NA	NA	NA	NA	NA
130116_2	1	NA	NA	NA	NA	NA
130124_1	1	NA	NA	NA	NA	NA
130124_2	1	NA	NA	NA	NA	NA
130206_1	1	NA	NA	NA	NA	NA
130206_2	1	NA	NA	NA	NA	NA
130214_1	3	47.412	2.8045	122.511	8.3308	2.7866
130214_2	3	47.9964	2.2114	121.511	9.288	2.733
130221_1	3	-	-	-	-	-
130221_2	3	43.5223	1.73736	126.272	7.5224	2.7326
130228_1	3	43.5682	0.6538	120.842	1.9424	2.7255
130228_2	3	44.0175	0.7193	121.674	2.5698	2.7405
130328_1	4	NA	NA	NA	NA	NA
130328_2	4	NA	NA	NA	NA	NA

Table 4 Continued

ID	Test type	Max Acc (rad/s^2)	Acc at Peaks (rad/s^2)	STD Peaks (ras/s^2)	Acc at Valley (rad/s^2)	STD Valleys (rad/s^2)
120531	2	2720.3239	1157.048484	216.168	1175.1428	419.463
120629	2	2876.4569	1262.672915	214.641	1843.550818	588.12
121218	2	2775.7371	1190.488041	100.494	1909.157362	425.236
121220_1	2	6220.9578	1553.295831	570.144	1991.216723	786.516
121220_2	2	4215.7348	1194.421281	331.201	1740.084693	951.547
130116_1	1	NA	NA	NA	NA	NA
130116_2	1	NA	NA	NA	NA	NA
130124_1	1	NA	NA	NA	NA	NA
130124_2	1	NA	NA	NA	NA	NA
130206_1	1	NA	NA	NA	NA	NA
130206_2	1	NA	NA	NA	NA	NA
130214_1	3	4227.4522	1326.508533	242.252	2263.369641	758.447
130214_2	3	6427.3506	1609.198863	893.166	2071.152617	693.027
130221_1	3	-	-	-	-	-
130221_2	3	2723	1169.785712	149.553	1775.808276	305.712
130228_1	3	2422.8336	1710.419105	242.822	1139.864369	65.9291
130228_2	3	2308.1449	1722.205746	234.978	1153.639004	116.432
130328_1	4	NA	NA	NA	NA	NA
130328_2	4	NA	NA	NA	NA	NA

Table 4 Continued¶

ID	Test type	Weight (kg)	max change nthi %	ICP Baseline (mmHg)	ICP max (mmHg)	ICP Max Avg (mmHg)	ICP total avg (mmHg)	ICP test avg (mmHg)
120531	2	-	NA	NA	NA	NA	NA	NA
120629	2	-	NA	NA	NA	NA	NA	NA
121218	2	-	NA	NA	NA	NA	NA	NA
121220_1	2	-	NA	NA	NA	NA	NA	NA
121220_2	2	-	NA	NA	NA	NA	NA	NA
130116_1	1	2.4	15.7	48.04	47.12	16.3562	-6.1	8.44
130116_2	1	2	16.4	19.532	12.988	9.18023	2.438	7.428
130124_1	1	2.162	21.3	-	-	-	-	-
130124_2	1	1.94	10.1	10.3121	22.1879	22.8111	1.2279	7.5979
130206_1	1	2.516	NA	NA	NA	NA	NA	NA
130206_2	1	2.887	20.3	4.0053	11.6547	5.52742	0.2097	4.1308
130214_1	3	1.643	4.63	NA	NA	NA	NA	NA
130214_2	3	2.004	9.35	NA	NA	NA	NA	NA
130221_1	3	2.163	15.94	NA	NA	NA	NA	NA
130221_2	3	2.126	6	NA	NA	NA	NA	NA
130228_1	3	2.372	5.52	NA	NA	NA	NA	NA
130228_2	3	2.06	8.5	NA	NA	NA	NA	NA
130328_1	4	2.337	-	NA	NA	NA	NA	NA
130328_2	4	-	0.2	NA	NA	NA	NA	NA

Table 4 Continued

ID	Test type	% Area injury	Eye Hemorrhage	RCNAC	Comp cycles	Notes
120531	2	0.00580584	eo	0	NA	male
120629	2	0.03673957	none	0	NA	
121218	2	0	eo, id	0	NA	
121220_1	2	0.05703812	none	0	NA	
121220_2	2	0.04002971	none	0	NA	
130116_1	1	0.03433491	na	0	NA	NIRS data may not be good due to poor adhesion of tape
130116_2	1	0.00804332	na	0	NA	
130124_1	1	0.0247197	na	0	NA	No Data collected from the DAQ, no ICP data
130124_2	1	0.03928204	id	0	NA	
130206_1	1	NA	none	0	NA	Quite a bit of leaking up cannula near the end
130206_2	1	0.01131908	eo	0.08153	NA	
130214_1	3	0	cb	0	8	
130214_2	3	0.0436758	none	0	9	
130221_1	3	0.07368664	none	0	7	No recorded cyclic data, slipped off bite plate about halfway through
130221_2	3	0.06194747	sc, eo	0	10	slipped off bite plate with appox 3 sec left
130228_1	3	0.01482363	eo	0	9	
130228_2	3	0.09173211	eo, rh	0	9	
130328_1	4	0.03884708	v	0	9	Animal had chest compressions applied
130328_2	4	0.04877472	eo	0	9	Used as thor. Compr. Control

APPENDIX B

CHAPTER 3 APPENDIX

B.1 Calculations of Clamping Forces

Figure 32 shows the free body diagram used to calculate the clamping forces seen at the optic nerve. The forces at the optic nerve were assumed to be perpendicular to the clamping face. Taking the sum of the moments about point O to be equal to zero, we get Eq. A3.1.

$$\sum M_O = 0 = -D_1 * F_{ON} - Fcos(\theta) * D_2 \qquad \text{A3.1}$$

where M_O is the moment about point O, D1 is the distance from the application of the force applied to the optic nerve to point O, F_{ON} is the force on the optic nerve, F is the handle force recorded by the load cell, θ is the angle required to find the force normal to D_2, and D_2 is the distance from the application of the handle force to point O. F_{ON} was then solved for. D_1 and θ were variable depending on the location of the optic nerve, and on how closed or open the forceps were. When solving for $F_{ON,}$ a D_1 roughly in the middle of the clamping portion of the forceps, and a θ in the nearly closed position were chosen which was thought to most accurately represent the actual test conditions.

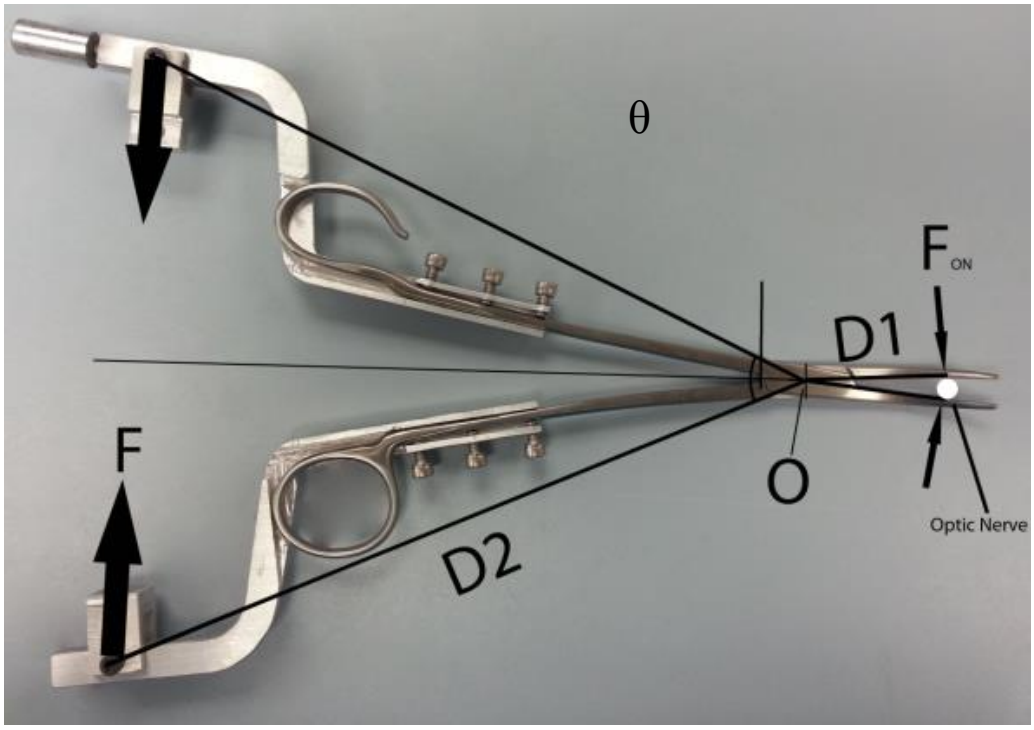

Figure 32: Free body diagram of the clamping assembly, note that F_{ON} is the force on the optic nerve and not the reaction force on the clamps.

B.2 MATLAB Code to Extract Force Data

```
clear,clc

A = uiimport;      This is going to open a user interface to import the file you want
pause

Once you have selected your file and named it put your cursor in the command window
and press enter

data = A.data;  creates a variable and extracts "data" out of struct A
ID = A.textdata{2,1};
forceRaw = data(:,1);
Fs = 300;        Sampling Frequency
N = 2;           Order
Fc = 3.5;        Cutoff Frequency

Construct an FDESIGN object and call its BUTTER method.
h = fdesign.lowpass('N,F3dB', N, Fc, Fs);
Hd = design(h, 'butter');
t = 0:1/Fs:(length(forceRaw)-1)/Fs;
t = round((t.*10000))./10000;

Filter the force data at cut off freq
a = filter(Hd,forceRaw);
b = flipud(a);
c = filter(Hd,b);
force = flipud(c);

PlotTitle = 'Pick bounding points for the regions of interest then press enter. ';
PlotTitle = strcat(PlotTitle, ID);
plot(force)
title(PlotTitle)
[boundsx boundsy] = ginput;
boundsx = round(boundsx);

j = 2;
for i = 1:2:length(boundsx)

  figure(j)
  plot(t(boundsx(i):boundsx(i+1))-t(boundsx(i)),force(boundsx(i):boundsx(i+1)).*4)
  xlabel('Time (s)')
  ylabel('Force (lbs)')
  maxF = max(force(boundsx(i):boundsx(i+1)));
  minF = abs(min(force(boundsx(i):boundsx(i+1))));
  maxForce(j-1) = max([maxF,minF]);
```

```
  j = j+1;
end
```

pick 8 points and export them, start point, two points in the linear force application region, 2 within the steady state plateau, 1 at the peak force 1 at the end of the plateau, finally 1 at the end point

```
for k = 1:length(cursor_info)
  coor(k,:) = cursor_info(1,k).Position;
end

coor = flipud(coor);
for l = 1:length(coor)
  indx(l) = find(t==coor(l,1));
end

 forRate = polyfit(t(indx(2):indx(3))',force(indx(2):indx(3)),1);
 forMax  = max(force(indx(1):indx(8)));
 forMean = mean(force(indx(4):indx(5)));
 platTime = t(indx(7))-t(indx(6));
 totTime = t(indx(8))-t(indx(1));
```

cyclic frequency and time extraction

use data cursor to select the start of the first peak as the first point and then a set of continuous peaks choose the end of the last peak as the final point

```
for k = 1:length(cursor_info)
  coor(k,:) = cursor_info(1,k).Position;
end

coor = flipud(coor);
totCyclicTime = coor(end,1)-coor(1,1); extracts the total time of the clamping
numOfPeaks = length(coor)-2;       extracts the total number of peaks minus the first and last
cyclicTime = coor(end-1,1)-coor(2,1);  finds the time between the second point and second to last point
cyclicFreq = numOfPeaks/cyclicTime;    calculates frequency by the total number of peaks in a time frame.
```

B.3 Percentage of Vessel Diameter Change

Table 5: Vessel diameter changes by group and eye. Action is the current state of the clamping sequence for the reported value. The grey highlighted cells indicate a positive change in vessel diameter.

Group (Eye # Initial state)	Action	Peak Force (lbs)	Proximal Change	Distal Change	Proximal Change from prior step	Distal Change from prior step	Hemorrhage
1 (1 Clamped)	Post Clamp 1	-	-7.63%	8.87%	-	-	No
	Clamp 2	3.65	35.17%	7.77%	42.80%	-1.10%	No
	Post clamp 2	-	26.58%	10.86%	-8.59%	3.09%	No
	Clamp 3	2.91	58.01%	36.51%	31.43%	25.65%	No
	Post clamp 3	-	79.20%	41.38%	21.20%	4.87%	Yes
1 (2 Preclamp)	Clamp 1	5.39	-63.49%	-14.86%	-	-	No
	Post clamp 1	-	43.98%	-9.37%	107.47%	5.49%	No
	Clamp 2	5.31	-56.36%	-53.59%	-100.34%	-44.22%	No
	Post clamp 2	-	-36.84%	-37.53%	19.53%	16.06%	No
2 (1 Preclamp)	Clamp 1	2.13	-14.53%	-5.43%	-	-	No
	Post clamp 1	2.05*	-22.66%	-9.48%	-8.14%	-4.05%	No†
2 (2 Preclamp)	Preclamp TC	-	2.05%	-10.79%	-	-	No
	Clamp 1	6.29	15.26%	-7.75%	13.20%	3.04%	No
	Clamp 2	6.22	25.76%	34.07%	10.50%	41.82%	Yes
2 (3 Preclamp)	Post clamp 1	4.58*	-5.99%	-14.05%	-	-	No
2 (4 Post clamp)	Post clamp 2	4.33	-14.77%	-7.18%	-	-	No
3 (1 Preclamp)	Post clamp 1	5.78*	4.51%	-3.88%	-	-	No
	Post clamp 3	~4*	28.35%	-2.51%	23.84%	1.37%	No

* indicates the peak force experienced and was not the force represented at that clamped state.
† indicates a hemorrhage occurred but there were no vessel diameters available to measure.

Table 6: Collected data from ON clamping study.

Animal	Group	Max Force Handle (lbs)	Max Force ON (lbs)	Average Plateau Force Handle (lbs)	Average Plateau Force ON (lbs)	Rate of Force Application (lbs/s)	Total Time (minutes)	Plateau Time (minutes)	Cyclic Time (minutes)	Frequency (Hz)	Hemorrhage (Y/N)
130509_1L	1	0.915	3.658	0.864	3.454	0.058	3.398	2.578	NA	NA	N
130509_1L	1	0.730	2.918	0.599	2.396	0.244	5.450	5.367	NA	NA	Y
130509_1R	2	0.534	2.134	0.368	1.474	0.032	2.320	1.859	NA	NA	N
130509_1R	2	0.512	2.046	0.330	1.318	0.128	1.391	1.229	NA	NA	Y
130509_2R	2	1.574	6.294	1.464	5.856	0.048	1.581	0.798	NA	NA	N
130509_2R	2	1.555	6.220	1.428	5.713	0.059	3.811	1.738	NA	NA	Y
130509_2L	1	1.350	5.399	1.213	4.853	0.057	4.061	3.545	NA	NA	N
130509_2L	1	-	5.311	1.129	4.514	-	-	-	NA	NA	N
130510_1R	2	1.056	4.224	0.972	3.887	0.035	1.666	0.655	NA	NA	N
130510_1R	2	1.083	4.331	0.958	3.831	0.021	5.870	5.421	NA	NA	N
130510_1R	3	NA	NA	NA	NA	NA	NA	NA	1.400	0.468	N
130510_1R	3	NA	NA	NA	NA	NA	NA	NA	0.9	-	N
130510_2R	2	1.019	4.078	0.845	3.380	0.081	5.318	5.174	NA	NA	N
130510_2R	2	1.145	4.579	1.069	4.276	0.462	2.252	2.186	NA	NA	N
130510_2L	2	1.445	5.781	1.292	5.169	0.066	4.989	4.578	NA	NA	N
130510_2L	2	1.407	5.629	1.246	4.984	0.049	7.591	6.826	NA	NA	N
130510_2L	3	NA	NA	NA	NA	NA	NA	NA	1.000	0.612	N
130510_2L	3	NA	NA	NA	NA	NA	NA	NA	0.367	0.920	N

- Data not available

APPENDIX C

CHAPTER 4 APPENDIX

C.1 **Arduino** Code

C.1.1 Cyclic Arduino Code

```
Variable declarations
 int StepPin=13;
 int DirPin=12;
 int NumSteps, NumIndent, dwell, StepTime, i, j, m, k;
 MSx is a pin on the stepper driver to control the microstepping. See documentation for
stepper driver to set

 int MS3=8;
 int MS2=9;
 int MS1=10;
 int IndentRate;
 float depth;
 char LR, center;
 unsigned long TimeStart;

void setup()
{
  Serial.begin(38400);
  Serial.read();
  Declares which pins will be used
  pinMode(StepPin, OUTPUT);
  pinMode(DirPin, OUTPUT);
  pinMode(MS3, OUTPUT);
  pinMode(MS2, OUTPUT);
  pinMode(MS1, OUTPUT);

  Microstepping is set for eighth steps to zero the LVDT
  digitalWrite(MS3, LOW);
  digitalWrite(MS2, HIGH);
```

```
  digitalWrite(MS1, HIGH);

  Initializes center to enter the loop to center LVDT
  center = 'N';

  StepTime=300;
  This is used to zero the LVDT
   while(center=='N'||center=='n')
   {
    j = 1;  initializes or resets the centering counter

    Serial.println("Do you need to go Left or Right? L/R");
    while(Serial.available() ==0){}
    LR = Serial.read();

    Serial.println("Enter the number of steps you would like to move.");
    while(Serial.available()==0){}
    NumSteps=Serial.parseInt();

    Sets the direction of the stepper motor
    if (LR=='L'||LR=='l')
    {
     digitalWrite(DirPin,HIGH);
    }

    else
    {
     digitalWrite(DirPin,LOW);
    }

    Steps the number of steps entered
    for(j; j<=NumSteps; j++)
     {
      digitalWrite(StepPin, HIGH);
      delayMicroseconds(StepTime);
      digitalWrite(StepPin, LOW);
      delayMicroseconds(StepTime);

     }

    Serial.println("Is the LVDT zeroed? Y/N");
    while(Serial.available() ==0){}
    center = Serial.read();
   }
}
```

```
void loop()
{
 This section controls the actual indentation
 Serial.println("Enter the depth of indentation in mm.");
 while(Serial.available() ==0){}
 depth=Serial.parseFloat();
 This sets the microstepping to quarter steps
 digitalWrite(MS3, LOW);
 digitalWrite(MS2, HIGH);
 digitalWrite(MS1, LOW);

 Serial.print("Depth ");
 Serial.print(depth);
 Serial.println("mm Cyclic.");

 NumSteps=depth/12.7*180/3.14159/.225;
 dwell=5;
 StepTime=.9/4*3.14159/180/2/(depth*2/.33/12.7)*1000*1000;

 starts recording time for the thirty second cycle
 TimeStart = millis();

 do
 {


    i=0;    counter for steps in
    k=0;    counter for steps out

   for(i; i<=NumSteps; i++)
   {
    digitalWrite(DirPin, LOW);
    digitalWrite(StepPin, HIGH);
    delayMicroseconds(StepTime);
    digitalWrite(StepPin, LOW);
    delayMicroseconds(StepTime);
   }

    delayMicroseconds(StepTime);
   for(k; k<=NumSteps; k++)
   {
    digitalWrite(DirPin, HIGH);
    digitalWrite(StepPin, HIGH);
    delayMicroseconds(StepTime);
    digitalWrite(StepPin, LOW);
    delayMicroseconds(StepTime);
```

```
    }


  }while(millis()-TimeStart<=30000);
}
```

C.1.2 Single Indentation Arduino Code

```
Variable declarations
 int StepPin=13;
 int DirPin=12;
 int NumSteps, NumIndent, dwell, StepTime, i, j, m, k;
 MSx is a pin on the stepper driver to control the microstepping.  See documentation for
stepper driver to set
 int MS3=8;
 int MS2=9;
 int MS1=10;

 int IndentRate;
 float depth;
 char LR, center;

void setup()
{
  Serial.begin(38400);
  Serial.read();
  Declares which pins will be used
  pinMode(StepPin, OUTPUT);
  pinMode(DirPin, OUTPUT);
  pinMode(MS3, OUTPUT);
  pinMode(MS2, OUTPUT);
  pinMode(MS1, OUTPUT);

  Microstepping is set for eighth steps to zero the LVDT
  digitalWrite(MS3, LOW);
  digitalWrite(MS2, HIGH);
  digitalWrite(MS1, HIGH);

  Initializes center to enter the loop to center LVDT
  center = 'N';
  StepTime=300;

  This is used to zero the LVDT
   while(center=='N'||center=='n')
```

```
  {
   j = 1;  initializes or resets the centering counter
   Serial.println("Do you need to go Left or Right? L/R");
   while(Serial.available() ==0){}
   LR = Serial.read();

   Serial.println("Enter the number of steps you would like to move.");
   while(Serial.available()==0){}
   NumSteps=Serial.parseInt();

   Sets the direction of the stepper motor
   if (LR=='L'||LR=='l')
   {
    digitalWrite(DirPin,HIGH);
   }
   else
   {
    digitalWrite(DirPin,LOW);
   }

   Steps the number of steps entered
   for(j; j<=NumSteps; j++)
    {
     digitalWrite(StepPin, HIGH);
     delayMicroseconds(StepTime);
     digitalWrite(StepPin, LOW);
     delayMicroseconds(StepTime);
    }
   Serial.println("Is the LVDT zeroed? Y/N");
   while(Serial.available() ==0){}
   center = Serial.read();
  }
}

void loop()
{
 This section controls the actual indentation
 Serial.println("Enter the depth of indentation in mm.");
 while(Serial.available() ==0){}
 depth=Serial.parseFloat();

 Serial.println("Enter the indentation rate in mm/s.");
 while(Serial.available() ==0){}
 IndentRate=Serial.parseInt();

 Controls the low rate stepping
```

```
if(IndentRate==1)
{
 Serial.print("Depth ");
 Serial.print(depth);
 Serial.println("mm Low Rate.");
 This sets the microstepping to quarter steps
 digitalWrite(MS3, LOW);
 digitalWrite(MS2, HIGH);
 digitalWrite(MS1, LOW);

 NumSteps=depth/12.7*180/3.14159/.225;
 NumIndent=1;
 dwell=5;
 StepTime=25;

 m=1;    counter for indentations
 i=0;    counter for steps in
 k=0;    counter for steps out

 delay(500);

 for(m; m<=NumIndent; m++)
 {
  i=0;    counter for steps in
  k=0;    counter for steps out

  for(i; i<=NumSteps; i++)
  {
   digitalWrite(DirPin, LOW);
   digitalWrite(StepPin, HIGH);
   delay(StepTime);
   digitalWrite(StepPin, LOW);
   delay(StepTime);
  }

  delay(dwell*1000);

  for(k; k<=NumSteps; k++)
  {
   digitalWrite(DirPin, HIGH);
   digitalWrite(StepPin, HIGH);
   delay(StepTime);
   digitalWrite(StepPin, LOW);
   delay(StepTime);
  }
    delay(500);
```

```
    Serial.read();
   }
  }

Controls the high rate stepping
   if(IndentRate==100)
  {
   Serial.print("Depth ");
   Serial.print(depth);
   Serial.println("mm High Rate.");
   This sets the microstepping to quarter steps
   digitalWrite(MS3, LOW);
   digitalWrite(MS2, HIGH);
   digitalWrite(MS1, LOW);

   NumSteps=depth/12.7*180/3.14159/.225;
   NumIndent=1;
   dwell=5;
   StepTime=600;

   m=1;    counter for indentations
   i=0;    counter for steps in
   k=0;   counter for steps out

   delay(dwell);

   for(m; m<=NumIndent; m++)
   {
    i=0;    counter for steps in
    k=0;    counter for steps out

   for(i; i<=NumSteps; i++)
   {
    digitalWrite(DirPin, LOW);
    digitalWrite(StepPin, HIGH);
    delayMicroseconds(StepTime);
    digitalWrite(StepPin, LOW);
    delayMicroseconds(StepTime);
   }
   delay(dwell*1000);

   for(k; k<=NumSteps; k++)
   {
    digitalWrite(DirPin, HIGH);
    digitalWrite(StepPin, HIGH);
    delayMicroseconds(StepTime);
```

```
      digitalWrite(StepPin, LOW);
      delayMicroseconds(StepTime);
     }
     delay(dwell);
    }
   }
   Serial.read();
}
```

C.2 MATLAB Code

C.2.1 Single Indentation Data

```
clear,clc

A = uiimport;          This is going to open a user interface to import the file you want
                       Once you have selected your file and named it put your cursor in
                       the command window and press enter

UIData = A.data;    creates a variable and extracts "data" out of struct A

extract data streams
pressureRaw = UIData(:,1).*94.51-161.25;       converts voltage to pressure (mmHg)
dispRaw     = UIData(:,2).*(25.4/1.1401/15);   converts   voltage to displacement (mm)
forceRaw    = UIData(:,3).*4.448;              extracts force in lbs

R = length( UIData);

samFreq = 300;       change this to the sample frequency from the imported file
t = 0:1/samFreq:(R-1)/samFreq;
t = 10000.*t;
t = round(t);
t = t./10000;

if samFreq==10000
   t = t(1:33:end);
   pressureRaw = pressureRaw(1:33:end);
   dispRaw = dispRaw(1:33:end);
   forceRaw = forceRaw(1:33:end);

end
load('Filter_30hz.mat')

filters pressure data
a = filter(Filter_30hz,pressureRaw);
b = flipud(a);
c = filter(Filter_30hz,b);
pressureFil = flipud(c);

filters displacement data
a = filter(Filter_30hz,dispRaw);
b = flipud(a);
c = filter(Filter_30hz,b);
dispFil = flipud(c);
```

```
filters force data
a = filter(Filter_30hz,forceRaw);
b = flipud(a);
c = filter(Filter_30hz,b);
forceFil = flipud(c);

DispBaseline = mean(dispFil(1:100));   Finds the avg of the first 100 disp points
AdjDisp = dispFil-DispBaseline;       Subtracts the avg from the disp plots to zero the plot

figure(1)
plot(pressureFil)
title('Pick 2 plateau points then press enter')

[numpick, Ppick] = ginput;              Always pick 5 points
rnumpick = round(numpick);
clf

This plot is to choose points to calc the leading slope pressure
figure(1)
plot(t(rnumpick(2):rnumpick(3)),pressureFil(rnumpick(2):rnumpick(3)))
title('Pick 2 points with data cursor export as cursor_info')

calculates Pressure vs Disp correlation (slope) leading slope
xval1 = cursor_info(2).DataIndex+rnumpick(2);
xval2 = cursor_info(1).DataIndex+rnumpick(2);
leadSlopeP = polyfit(dispFil(xval1:xval2),pressureFil(xval1:xval2),1);

This plot is to choose points to calculate the end slope pressure
figure(1)
plot(t(rnumpick(4):rnumpick(5)),pressureFil(rnumpick(4):rnumpick(5)))
title('Pick 2 points then press enter')

calculates Pressure vs Disp correlation (slope) trailing slope
xval1 = cursor_info(2).DataIndex+rnumpick(4);
xval2 = cursor_info(1).DataIndex+rnumpick(4);
endSlopeP = polyfit(dispFil(xval1:xval2),pressureFil(xval1:xval2),1);

This plot is to choose points to calculate the leading slope force
figure(1)
plot(t(rnumpick(2):rnumpick(3)),forceFil(rnumpick(2):rnumpick(3)))
title('Pick 2 points then press enter')

xval1 = cursor_info(2).DataIndex+rnumpick(2);
xval2 = cursor_info(1).DataIndex+rnumpick(2);
endSlopeP = polyfit(dispFil(xval1:xval2),pressureFil(xval1:xval2),1);
```

```
This plot is to choose points to calculate the end slope force
figure(1)
plot(t(rnumpick(4):rnumpick(5)),forceFil(rnumpick(4):rnumpick(5)))
title('Pick 2 points then press enter')
[xvalfe,yvalfe] = ginput;            Pick 2 points only
xvalfe = round(xvalfe.*10000)./10000;
clf

This plot is to choose points to calculate the leading slope disp
figure(1)
plot(t(rnumpick(2):rnumpick(3)),dispFil(rnumpick(2):rnumpick(3)))
title('Pick 2 points then press enter')
[xvald,yvald] = ginput;            Pick 2 points only
xvald = round(xvald.*10000)./10000;
clf

This plot is to choose points to calculate the end slope disp
figure(1)
plot(t(rnumpick(4):rnumpick(5)),dispFil(rnumpick(4):rnumpick(5)))
title('Pick 2 points then press enter')
[xvalde,yvalde] = ginput;            Pick 2 points only
xvalde = round(xvalde.*10000)./10000;
clf

This calculates the leading slope
leadSlopeP = (yval(2)-yval(1))/(xval(2)-xval(1));        pressure
leadSlopeF = (yvalf(2)-yvalf(1))/(xvalf(2)-xvalf(1));    force
leadSlopeD = (yvald(2)-yvald(1))/(xvald(2)-xvald(1));

This calculates the slope on the trailing side.
endSlopeP = (yvale(2)-yvale(1))/(xvale(2)-xvale(1));     pressure
endSlopeF = (yvalfe(2)-yvalfe(1))/(xvalfe(2)-xvalfe(1)); force
endSlopeD = (yvalde(2)-yvalde(1))/(xvalde(2)-xvalde(1));

This calc. the avg plateau value
platavg = mean(pressureFil(rnumpick(3):rnumpick(4)));
platslope= polyfit(pressureFil(rnumpick(3):rnumpick(4)),t(rnumpick(3):rnumpick(4))',1);

[maxPress MPI]= max(pressureFil);
[maxDisp MDI]= max(AdjDisp);
[maxForce MFI]= min(forceFil);

datacollection = [endSlopeD endSlopeF endSlopeP leadSlopeD leadSlopeF...
    leadSlopeP maxDisp maxForce maxPress platavg];

close('1')
```

```
figure(2)
plot(t(rnumpick(1):rnumpick(5)),pressureRaw(rnumpick(1):rnumpick(5))...
    ,t(rnumpick(1):rnumpick(5)),pressureFil(rnumpick(1):rnumpick(5)))
title('Filtered and Raw Pressure data')
xlabel('time (s)')
ylabel('mmHg')

figure(3)
plot(t(rnumpick(1):rnumpick(5)),dispRaw(rnumpick(1):rnumpick(5))...
    ,t(rnumpick(1):rnumpick(5)),dispFil(rnumpick(1):rnumpick(5)))
title('Filtered and Raw displacement data')
xlabel('time (s)')
ylabel('mm')

figure(4)
plot(t(rnumpick(1):rnumpick(5)),forceRaw(rnumpick(1):rnumpick(5))...
    ,t(rnumpick(1):rnumpick(5)),forceFil(rnumpick(1):rnumpick(5)))
title('Filtered and Raw force data')
xlabel('time (s)')
ylabel('N')
```

C.2.2 Plateau Values

```
clear,clc

A = uiimport;          This is going to open a user interface to import the file you want
pause

Once you have selected your file and named it put your cursor in the command  window
and press enter

UIData = A.data;    creates a variable and extracts "data" out of struct A

extract data streams
pressureRaw = UIData(:,1).*94.51-161.25;    converts voltage to pressure  (mmHg)
dispRaw     = UIData(:,2).*(25.4/1.1401/15);     converts voltage to displacement (mm)
forceRaw    = UIData(:,3).*4.448;               extracts force in N
R = length( UIData);
samFreq = 300;             The if statement below changes this if sample freq is not 300 Hz.
t = 0:1/samFreq:(R-1)/samFreq;
Fs = 300;        Sampling Frequency
N  = 2;          Order
Fc = 21;          Cutoff Frequency

Construct an FDESIGN object and call its BUTTER method.
h  = fdesign.lowpass('N,F3dB', N, Fc, Fs);
Hd = design(h, 'butter');

if strcmp(A.textdata{3,1},'Sample Clock Rate,10000.00')
   samFreq = 10000;         change this to the sample frequency from the imported file
   t = 0:1/samFreq:(R-1)/samFreq;
   t = 10000.*t;
   t = round(t);
   t = t./10000;

   Fs = 10000;           Sampling Frequency
   N  = 2;        Order
   Fc = 147;     Cutoff Frequency

Construct an FDESIGN object and call its BUTTER method.
   h  = fdesign.lowpass('N,F3dB', N, Fc, Fs);
   Hd = design(h, 'butter');
   t = t(1:33:end);
   pressureRaw = pressureRaw(1:33:end);
   dispRaw = dispRaw(1:33:end);
   forceRaw = forceRaw(1:33:end);
end
```

```
filters pressure data
a = filter(Hd,pressureRaw);
b = flipud(a);
c = filter(Hd,b);
pressureFil = flipud(c);

filters displacement data
a = filter(Hd,dispRaw);
b = flipud(a);
c = filter(Hd,b);
dispFil = flipud(c);

filters force data
a = filter(Hd,forceRaw);
b = flipud(a);
c = filter(Hd,b);
forceFil = flipud(c).*-1;

DispBaseline = mean(dispFil(1:100));   Finds the avg of the first 100 disp points
AdjDisp = dispFil-DispBaseline;
AdjForce = forceFil-mean(forceFil(1:100));

figure(1)
plot(pressureFil)
title('Pick 2 plateau points then press enter')

[numpick, Ppick] = ginput
rnumpick = round(numpick);
close all

avgPlatForce = mean(forceFil(rnumpick(1):rnumpick(2)));
avgPlatPress = mean(pressureFil(rnumpick(1):rnumpick(2)));
```

C.2.3 Cyclic Indentations

```
clear,clc

A = uiimport;          This is going to open a user interface to import the file you want
pause

Once you have selected your file and named it put your cursor in the command  window
and press enter

UIData = A.data;    creates a variable and extracts "data" out of struct A

extract data streams
pressureRaw = UIData(:,1).*94.51-161.25;    converts voltage to pressure (mmHg)
dispRaw     = UIData(:,2).*(25.4/1.1401/15);     converts voltage to displacement (mm)
forceRaw    = UIData(:,3).*4.448;               extracts force in N

R = length( UIData);

samFreq = 300;         The if statement below changes this if sample freq is not 300 Hz.
t = 0:1/samFreq:(R-1)/samFreq;

Fs = 300;        Sampling Frequency
N  = 2;          Order
Fc = 21;         Cutoff Frequency

Construct an FDESIGN object and call its BUTTER method.
h  = fdesign.lowpass('N,F3dB', N, Fc, Fs);
Hd = design(h, 'butter');

if strcmp(A.textdata{3,1},'Sample Clock Rate,10000.00')
   samFreq = 10000;         change this to the sample frequency from the imported file
   t = 0:1/samFreq:(R-1)/samFreq;
   t = 10000.*t;
   t = round(t);
   t = t./10000;
   Fs = 10000;           Sampling Frequency
   N  = 2;        Order
   Fc = 21;       Cutoff Frequency

Construct an FDESIGN object and call its BUTTER method.
   h  = fdesign.lowpass('N,F3dB', N, Fc, Fs);
   Hd = design(h, 'butter');
   t = t(1:33:end);
   pressureRaw = pressureRaw(1:33:end);
   dispRaw = dispRaw(1:33:end);
```

```
   forceRaw = forceRaw(1:33:end);
end

filters pressure data
a = filter(Hd,pressureRaw);
b = flipud(a);
c = filter(Hd,b);
pressureFil = flipud(c);

filters displacement data
a = filter(Hd,dispRaw);
b = flipud(a);
c = filter(Hd,b);
dispFil = flipud(c);

filters force data
a = filter(Hd,forceRaw);
b = flipud(a);
c = filter(Hd,b);
forceFil = flipud(c).*-1;

DispBaseline = mean(dispFil(1:100));   Finds the avg of the first 100 disp points
AdjDisp = dispFil-DispBaseline;
AdjForce = forceFil-mean(forceFil(1:100));

figure(1)
plot(pressureFil)
title('Pick the first peak then press enter')

[numpick, Ppick] = ginput;
rnumpick = round(numpick);
clf

for i=1:86
   [PressMax(i) PressLoc(i)] = max(pressureFil(rnumpick:rnumpick+100));
   [DispMax(i) DispLoc(i)] = max(AdjDisp(rnumpick:rnumpick+100));
   [ForceMax(i) ForceLoc(i)] = max(AdjForce(rnumpick:rnumpick+100));
   tnew = t(rnumpick:rnumpick+100);
   tpmax(i) = tnew(PressLoc(i));
   tdmax(i) = tnew(DispLoc(i));
   tfmax(i) = tnew(ForceLoc(i));
   rnumpick = rnumpick+PressLoc(i)+50;

end

combinedData = [PressMax; DispMax; ForceMax];
```

```
plot(t,pressureFil,tpmax,PressMax,'rx')
title('Filtered Pressure and its peaks')
xlabel('Time (s)')
ylabel('Pressure (mmHg)');
legend('Filtered data','Peaks')

FileId = fopen('CyclicResults\120731_27C1.csv','a');
fprintf(FileId,'%4.4f        %4.4f        %4.4f\r\n', combinedData);
fprintf(FileId,'\nEof\n');

fclose('all');
```

C.2.4 Cyclic Pressurization Rate

```
clear,clc

A = uiimport;       This is going to open a user interface to import the file you want
pause

Once you have selected your file and named it put your cursor in the command window
and press enter

UIData = A.data;    creates a variable and extracts "data" out of struct A


extract data streams
pressureRaw = UIData(:,1).*94.51-161.25;    converts voltage to pressure ( mmHg)
dispRaw     = UIData(:,2).*(25.4/1.1401/15);     converts voltage to displacement (mm)
forceRaw    = UIData(:,3).*4.448;               extracts force in lbs

R = length( UIData);

samFreq = 300;         The if statement below changes this if sample freq is not 300 Hz.
t = 0:1/samFreq:(R-1)/samFreq;
Fs = 300;          Sampling Frequency
N  = 2;            Order
Fc = 21;           Cutoff Frequency

Construct an FDESIGN object and call its BUTTER method.
h  = fdesign.lowpass('N,F3dB', N, Fc, Fs);
Hd = design(h, 'butter');

if strcmp(A.textdata{3,1},'Sample Clock Rate,10000.00')
   samFreq = 10000;         change this to the sample frequency from the imported file
   t = 0:1/samFreq:(R-1)/samFreq;
   t = 10000.*t;
   t = round(t);
   t = t./10000;
   Fs = 10000;           Sampling Frequency
   N  = 2;         Order
   Fc = 21;        Cutoff Frequency

Construct an FDESIGN object and call its BUTTER method.
   h  = fdesign.lowpass('N,F3dB', N, Fc, Fs);
   Hd = design(h, 'butter');

   t = t(1:33:end);
   pressureRaw = pressureRaw(1:33:end);
```

```
    dispRaw = dispRaw(1:33:end);
    forceRaw = forceRaw(1:33:end);
end

filters pressure data
a = filter(Hd,pressureRaw);
b = flipud(a);
c = filter(Hd,b);
pressureFil = flipud(c);

filters displacement data
a = filter(Hd,dispRaw);
b = flipud(a);
c = filter(Hd,b);
dispFil = flipud(c);

filters force data
a = filter(Hd,forceRaw);
b = flipud(a);
c = filter(Hd,b);
forceFil = flipud(c).*-1;

figure(2)
plot(t,pressureFil)
 title('Zoom in on several of the peaks and select 2 points in the linear region of each')
xlabel('Time (s)')
ylabel('Pressure (mmHg)');

clear('coor','modulus', 'indentRate')

for k = 1:length(cursor_info)
    coor(k)  = cursor_info(k).DataIndex;
end
coor = coor';

coor = flipud(coor);

k = 1;
for i=1:2:length(coor)

    modulus(k,:)     = polyfit(dispFil(coor(i):coor(i+1)),pressureFil(coor(i):coor(i+1)),1);
    indentRate(k,:)  = polyfit(t(coor(i):coor(i+1))',dispFil(coor(i):coor(i+1)),1);
    k = k+1;
end

avgModulus = mean(modulus(:,1));
```

```
avgIndentRate = mean(indentRate(:,1));
```

C.3 Single Indentation Data

Table 7: Collected Data from Single Indentation Studies

Animal #	Indentation rate (mm/s)	Return rate (mm/s)	Indentation Depth (mm)	Rate of Force Application (N/s)	Rate of Force Retraction (N/s)	Max Force (N)	Avg. Plateau Force (N)
2	0.99	-1.06	0.93	-0.08	0.05	0.19	0.12
2	53.62	-48.73	1.00	-3.22	2.40	0.26	0.12
2	0.94	-0.99	1.85	-0.08	0.04	0.26	0.22
2	54.45	-52.61	1.89	-7.57	2.03	0.37	0.16
2	0.94	-0.98	2.79	-0.05	0.08	0.28	0.17
2	55.14	-54.21	2.76	-9.44	1.83	0.48	0.35
2	0.94	-1.00	3.82	-0.12	0.11	0.37	0.20
2	48.77	-52.55	3.78	-9.56	12.04	0.50	0.22
2	0.93	-0.98	4.73	-0.05	0.08	0.38	0.31
2	53.28	-52.74	4.71	-9.71	4.33	0.85	0.25
2	0.94	-0.97	5.71	-0.08	0.09	0.56	0.25
2	55.66	-54.79	5.68	-10.12	7.99	0.99	0.45
2	0.91	-0.94	6.69	-0.06	0.10	0.58	0.28
2	56.31	-56.82	6.83	-6.74	10.44	0.85	0.34
2	55.90	-58.02	6.72	-8.97	17.89	0.99	0.60
3	1.04	-0.99	1.09	-0.04	0.07	0.24	0.42
3	51.02	-62.15	0.96	-1.56	0.96	0.21	0.46
3	0.93	-0.99	1.91	-0.07	0.06	0.27	0.81
3	52.27	-57.80	1.87	-2.60	1.06	0.32	0.42
3	0.94	-0.95	2.85	-0.06	0.07	0.31	0.48
3	52.93	-57.50	2.81	-4.15	1.95	0.48	0.66
3	0.93	-0.99	3.79	-0.06	0.06	0.35	0.11
3	55.44	-52.46	3.79	-7.79	0.80	0.46	0.12
3	0.93	-0.98	4.75	-0.07	0.05	0.60	0.19
3	52.14	-55.59	4.72	-7.97	7.45	0.75	0.17
3	0.94	-0.98	5.74	-0.10	0.09	0.65	0.17
3	54.49	-56.96	5.72	-6.59	1.16	0.66	0.26
3	0.96	-0.99	6.70	-0.13	0.12	0.66	0.19
3	56.86	-55.27	6.67	-7.97	7.43	1.00	0.21
4	-1.70	-1.00	1.02	-0.18	0.35	0.38	0.28
4	13.91	-22.33	1.01	-0.22	2.16	0.34	0.42
4	0.92	-0.96	1.93	-0.09	0.13	0.48	0.49
4	35.10	-42.90	1.93	-1.32	4.12	0.54	0.25
4	0.92	-0.97	2.93	-0.11	0.10	0.43	0.25
4	54.13	-55.27	2.91	-10.22	4.21	0.49	0.70
4	49.39	-52.92	2.98	-14.34	4.64	0.67	0.31
4	51.46	-56.12	2.98	-19.20	11.77	0.83	0.35
4	0.98	-0.95	3.90	-0.13	0.19	0.63	0.57
4	57.78	-55.09	3.88	-17.78	16.12	1.12	0.43
4	0.95	-0.96	4.86	-0.19	0.29	0.96	0.30
4	56.18	-57.09	4.80	-12.64	5.44	1.13	0.96
4	0.94	-0.97	5.83	-0.26	0.35	1.43	0.89
4	57.02	-60.68	5.11	-21.11	19.79	1.64	0.44
4	58.37	-62.53	5.80	-24.56	34.69	1.61	0.52
4	0.95	-0.95	6.79	-0.15	0.31	1.28	0.44
4	58.42	-60.16	5.98	-21.16	20.93	1.90	1.29

Table 7 continued

Animal #	Pressurization Rate (mmHg/s)	Depressurization Rate (mmHg/s)	Max Pressure (mmHg)	Avg. Plateau Pressure (mmHg)
2	19.26	-3.64	24.42	16.79
2	986.89	-1015.11	25.56	15.96
2	15.04	-8.75	30.79	22.33
2	1478.50	-239.19	58.67	23.64
2	11.99	-12.12	38.72	28.94
2	1438.78	-550.57	74.65	27.44
2	12.00	-11.50	52.05	35.19
2	1214.58	-813.39	82.86	35.03
2	9.11	-9.27	54.63	37.50
2	1603.22	-768.30	131.42	41.64
2	12.31	-9.66	83.95	59.11
2	1789.01	-1167.10	175.94	63.66
2	9.47	-9.88	85.14	62.04
2	1296.04	-1032.31	141.81	67.81
2	1688.04	-1353.59	177.96	86.99
3	6.40	-10.42	20.63	16.56
3	938.99	-802.21	28.76	17.14
3	12.70	-12.59	38.19	26.34
3	1331.82	-934.73	46.39	24.40
3	9.69	-10.27	41.07	31.64
3	1217.50	-1207.82	71.94	32.08
3	9.00	-11.01	49.62	37.39
3	1241.89	-737.62	82.93	37.39
3	9.46	-9.85	65.88	48.88
3	1566.88	-674.43	130.02	54.09
3	13.65	-9.70	94.52	67.41
3	1197.45	-1024.06	108.02	45.25
3	20.77	-18.18	98.06	71.54
3	1746.72	-1031.76	171.70	69.54
4	21.25	-18.55	61.93	50.55
4	26.96	-102.40	75.61	42.72
4	9.95	-16.37	79.63	59.50
4	104.69	-375.34	115.74	51.84
4	41.73	-13.25	95.37	64.82
4	836.42	-552.50	82.49	61.77
4	92.50	-819.60	73.91	42.90
4	2192.94	-1376.39	131.76	89.51
4	11.51	-27.11	101.18	77.88
4	1901.89	-1716.44	173.82	125.00
4	31.74	-43.95	155.29	111.85
4	1603.08	-1268.14	159.42	103.20
4	31.91	-71.78	204.73	146.47
4	1951.83	-1807.08	220.06	153.18
4	2797.58	-1906.89	241.91	151.66
4	14.50	-48.76	185.36	124.47
4	2398.71	-3022.00	279.18	231.35

REFERENCES

[1] M. Faul, L. Xu, M. Wald and V. Coronado, "Traumatic brain injury in the United States: emergency department visits, hospitalizations, and deaths. 2002-2006," CDC, N.C.f.l.P.a.C., Atlanta, 2010.

[2] J. Friedman, P. Reed, P. Sharplin and P. Kelly, "Primary prevention of pediatric abusive headtrauma: A cost audit and cost-utility analysis," *Child Abuse & Neglect,* vol. 36, pp. 760-770, 2012.

[3] K. M. &. M. R. A. Barlow, "Annual incidence of shaken impact syndrome in young children.," *The Lancet,* vol. 356, no. 1, p. 1571–1572, 2000.

[4] A. C. Duhaime, T. A. Gennarelli, L. E. Thibault, D. A. Bruce, S. S. Margulies and R. Wiser, "The shaken baby syndrome: A clinical, pathological, and biomechanical study," *Journal of Neurosurgery,* vol. 66, pp. 409-415, 1987.

[5] B. Harding, R. Risdon and H. Krous, "Shaken Baby Syndrome," *British Medical Journal,* vol. 328, no. 7442, pp. 720-721, 2004.

[6] C. H. Kempe, F. N. Silverman, B. F. Steele, W. Droegemueller and H. K. Silver, "The Battered-Child Syndrome," *The Journal of the American Medical Association,* vol. 181, pp. 17-24, 1962.

[7] J. Caffey, "The Whiplash Shaken Infant Syndrome: Manual Shaking by the Extremities With Whiplash-Induced Intracranial and Intraocular Bleedings, Linked with Residual Permanent Brain Damage and Mental Retardation," *Pediatrics,* vol. 54, pp. 396-403, 1974.

[8] T. A. Gennarelli, L. E. Thibault, J. H. Adams, D. I. Graham, C. J. Thompson and R. P. Marcincin, "Diffuse Axonal Injury and Traumatic Coma in the Primate.," *Annals of Neurology,* vol. 12, no. 6, pp. 564-574, 1982.

[9] M. T. Prange, B. Coats, A. C. Duhaime and S. S. Margulies, "Anthropomorphic simulations of falls, shakes, and inflicted impacts in infants," *Journal of Neurosurgery,* vol. 99, pp. 143-150, 2003.

[10] J. W. Finnie, P. C. Blumbergs and M. R. V, "Pattern of cerebrospinal immediate early gene c-fos expression in an ovine model of non-accidental head injury," *Journal of Clinical Neuroscience,* vol. 20, no. 12, pp. 1759-1761, 2013.

[11] J. W. Finnie, P. C. Blumbergs, J. Manavis, R. J. Turner, S. Helps, V. R, R. W. Byard, G. Chidlow, B. Sandoz, J. Dutschke and R. Anderson, "Neuropathological changes in a lamb model of non-accidental head injury (the shaken baby syndrome)," *Journal of Clinical Neuroscience,* vol. 19, no. 8, pp. 1159-1164, August 2012.

[12] J. W. Finnie, J. Manavis and P. C. Blumbergs, "Diffuse neuronal perikaryal amyloid precursor protein immunoreactivity in an ovine model of non-accidental head injury (the shaken baby syndrome)," *Journal of Clinical Neuroscience,* vol. 17, no. 2, pp. 237-240, February 2010.

[13] C. Bonnier, B. Mesples and P. Gressens, "Animal models of shaken baby syndrome: revisiting the pathophysiology of this devastating injury," *Pediatric rehabilitation,* vol. 7, no. 3, pp. 165-171, 2004.

[14] C. Bonnier, B. Mesples, S. Carpentier, D. Henin and P. Gressens, "Delayed White Matter Injury in a Murine Model of Shaken Baby Syndrome," *Brain Pathology,* vol. 12, no. 3, pp. 320-328, 2002.

[15] B. Coats, G. Binenbaum, R. L. Peiffer, S. Sullivan, J. Ralston, T. Akella, C. Smith, A.-C. Duhaime and S. Margulies, "Ocular and Neuropathology from Cyclic, Low Velocity Head Rotations in Immature Pigs," in *National Neurotrauma Symposium*, Fort Lauderdale,, 2011.

[16] B. M. Togioka, M. A. Arnold, M. A. Bathurst, S. M. Ziegfeld, R. Nabaweesi, P. M. Colombani, D. Chang and F. Abdullah, "Retinal Hemorrhages and Shaken Baby Syndrome: An Evidence Based Review," *The Journal of Emergency Medicine,* pp. 98-106, 2009.

[17] K. Bechtel, K. Stoessel, J. Leventhal, E. Ogle, B. Teague, S. Lavietes, B. Banyas, K. Allen, J. Dziura and C. Duncan, "Characteristics That Distinguish Accidental From Abusive Injury in Hospitalized Young Children with Head Trauma," *Pediatrics,* vol. 114, pp. 165-168, 2004.

[18] M. Vinchon, S. Defoort-Dhellemmes, M. Desurmont and P. Dhellemmes, "Accidental and nonaccidental head injuries in infants: a prospective study.," *Journal of Neurosurgery,* vol. 102, no. 4, pp. 380-384, 2005.

[19] L. Ewing-Cobbs, L. Kramer, M. Prasad, D. N. Canales, P. T. Louis, J. M. Fletcher, H. Vollero, S. H. Landry and K. Cheung, "Neuroimaging, Physical, and Developmental Findings After Inflicted and Noninflicted Tramuatic Brain Injury in Young Children," *Pediatrics,* vol. 102, no. 2, pp. 300-307, 1998.

[20] Y. Morad, T. Wygnansky-Jaffe and A. V. Levin, "Retinal haemorrhage in abusive head trauma," *Clinical Experimental Ophthalmology,* vol. 38, no. 5, pp. 514-520, 2010.

[21] V. M. Elner, "Ocular Manifestations of Child Abuse," *Archives of Ophthalmology,* vol. 126, no. 8, pp. 1141-1142, 2008.

[22] B. Harcourt and D. Hopkins, "Ophthalmic Manifestations of the Battered-baby Syndrome," *British Medical Journal,* vol. 14, pp. 398-401, 1971 .

[23] H. T. Keenan, D. K. Runyan, S. W. Marshall, M. A. Nocera and D. F. Merten, "A Population-Based Comparison of Clinical and Outcome Characteristics of Young Children With Serious Inflicted and Noninflicted Traumatic Brain Injury," *Pediatrics,* vol. 114, pp. 633-639, 2004.

[24] M. S. Dias, K. Smith, K. deGuehery, P. Mazur, V. Li and M. L. Shaffer, "Preventing Abusive Head Trauma Among Infants and Young Children: A Hospital-Based, Parent Education Program," *Pediatrics,* vol. 115, no. 4, pp. e470-e477, 2005.

[25] C. Z. Cory and M. D. Jones, "Can Shaking Alone Fatal Brain Injury?: A biomechanical assessment of the Duhaime shaken baby syndrome model," *Medicine, Science and the Law,* vol. 43, no. 4, pp. 317-333, 2003.

[26] D. N. Abrous, J. Rodriguez, M. le Moal, P. C. Moser and P. Barneoud, "Effects of mild traumatic brain injury on immunoreactivity for the inducible transcription factors c-Fos, c-Jun, JunB, and Krox-24 in cerebral regions associated with conditioned fear responding," *Brain Research,* vol. 826, pp. 181-192, 1999.

[27] C. Adamsbaum, S. Grabar, N. Mejean and C. Rey-Salmon, "Abusive Head Trauma: Judicial Admissions Highlight Violent and Repetitive Shaking," *Pediatrics,* vol. 126, pp. 546-555, 2010.

[28] R. G. Barr, R. B. Trent and C. J, "Age-related incidence curve of hospitalized Shaken Baby Syndrome cases: Convergent evidence for crying as a trigger to shaking," *Child Abuse and Neglect,* vol. 30, pp. 7-16, 2006.

[29] I. Talvik, R. C. Alexander and T. T, "Shaken baby syndrome and a baby's cry," *Acta Paediatrica,* vol. 97, pp. 782-785, 2008.

[30] J. Brazy, "Effects of crying on cerebral blood volume and cytochrome aa3.," *Journal of Pediatrics,* vol. 112, pp. 457-461, 1988.

[31] B. Kornum and K. G, "Cognitive testing of pigs (Sus scrofa) in translational biobehavioral research," *Neuroscience and Biobehavioral Reviews,* vol. 35, pp. 437-451, 2011.

[32] H. Hagberg, R. Ichord, C. Palmer, J. Y. Yager and S. J. Vannucci, "Animal Models of Developmental Brain Injury: Relevance to Human Diseases," *Developmental Neuroscience,* vol. 24, pp. 364-366, 2002.

[33] N. M. Lind, A. Moustgaard, J. Jelsing, G. Vajta, P. Cumming and A. Hansen, "The use of pigs in neuroscience: Modeling brain disorders," *Neuroscience and Biobehavioral Reviews,* vol. 31, pp. 728-751, 2007.

[34] S. F. S. Sullivan, J. Ralston, C. Smith, K. Propert, P. Rapp and S. Margulies, "Behavioral Deficits and Axonal Injury Persistence after Rotational Head Injury Are Direction Dependent," *Journal of Neurotrauma,* vol. 30, pp. 538-545, 2013.

[35] N. G. Ibrahim, J. Ralston, C. Smith and S. Margulies, "Phyisological and Pathological Responses to Head Rotations in Toddler Piglets," *Journal of Neurotrauma,* vol. 27, pp. 1021-1035, 2010.

[36] F. Ratjen, A. Trost, J. Welker, P. Spangenberg and H. G. Wiesemann, "The Effect of Rapid Thoracoabdominal Compressions on Intracranial Pressure in Newborn Lambs," *Pediatric Research,* vol. 38, no. 5, pp. 664-667, 1995.

[37] S. Eucker, "PhD Dissertation: Effect of head rotation direction on closed head injury in neonatal piglets.," *University of Pennsylvania,* 2009.

[38] B. Yu, D. Gabriel, N. Larry and K. An, "Estimate of the Optimum Cutoff Frequency for the Butterworth Low-Pass Digital Filter," *Journal of Applied Biomechanics,* vol. 15, no. 3, pp. 318-329, 1999.

[39] I. M. Medana and M. M. Esiri, "Axonal damage: a key predictor of outcome in human CNS diseases," *Brain,* vol. 126, no. 3, pp. 515-530, 2003.

[40] P. Brodal, The Central Nervous System Structure and Function, New York: Oxford University Press, Inc., 1992.

[41] J. F. Geddes, H. L. Whitwell and D. I. Graham, "Traumatic or diffuse axonal injury? Author's response," *Neuropathology and Applied Neurobiology,* vol. 26, no. 5, p. 491, 2000.

[42] Y. Han, T. J. McCulley and J. C. Horton, "No Correlation between Intraocular Pressure and Intracranial Pressure," *Annals of Neurology,* vol. 64, no. 2, pp. 221-224, 2008.

[43] T. Kirk, K. Jones, S. Miller and J. Corbett, "Measurement of Intraocular and Intracranial Pressure: Is there a Relationship," *Annals of Neurology,* vol. 70, no. 2, pp. 323-326, 2011.

[44] M. K. Lashutka, A. Chandra, H. N. Murray, G. S. Phillips and B. C. Hiestand, "The Relationship of Intraocular Pressure to Intracranial Pressure," *Annals of Emergency Medicine,* vol. 43, no. 5, pp. 585-591, 2004.

[45] Z. Li, Y. Yang, Y. Lu, D. Liu, E. Xu, J. Jia, D. Yang, X. Zhang, H. Yang, D. Ma and N. Wang, "Intraocular pressure vs intracranial pressure in disease conditions: A prospective cohort study (Beijing iCOP study)," *BMC Neurology,* vol. 12, no. 66, 2012.

[46] S. C. Gabaeff, "Challenging the Pathophysiologic Connection between Subdural Hematoma, Retinal Hemorrhage and Shaken Baby Syndrome," *Western Journal of Emergency Medicine,* vol. 12, no. 2, pp. 144-158, 2011.

[47] T. Shiau and A. V. Levin, "Retinal Hemorrhage in Children: The Role of Intracranial Pressure," *Archives of Pediatric Adolescent Medicine,* vol. 166, no. 7, pp. 623-628, 2012.

[48] G. Binenbaum, D. L. Rogers, B. J. Forbes, A. V. Levin, S. A. Clark, C. W. Christian, G. T. Liu and R. Avery, "Patterns of Retinal Hemorrhage Associated With Increased Intracranial Pressure in Children," *Pediatrics,* vol. 132, pp. 430-434, 2013.

[49] A. H. S. Holbourn, *Private communication to Dr. Sabina Strich.,* 1956.

[50] A. K. &. H. A. E. Ommaya, " Tolerance for cerebral concussion from head impact and whiplash in primates.," *Journal of Biomechanics,* vol. 4, no. 1, pp. 13-21, 1971.

[51] K. L. Thibault and S. S. Margulies, "Age-dependent material properties of the porcine cerebrum: effect on pediatric inertial head injury criteria," *Journal of Biomechanics,* vol. 31, pp. 1119-1126, 1998.

[52] M. T. Prange and S. S. Margulies, "Regional, Directional, and Age-Dependent Properties of the Brain Undergoing Large Deformation," *Journal of Biomechanical Engineering,* vol. 124, pp. 244-252, 2002.

[53] R. C. Augusteyn, D. Nankivil, A. Mohamed, B. Maceo, F. Pierre and J.-M. Parel, "Human ocular biometry," *Experimental Eye Research,* vol. 102, pp. 70-75, 2012.

[54] G. Ancora, E. Maranella, A. Aceti, L. Pierantoni, S. Grandi, L. Corvaglia and G. Faldella, "Effect of Posture on Brain Hemodynamics in Preterm Newborns Not Mechanically Ventilated," *Neonatology,* vol. 97, pp. 212-217, 2009.

[55] Y. Hoshi and M. Tamura, "Detection of dynamic changes in cerebral oxygenation coupled to neuronal function during mental work in man," *Neuroscience Letters,* vol. 150, pp. 5-8, 1993.

[56] A. Villringer, J. Planck, C. Hock, L. Schleinkofer and U. Dirnagl, "Near infrared spectroscopy (NIRS): a new tool to study hemodynamic changes during activation of brain function in adults," *Neuroscience Letters,* vol. 154, pp. 101-104, 1993.

[57] G. Strangman, D. A. Boas and J. P. Sutton, "Non-invasive neuroimaging using near-infrared light," *Biological Psychiatry,* vol. 52, no. 7, pp. 679-693, 2002.

[58] G. Strangman, M. A. Franceschini and D. Boas, "Factors affecting the accuracy of near-infrared spectroscopy concentration calculations for focal changes in oxygenation parameters," *NeuroImage,* vol. 18, no. 4, pp. 865-879, 2003.

[59] S. S. Hayreh, "Occlusion of the central retinal vessels," *British Journal of Ophthalmology,* vol. 49, pp. 626-645, 1965.

[60] T. Y. Wong and I. U. Scott, "Retinal-Vein Occlusion," *The New England Journal of Medicine,* vol. 363, pp. 2135-2144, 2010.

[61] M. C. Pierce and G. Bertoocci, "Injury Biomechanics and Child Abuse," *The Annual Review of Biomedical Engineering,* vol. 10, pp. 85-106, 2008.

[62] P. Riordan-Eva, J. Whitcher, D. Vaughan and T. Asbury, Vaughan and Asbury's General Ophthalmology, New York: McGraw Hill, 2008.

[63] B. Coats, G. Binenbaum, R. I. Peiffer, B. J. Forbes and S. S. Margulies, "Ocular Hemorrhages in Neonatal Porcine Eyes From Single, Rapid Rotational Events," *Investigative Ophthalmology & Visual Science,* vol. 51, no. 9, pp. 4792-4797, 2010.

[64] S. A. Sajjadi, M. H. Harirchian, N. Sheikhbahaei, M. R. Mohebbi, M. H. Malekmadani and H. Saberi, "The Relation between Intracranial and Intraocular Pressures: Study of 50 patients," *Annals of Neurology,* vol. 59, no. 5, pp. 867-870, 2006.

[65] J. Arrevalo, A. Mendoza, C. Fernandez, J. Yepez, D. Krivoy and F. Millan, "Decompression Retinopathy after intraocular surgery," *Arch Soc Esp Oftalmol,* vol. 82, pp. 629-634, 2007.

[66] S. K. Mukkamala, A. D. S. Patel, R. McGlynn, P. A. Sidoti, R. N. Weinreb, J. Rusoff, S. Rau and R. C. Gentile, "Ocular decompression retinopathy: A review," *Survey of Ophthalmology,* vol. 58, pp. 505-512, 2013.

[67] J. Saffioti, *Characterization of Pediatric Ocular Material Properties for Implementation in Finite Element Modeling.,* Salt Lake City: University of Utah, 2014.

[68] J. Colter, A. Williams, P. Moran and B. Coats, "Dynamic Moduli of Immature Ovine Vitreous using Spectrum Interconversion," *Journal of Mechanical Properties of*

Biomedical Materials, vol. In Review, 2014.

[69] E. O. Carew, J. E. Barber and I. Vesely, "Role of Preconditioning and Recovery Time in Repeated Testing of Aortic Valve Tissues: Validation Through Quasilinear Viscoelastic Theory," *Annals of Biomedical Engineering,* vol. 28, pp. 1093-1100, 2000.

[70] Y. Fung, "Elasticity of soft tissues in simple elongation," *American Journal of Physiology,* vol. 213, no. 6, pp. 1532-1544, 1967.

[71] G. R. Lopez Jaime, A. H. Kashani, S. Saati, G. Martin, G. Chader and M. Humayun, "Acute Variations in Retinal Vascular Oxygen Content in a Rabbit Model of Retinal Venous Occlusion," *PLOS ONE,* vol. 7, no. 11, 2012.

[72] R. A. W. Lehman, T. Krupin and S. M. Podos, "Experimental effect of intracranial hypertension upon intraocular pressure.," *The Journal of Neurosurgery,* vol. 36, no. 1, pp. 60-66, 1972.

[73] Y. Fung, "Chapter 7 Bioviscoelastic Solids," in *Biomechanics Mechanical Properties of Living Tissues* , Springer, 1993, pp. 242-320.

[74] J. Cheng, I. C. Howard and M. Rennison, "Study of an infant brain subjected to periodic motion via a custom experimental apparatus design and finite element modelling," *Journal of Biomechanics,* vol. 43, pp. 2887-2896, 2010.

[75] H. Ameri, J. G. Kim, T. Ratanapakorn, G. Chader and M. Humayun, "Intravitreal and subretinal injection of tissue plasinogen ativator (tPA) in the treatment of experimentally created retinal vein occlusion in Rabbits," *Retina,* vol. 28, no. 2, pp. 350-355, 2008.

[76] T. Wygnanski-Jaffe, A. V. Levin, A. Shafiq, C. Smith, R. W. Enzenauer, J. E. Elder, J. D. Morin, D. Stephens and E. Atenafu, "Postmortem Orbital Findings in Shaken Baby Syndrome," *American Journal of Ophthalmology,* vol. 142, no. 2, pp. 233-240, 2006.

[77] B. Curtin, "Physiopathologic Aspects of Scleral Stress-Strain.," *Transactions of the American Ophthalmological Society,* vol. 67, pp. 417-461, 1969.